Seismic velocity changes associated with the 2011 Tohoku-Oki earthquake (Mw9.0) as inferred from analyses of direct and coda waves of repeating earthquakes

Doctoral Thesis
博士論文

Seismic velocity changes associated with the 2011 Tohoku-Oki earthquake (Mw 9.0) as inferred from analyses of direct and coda waves of repeating earthquakes

繰り返し地震の直達波とコーダ波の解析により推定された 2011 年東北地方太平洋沖地震（Mw9.0）に伴う地震波速度変化

東北大学大学院理学研究科
地球物理学専攻

Jose Jesus Karim Pacheco Vivero

論文審査委員
西村　太志　教授　（指導教員・主査）
松澤　暢　　教授
三浦　哲　　教授
岡田　知己　准教授
中原　恒　　准教授

2014
平成 26 年

Acknowledgements:

I want to express my gratitude to Professor Takeshi Nishimura. This work could not be completed without his guidance and helpful comments. I am very grateful for his assistance and the time he spent discussing with me on my work and for his help during my stay in Japan. I also want to express my gratitude to Associate Professor Hisashi Nakahara for his useful and constructive comments on my work and during the weekly seminars at Solid Earth Physics Laboratory. I would like to thank them for sharing with me their knowledge and expertise.

I am very thankful to Professor Toru Matsuzawa, Professor Satoshi Miura and Associate Professor Tomomi Okada, for their invaluable comments on this study. Also, I express my gratitude to all the professors of the Research Center for Prediction of Earthquakes and Volcanic Eruptions.

I would like to thank Associate Professor Mare Yamamoto, Dr. Kentaro Emoto and Dr. Tomofumi Kozono for their suggestions on my work and for their help during my studies at the Solid Earth Physics Laboratory. Their professionalism and knowledge are unparalleled.

Also, I like to thank all of the students, clerical and technical staff of Solid Earth Physics Laboratory. They helped me in my study and daily life. Many thanks to Ms.Chika Kamada for all her help, especially on administration matters related to my stay and study in Japan.

I want to thank my wife for her support and encouragement that helped me put many hours on my studies during our stay in Japan. I would like to express all my gratitude to my father, my mother and my brothers for their unconditional support during my time in Japan.

I would like to thank the Monbukagakusho scholarship and the research assistant funding of Tohoku University that enabled me to study in Japan. I am also grateful to the National Research Institute for Earth Science and Disaster Prevention for providing Hi-net and KiK-net data used in this study.

Abstract:

Detecting seismic velocity changes in the solid earth has been of major interest and important to understand geophysical underground phenomena for many years. Since a pioneer work of Poupinet et al. (1984), seismic velocity changes have been measured with high resolution and reliability by using the waveforms excited from controlled artificial sources and natural repeating earthquakes that occur at same locations with the same mechanisms. Recently, seismic interferometry techniques using ambient noises or coda waves, which do not need same sources, are used to detect subtle medium changes. As a result, decreases of seismic wave velocity have been detected associated with the occurrences of large earthquakes at many fields. Examples are summarized in Chapter 1. The observed seismic wave velocity changes associated with the large earthquakes have been often considered to be caused by mechanisms such as near surface damage due to strong motions [e.g., Rubinstein & Beroza, 2005]. Also, stress changes in the medium have been inferred as a mechanism to generate seismic velocity changes in the subsurface and crust [e.g., Brenguier et al., 2008, Nishimura et al., 2005; Anggono et al., 2012]. There is a report on the velocity changes in the upper and lower crust during slow slip events that do not generate strong motions affecting the subsurface [Rivet et al., 2012]. However, the mechanism and depth extents of these seismic wave velocity changes are still matters under debate.

The 2011 Tohoku-Oki earthquake (Mw 9.0) provided us with an important opportunity to better understand seismic wave velocity changes occurring at shallow and deeper zones in the crust, because seismic waves are recorded by high-density seismic networks in a wide area of NE Japan that is subject to strong motions and large deformations. Several studies have already reported seismic wave velocity drops of up to 10 % in the subsurface due to strong motions after this earthquake from analyses of the records of the borehole and ground surface sensors [e.g. Nakata & Snieder, 2011; Takagi & Okada 2012]. Seismic wave velocity changes have been also inferred at deeper zones down to 10 km from analyses of Rayleigh waves retrieved from ambient noises [Brenguier et al., 2014]. The enormous strain induced by the Tohoku-Oki earthquake might have introduced subtle changes in seismic wave velocity that extends deep in the crust beneath NE Japan. However, it is still unknown whether or not deeper crust has changed its seismic velocity associated with the Tohoku-Oki earthquake.

In the present study, we use direct body waves generated from repeating earthquakes. The analyses of repeating earthquakes have a merit in that the body-waves sample deeper zone between the sources and the receivers, which have not yet been analyzed for the case of the Tohoku-Oki earthquake. However, accurate measurement of changes in travel times of direct P- and S-waves is strongly dependent on the precision of the repeating earthquake locations, and because a large area of NE Japan

was damaged, usual relocation methods of repeating earthquakes are not applicable. Therefore, we develop a new inversion method to detect subtle velocity changes in the medium as well as hypocenter parameters of repeating earthquakes. The new method is applied to the Hi-net data to reveal spatial distributions of the seismic velocity change in NE Japan. We further analyze the seismograms of repeating earthquakes recorded on the ground surface and at depths of about 100 m to understand the wave properties we analyzed. Finally, we discuss the structural changes associated with the Tohoku-Oki earthquake based on our results and previous studies that report the seismic velocity changes.

In Chapter 2, the new inversion method using arrival time differences of direct P and S-waves is described. The inversion method simultaneously determines hypocenter parameters and station correction factors of travel times of direct P- and S-waves. Since arrival time differences of body waves from a pair of repeating earthquakes occurring before and after the target large earthquake are represented as linear equations of relative locations and origin times of the two earthquakes and station correction factors that account for the velocity changes of medium, we are able to determine these parameters by using the least square method. We apply this method to a set of 25 repeating earthquakes located at depths between 30 and 60 km in NE Japan with magnitudes ranging from 3.4 to 4.7. Each pair of repeating earthquakes consists of two events occurring before and after the Tohoku-Oki earthquake. Direct wave arrival time differences are measured from seismograms recorded by 454 stations of Hi-net seismic network. Using a cross-spectrum method, we estimate arrival time differences up to about 0.01 s and 0.04 s for P- and S-waves, respectively. The results show that a wide area of NE Japan locating at 37-40^{o} N in latitude, close to the large slip area of the Tohoku-Oki earthquake, indicates large station correction factors of about 0.005-0.04 s for S-wave. On the other hand, station correction factors for P-wave are much smaller. We examine temporal changes of the medium properties by dividing the 25 sets of repeating earthquakes in three groups and by analyzing a set of 15 repeating earthquakes that occurred only before the Tohoku-Oki earthquake. The results indicate no significant temporal change in the station correction factors. We further separately analyze the repeating earthquakes occurring in the north and the south regions of NE Japan, respectively. As a result, we observe significant spatial shifts of large station correction factors for S-wave: large station correction factors determined from the repeating earthquakes located in the north are shifted to the south area of NE Japan, while those from the repeating earthquakes in the south are shifted to the north area. This implies that the anomaly that decreased seismic velocity extends down to deep crust in the middle of the area where both large station correction factors are observed. We first determine the horizontal extent of the anomaly. We suppose that the horizontal extent of the anomaly is the region where station correction factors determined both from the north and south groups exceed a limit value

(0.015 s). As a result, the anomaly is determined at the area extending N-S directions in the middle of NE Japan. We further estimate the depth of the anomaly to be at approximately 25 km from analyses of S-wave ray tracing in a layered spherical earth. The average velocity change is estimated to be about 0.1%. We examine the stability and accuracy of the inversion method by using a Jackknife test, and confirm that the hypocenters are located at approximately same regions independently of the set of repeating earthquakes. These results suggest that our inversion method properly determines the station correction factors and hypocenter parameters.

In Chapter 3, to examine the area where the seismic waves of repeating earthquakes propagate, we analyze triggered seismograms recorded at borehole and ground surface sensors of KiK-net. Comparison between the results obtained from the sensors installed at different depths allows us to infer the regions where the waves are sampling in the medium. We measure arrival time differences of body waves from the seismograms of 6 repeating earthquakes located at depths from 43 to 53 km in NE Japan with magnitudes ranging between 3.4 and 4.7. We correct the origin times of repeating earthquakes using hypocenter parameters determined in the previous chapter and estimate travel time differences of direct waves to be up to 0.01 s for P-waves and about 0.04 s for S-waves. From multi-lapse time window analyses of S-coda, velocity changes are estimated to be up to 0.2% at some stations located mainly at Iwate and Fukushima Prefectures in Tohoku region. These travel time differences and velocity changes measured at the borehole and ground surface sensors are very similar to each other. This suggests that the waves we analyzed sample the same region and not mainly consist of reverberations at subsurface but originate from deeper in the medium.

In Chapter 4, we examine the origins of the velocity changes detected in this study. We first compare the results of this study with peak ground accelerations and strains associated with the occurrence of Tohoku-Oki earthquake. The results show no clear correlation among them. The results are then compared and discussed with results reported in previous studies on the velocity changes associated with the Tohoku-Oki earthquake. Our results from analyses of KiK-net data indicate that the waves we analyzed do not consist mainly of the waves propagating or reverberating at depths of a few hundred meters. This is confirmed by a poor spatial distribution of seismic velocity changes by this study with the results of KiK-net data analyses by Takagi & Okada (2012). On the other hand, we find good spatial correlations with results of relatively long period (about 1-10 s) Rayleigh waves [Brenguier et al., 2014] and S-coda at 1-2 Hz [Nishimura et al., 2013]. The estimated velocity changes are also in the same amplitude ranges of about 0.1 %. To reconcile all these observations, we present a model of structural changes that explains the observations from this study and previous studies. The structural model consists of shallow layers (few hundred meters) with velocity changes up to 10 % and crust with

velocity changes of about 0.1% that extends down to approximately 25 km beneath the middle of NE Japan, immediately west from the large slip area of the Tohoku-Oki earthquake. Although seismic wave velocity changes extending down to such depths in the lower crust are rarely reported, there is recently a reported example in which slow slip events generated a decrease of the seismic velocity in the crust beneath Mexico [Rivet et al., 2014].

In this study, we have succeeded in clarifying that seismic velocity changes associated with the Tohoku-Oki earthquake occurred not only at the subsurface but in the crust from our new inversion analyses of large number of arrival time data of repeating earthquakes. We found an anomaly of velocity change with about 0.1% extending down to approximately 25 km in the middle of NE Japan, close to the large slip area of the Tohoku-Oki earthquake. Considering the results from analyses of seismograms recorded at KiK-net stations and previous studies on the seismic velocity changes, we propose a structural model that consists velocity changes of up to 10% in subsurface (~100 m), and anomaly with an average velocity change of approximately 0.1% extending down to 25 km. This study has provided important evidence that seismic velocity changes associated with a megathrust earthquake are not limited to the shallow subsurface, but extend deeper in the crust.

CONTENTS

1. Introduction

1.1. Seismic velocity changes of the Earth's crust

Seismic wave velocity changes in the crust before and/or after a large earthquake have been investigated since early 1960s. Savarensky (1968) reported an increase in travel time of compressional waves after an earthquake. Anomalies of seismic velocities before earthquakes were sometimes reported to be as large as 10% [e.g., Wyss et al., 1975] or less than 1% [e.g., Kanamori and Fuis, 1976]. However, such results are generally based on the estimation with low accuracy often comparable to the errors of observation [Dolbilkina et al., 1979], because they often used natural earthquakes occurring close to each other but not similar earthquakes that have almost same waveforms at each station. Poupinet et al. (1984) first proposed the use of earthquake doublets (repeating earthquakes) for monitoring seismic wave velocities in the Earth's crust with high accuracy. They analyzed earthquake doublets that generate same waveforms from a same location of hypocenters. To eliminate errors of the origin times of earthquake doublets, they examine small phase differences of coda-waves between the two events by applying a moving window cross-correlation technique. As a result, they succeeded in precisely estimating velocity decreases up to 0.2 % after the 1979 Coyote Lake earthquake (M5.9).

Since Poupinet et al. (1984)'s pioneer work, seismic velocity changes have been measured with reliable accuracy using sources set at same locations with same mechanisms such as repeating earthquakes [Rubinstein & Beroza, 2005; Schaff & Beroza, 2004; Rubinstein et al., 2007] and controlled sources [Nishimura et al., 2005; Li et al., 2006]. Seismic velocity measurements using ambient seismic noise [e.g., Meier et al., 2010; Wegler et al., 2009; Brenguier et al., 2008] are recently developed and now widely used at many regions. Each technique has its benefits and disadvantages. Controlled sources allow the measurements at discrete points with a high signal to noise ratio. But the sources may be limited in space and time because of expensive costs. Repeating earthquakes occur in nature and allows the measurement of direct P- and S-waves separately with good signal to noise ratio, since its energy is relatively larger than the others. The main disadvantages are that temporal sampling is sometimes insufficient, the source is not available everywhere, and more importantly, an accurate measurement is dependent on the precision of the repeating earthquake locations and origin times [Schaff 2012]. Recently developed techniques using ambient seismic noise enables us to continuously monitor seismic velocity changes at regions where at least two seismometers are installed. Hence, it is possible to determine three dimensional velocity changes where a dense seismic network is available. However, it is necessary to use large amount of data (sometimes days, months, or more) to retrieve the

seismic waves propagating between the stations. Temporal changes in the distribution of the ambient noise sources also affect measurements and introduce errors affecting the velocity change estimation.

Seismic velocity changes associated with large earthquakes have been investigated and the mechanisms to cause the observed velocity changes have been discussed. Rubinstein & Beroza (2005) analyzed direct S-wave and S-coda waves by using a moving window cross-correlation technique and observed time delays in the S-wave and S-coda. They observed that seismic velocity changes after a large earthquake are characterized by a decrease of seismic wave velocity after the main shock, followed by a gradual recovery. They attributed the observed travel time changes to cracks formed or opened due to strong shaking at less than 100 m after the occurrence of the Parkfield earthquake (Mw 6.0). Seismic velocity decreases up to 5% were also observed in the shallow medium after the Iwate-Miyagi earthquake (Mw 7.2) which are interpreted to be related to strong motions [Takagi et al., 2012]. On the other hand, S-wave velocity decreases by 0.08 % have been discussed with crustal stresses and stress relaxation after large earthquakes such as the Mw 6.6 Mid-Niigata earthquake [Wegler et al., 2009] and the Mw 6.5 San Simeon earthquake [Brenguier et al., 2008]. Changes in the deep crust have also been observed during slow slip events (SSE), which does not accompany strong motions, associated with the convergence between Cocos and North America plates [Rivet et al. 2011-2014] from analyses of long period ambient noise (>12 s) that are generated by the SSE. Seismic velocity increases are also observed in association with deflations at Miyakejima volcano in 2000 [Anggono et al., 2012]. Seasonal variations of water level changes and Earth tides also generate velocity changes in the shallow structure [Takano et al., 2014].

1.2. The Mw9.0 Tohoku-Oki earthquake

The Tohoku-Oki earthquake (Mw 9.0) took place in NE Japan, on March 11th 2011. This earthquake is a megathrust event in a subduction zone accompanying a large fault slip of about 50 m [e.g., Lay et al., 2011; Koketsu et al., 2012]. Studies based on source inversions indicate that the earthquake consists of three main ruptures [e.g., Yokota et al., 2011]. After a small bilateral rupture in the initial 40 s, the first main rupture propagated to the easternmost shallow part and generated a compact shallow slip. Later, the second main rupture began to propagate northwestward and southward, and caused a large final slip of 35 m. The slip propagated to the westernmost area including the Miyagi-Oki region [Yokota et al., 2011]. The southward rupture finally reached west off Fukushima prefecture, approximately 200 km south of the hypocenter of the third main rupture stage. The source process lasted about 150 s, generating very large slip area (30 to 60 m) that produced large amplitude low-frequency radiation. High frequency waves were also radiated from down-dip of the hypocenter

[Tajima et al., 2013].

The Tohoku-Oki earthquake caused severe tsunami damage due to the slow rupture speed of 1.5~1.8 km/s [Koketsu 2012]. Such slow rupture growth of the earthquake source required larger fracture energy; therefore the resultant radiated energy became smaller based on the energy budget [Kanamori and Heaton, 2000]. Strong accelerations up to 2000 gal were detected [e.g. Ozawa et al. 2012] and the observed strong motion is smaller than the estimates from empirical ground motion prediction equations [Miyake et al., 2012]. Large crustal deformation exceeding 10^{-6} strain was detected in a wide area of the NE Japan [Takahashi et al., 2011].

Recent studies report that the Tohoku-Oki earthquake introduced significant seismic velocity decreases in shallow structures down to about a hundred meters from analyses of seismograms recorded at boreholes and on the ground surface. Nakata & Snieder (2011) measured a reduction in S-wave velocity of about 10 % after the main shock by applying deconvolution analyses to the waveforms of KiK-net array that consists of two accelerometers set on the ground surface and in a borehole at a depth of about 100 m. Their method applied to the vertical arrays cancels out the source process and the medium properties below the borehole sensors, and the velocity reduction detected represents changes in the medium between the two sensors. Takagi & Okada (2012) estimated temporal changes in shear wave velocity of up to 10% at near surface from cross-correlation analyses applied to the coda recorded by the KiK-net vertical arrays. They inferred that the velocity changes are well correlated with strong motion. Recently, using data from the same KiK-net seismic network, Nakahara (2014) calculated autocorrelations from S-coda of seismograms recorded at the surface sensor and applied deconvolution analysis using the surface and subsurface records. He estimated large velocity changes at shallow depths from observed phase delays associated with the Tohoku-Oki earthquake. He also considered strong motion to be the main cause of the observed delays. These studies indicate a large velocity decreases in the subsurface and associate the changes in seismic wave velocity with strong motions and related mechanisms such as none linear site response at some stations [Wu & Peng, 2011] and generation of omni-directional cracks near the surface [Sawazaki & Snieder, 2013].

Several studies report seismic velocity changes occurring at deeper zones after the Tohoku-Oki earthquake. Minato et al. (2012) analyzed long period surface waves (of about 10 s) and estimated velocity decreases as large as 1.5% after the 2011 Tohoku-Oki earthquake. They inferred that the velocity changes contain information from the crust down to a few kilometers, which may be caused by coseismic stress release in addition to shallower effects due to strong motion. Brenguier et al. (2014) retrieved Rayleigh waves from correlation analyses of ambient noise recorded by Hi-net seismic network. They estimated velocity changes of up to 0.12% by computing cross-correlation functions

averaged over the day of the Tohoku-Oki earthquake and 4 days after it. They concluded that the spatial distribution of velocity changes does not well correlate with strong ground motion or deformation at shallow medium. They show that the reductions are more likely related to dynamic stresses and weakening of the pressurized crust. In particular, they observe that coseismic velocity reductions are spatially correlated with the regions where pressurized volcanic fluids are present in the upper crust.

These previous studies suggest that the large strong-motions and stress/strain changes caused by the Tohoku-Oki earthquake affect the medium properties not only at the subsurface but also deeper zone.

1.3. Purpose of the study

Seismic velocity changes associated with the occurrence of large earthquakes have been detected at many regions around the world. These changes are often attributed to the damage of subsurface at a few hundred meters subject to strong-motions. However, several studies using long-period waves suggest medium changes occur in deeper zones at depths of a few kilometers or more, which are discussed with stress/strain changes and/or weakening of the medium. The Tohoku-Oki earthquake induced enormous stress/strain changes in a wide area of the NE Japan down to deep crust. Previous studies have already reported seismic velocity changes up to 10 % at shallow medium that are inferred to be caused by strong motions. Small velocity reduction up to 0.12% in the medium extending down to about 10 kilometers in the crust have been also suggested from analyses of long-period ambient noises.

To examine the region where seismic velocity changes are induced, we analyze direct P- and S-waves from repeating earthquakes occurring before and after the Tohoku-Oki earthquake. This method has merits in the points that (1) the medium properties are characterized from both of P- and S- waves; (2) the seismic velocity changes at deep zones along the paths of seismic ray are examined. Accurate measurements of arrival times of direct P- and S-waves are very sensitive to relative locations of the hypocenter of repeating earthquakes. Since NE Japan is widely damaged as the seismic velocity reduction of about 10 % are reported, it is necessary to take it into account for determination of the hypocenter parameters. In the present study, therefore, we develop an inversion method to simultaneously determine hypocenter parameters of repeating earthquakes and station correction factors of travel times of direct P- and S-waves. We apply this new inversion method to the data obtained at a large number of stations in NE Japan to obtain spatial distributions of the seismic velocity changes caused by the occurrence of Tohoku-Oki earthquake.

We further analyze waveforms recorded by KiK-net seismic network vertical arrays. The results are used to understand where the seismic wave we analyzed propagates in the medium. Also, the results are

compared with previous studies, and we discuss the region of the seismic velocity change, especially giving attentions to the depth extent.

2. Simultaneous inversion for hypocenter locations and station corrections of direct P- and S-wave travel times

We analyze repeating earthquakes occurring before and after the Tohoku-Oki earthquake. Repeating earthquakes, which are characterized by waveform similarity [Poupinet et al., 1984], are considered to be generated from almost a same fault with a same focal mechanism and moment rate function. Detailed analyses of arrival times of body waves using cross-correlations of waveforms reveal small differences in hypocenters with a few hundred meters [e.g., Igarashi et al., 2003]. Such differences in hypocenter location are necessary to be corrected to discuss slight changes in the medium. In order to detect such slight changes, previous studies generally use relocated repeating earthquakes that occur far from the region where seismic velocity changes are observed. However, in the case of the Tohoku-Oki earthquake, subsurface was heavily damaged in a wide area of NE Japan by the strong motions as up to 10 % of velocity reductions were observed at a depth of 100 m [Nakata and Snieder, 2011; Takagi and Okada, 2012]. This makes it difficult to relocate hypocenters of repeating earthquakes following the same procedures used in previous studies. In the present study, therefore, we develop a new method to determine travel time changes of body waves as well as hypocenter differences of a pair of repeating earthquakes. We apply this method to Hi-net data and clarify the seismic velocity changes associated with the Tohoku-Oki earthquake.

2.1. Simultaneous inversion method

One of the most common procedures to relocate hypocenters is known as the joint hypocenter determination (JHD) [e.g., Douglas, 1967; Pujol 1992]. The JHD method uses arrival times of seismic phases determined at several seismic stations to jointly relocate hypocenters for a set of earthquakes. An approach involving the joint determination of hypocenters, origin times and station correction terms was proposed several decades ago and the basic assumption of this method is that the station correction terms represents velocity variations confined to the vicinity of the stations [Pujol, 1992]. However, we need to consider temporal changes of seismic velocity changes inherent to stations for the case of the Tohoku-Oki earthquake. Instead of arrival times, therefore, we use arrival time differences of repeating earthquakes occurring before and after a target large earthquake (we call main earthquake hereafter) to simultaneously invert hypocenter parameters and station correction factors of travel times of direct P- and S-waves.

We represent arrival times of any particular seismic phase, τ_{ij} , corresponding to each pair of a

repeating earthquake that occur before and after a main earthquake as:

$$\tau_{ij}^{1} = t_j^{1} + T_{ij}(\mathbf{x}_j^{1}, \mathbf{x}_i), \tag{2.1}$$

$$\tau_{ij}^{2} = t_j^{2} + T_{ij}(\mathbf{x}_j^{2}, \mathbf{x}_i) + S_i, \tag{2.2}$$

where i and j represent the number of station and the number of pair of repeating earthquakes, respectively. Superscripts 1 and 2 indicate the earthquakes occurring before and after the main earthquake, respectively. t_j^1 and t_j^2 correspond to the origin times of the earthquakes before and after the main earthquake, respectively, T_{ij} is the travel time, and S_i represents the station correction factor that accounts for travel time change inherent to each station (Figure 2.1).

Two events of a repeating earthquake are closely located to each other so that eq.(2.2) can be represented as a Taylor expansion around the hypocenter of the earthquake occurring before the main earthquake. Hence eq.(2.2) is approximated as:

$$\tau_{ij}^{2} \cong t_j^{2} + T_{ij}(\mathbf{x}_j^{1}, \mathbf{x}_i) + \left.\frac{\partial T_{ij}}{\partial x_j}\right|_{\mathbf{x}=\mathbf{x}_j^1} \delta x_j + \left.\frac{\partial T_{ij}}{\partial y_j}\right|_{\mathbf{x}=\mathbf{x}_j^1} \delta y_j + \left.\frac{\partial T_{ij}}{\partial z_j}\right|_{\mathbf{x}=\mathbf{x}_j^1} \delta z_j + S_i. \tag{2.3}$$

In eq.(2.3), the spatial derivatives of travel time are evaluated at the location of $\mathbf{x}=\mathbf{x}^1$. Terms δx_j, δy_j, and δz_j represent the hypocenter parameter differences in location between the two events of the j-th repeating earthquake. Now taking the difference between τ^2_{ij} and τ^1_{ij} in eqs.(2.3) and (2.1) and omitting the vertical bar notations for simplicity, we can write:

$$\tau_{ij}^{2} - \tau_{ij}^{1} = t_j^{2} - t_j^{1} + \frac{\partial T_{ij}}{\partial x_j}\delta x_j + \frac{\partial T_{ij}}{\partial y_j}\delta y_j + \frac{\partial T_{ij}}{\partial z_j}\delta z_j + S_i. \tag{2.4}$$

To measure arrival time differences between the two events occurring before and after the main earthquake, cross-correlation or cross-spectrum method is often applied to the main phases of P- or S-waves. In such a case, the waveforms are generally cut out from arbitrary times (e.g., origin times of the earthquakes determined from routine hypocenter determinations). Here, we introduce the origin time routinely determined by general hypocenter determination methods, and rewrite eq.(2.4) as:

$$(\tau_{ij}^{2} - t_{j,r}^{2}) - (\tau_{ij}^{1} - t_{j,r}^{1}) = (t_j^{2} - t_{j,r}^{2}) - (t_j^{1} - t_{j,r}^{1}) + \frac{\partial T_{ij}}{\partial x_j}\delta x_j + \frac{\partial T_{ij}}{\partial y_j}\delta y_j + \frac{\partial T_{ij}}{\partial z_j}\delta z_j + S_i, \tag{2.5}$$

where the subscript r indicates the origin time obtained from routine hypocenter determination. The term in the left hand side of eq.(2.5) represents the arrival time difference of a particular phase between two events of the repeating earthquake. Therefore, we may rewrite eq.(2.5) as:

$$\Delta\tau_{ij} = (t_j^{2} - t_j^{1}) - (t_{j,r}^{2} - t_{j,r}^{1}) + \frac{\partial T_{ij}}{\partial x_j}\delta x_j + \frac{\partial T_{ij}}{\partial y_j}\delta y_j + \frac{\partial T_{ij}}{\partial z_j}\delta z_j + S_i. \tag{2.6}$$

Eq.(2.6) is further simplified by using the origin time differences

$$\Delta\tau_{ij} = \delta t_j - \Delta t_{j,r} + \frac{\partial T_{ij}}{\partial x_j}\delta x_j + \frac{\partial T_{ij}}{\partial y_j}\delta y_j + \frac{\partial T_{ij}}{\partial z_j}\delta z_j + S_i, \tag{2.7}$$

where $\Delta t_{j,r}$ represents the difference of origin times between the two events of the j-th repeating earthquake which are previously obtained from routine hypocenter determination. δt_j represents the origin time difference between the two events of the j-th repeating earthquake. Using eq.(2.7), we relate the arrival time differences of P- and S- waves to the partial derivatives of the travel time in the set of equations:

$$\Delta\tau^P{}_{ij} = \frac{\partial T_{ij}}{\partial x_j}\delta x_j + \frac{\partial T_{ij}}{\partial y_j}\delta y_j + \frac{\partial T_{ij}}{\partial z_j}\delta z_j + \delta t_j - \Delta t_{j,r} + S^P{}_i. \tag{2.8}$$

$$\Delta\tau^S{}_{ij} = \frac{\partial T_{ij}}{\partial x_j}\delta x_j + \frac{\partial T_{ij}}{\partial y_j}\delta y_j + \frac{\partial T_{ij}}{\partial z_j}\delta z_j + \delta t_j - \Delta t_{j,r} + S^S{}_i, \tag{2.9}$$

where $S^P{}_i$ and $S^S{}_i$ represent the station correction factors for P- and S-waves, respectively. Eqs.(2.8) and (2.9) indicate that the arrival time differences of P- and S-waves between the two events are represented as a linear combination of the hypocenter parameters and the station correction factors.

The hypocenter parameters and station correction factors can be determined from eqs.(2.8) and (2.9) using the least squares method. However, our numerical tests indicate significant tradeoffs between he model parameters and we could not determine hypocenter parameters and the station correction factors correctly. In the present study, therefore, we introduce a constraint in the origin time differences:

$$\sum(\delta t_j - \Delta t_{j,r}) = 0 \tag{2.10}$$

Eq.(2.10) can be introduced by assuming that the differences of origin times are randomly distributed.

We solve the inverse problem in the system of eqs.(2.8) and (2.9) subject to the constraint of eq.(2.10) by applying the least square method using singular value decomposition.

2.2. Measurement of arrival time differences of direct P- and S-waves

We measure arrival time differences of direct P- and S-waves between the first and second events of a pair of repeating earthquake by using the cross-spectrum method [e.g., Poupinet et al., 1984]. We set a time window starting 1 s before the arrival of direct P- and S-waves. After applying a 10% cosine taper to both signals, the cross-spectrum is calculated from the spectrum of the signals of the first event, $A_1(f)$, and that of the second event, $A_2(f)$ by:

$$S_{12} = A^*{}_1(f)A_2(f) \tag{2.11}$$

where the asterisk denotes the complex conjugate. The time difference, $\Delta\tau$, between the two highly

similar signals of the first and second events are related to the phase differences $\phi(f)$ estimated from the cross-spectrum by:

$$\phi(f) = 2\pi f \Delta\tau . \tag{2.12}$$

By this procedure, the travel time differences of P- and S-waves between waveforms occurring before and after the Tohoku-Oki earthquake are estimated.

2.3. Data

We use seismic waveform data recorded by the Hi-net seismic network in Japan operated by the National Research Institute for Earth Science and Disaster Prevention (NIED). Each station is equipped with a 3-component short-period velocity sensor with a natural period of 1s. The sensors are installed at the bottom of a borehole at a depth of 100 m or more [Okada et al., 2004].

We select repeating earthquakes occurring before and after the Tohoku-Oki earthquake for the period from 2005 to 2013. We first select candidates of repeating earthquakes that have similar waveforms based on the hypocenter locations routinely determined by Japan Meteorological Agency (JMA). Because a wide area in the NE Japan is expected to change its medium properties, we search large repeating earthquakes with magnitudes ranging from 3.7 to 4.7. Then, we calculate cross-correlation coefficients of waveforms at stations located in NE Japan and select the events that have high waveform similarity with coherence of more than 0.8 for both P- and S-waves at many stations. As a result, we analyze 25 repeating earthquakes occurring at depths from 30 to 60 km. A total of 454 stations located in the area of 137˚ E and 146˚ E in longitude and between 34˚ N and 46˚ N in latitude are used (Figure 2.2 and Table 2.1). Occurrence dates of the first and second events that occur before and after the Tohoku-Oki earthquake, respectively, are also shown in Figure 2.3. The numbers of observed arrival time differences are about 22,700 for both P- and S-waves, and the number of model parameters is 1008.

We calculate partial derivatives of the travel times indicated in eqs.(2.8) and (2.9) from a travel time table of JMA [Ichikawa and Mochizuki, 1971] by applying a cubic spline interpolation to the arrival times of P- or S-waves at the depth and distance of interest.

We cut out seismograms of repeating earthquakes from the origin times of the earthquakes and S-waves from 5 s before the expected arrival times. Then, we measure arrival time differences of P- and S-waves at 1-2 Hz. The arrival time differences of P-waves are measured on the vertical component and those of the S-waves on the E-W component by using the cross-spectrum method with a 5 s time window. Arrival time differences of S-waves in N-S components are almost the same as those of E-W

components. Figures 2.4-2.9 show the observed arrival time differences ($\Delta\tau^{P}_{ij}$, $\Delta\tau^{S}_{ij}$) for the case of events 1 to 6. The plots for all the other 19 repeating earthquakes are shown in the Appendix. In each figure, the left panels show the observed arrival time differences. Positive values represent travel time increase after the Tohoku-Oki earthquake. In most of the cases, P-wave arrival time differences are estimated to be nearly zero and very small (<0.01 s) at most of the stations. Some stations show negative values. On the other hand, S-wave arrival time differences show positive values up to about 0.04 s at the region in the middle of NE Japan (36˚ N-39˚N). In the case of event 1, a wide region west of the large slip area of the Tohoku-Oki earthquake shows an increase in the arrival time differences of S-waves after the Tohoku-Oki earthquake. In the case of event 5, there seem to be some positive offsets in the values of arrival time differences compared with the case of event 1 or the other events. Such offsets mean that the arrival time differences are shifted systematically, which may be caused by differences in hypocenter locations routinely reported in the catalog of the JMA.

2.4. Inversion results for the set of 25 repeating earthquakes

We apply our inversion method to all of the data set of 25 repeating earthquakes. Figure 2.10 shows the estimated station correction factors of P- and S-waves. Station correction factors range mainly between 0.005 and 0.015 s for the P-wave and 0.005 and 0.04 s for the S-wave. Large values up to 0.04 s for S-waves are observed in the region between 37˚ N and 40˚ N in latitude, which spans a very wide zone of approximately 400 km length in the N-S direction. For the P-wave, relatively large values up to 0.01 s are observed in approximately the same area of that for S-wave. These regions are close to the large slip area of the Tohoku-Oki earthquake. Station correction factors mainly display changes in the N-S direction but do not significantly change in the E-W direction. In the figure, we plot the station correction factors with error bars against latitude. In the case of the P-wave, the errors estimated from the model covariance matrix with unitary standard deviation are higher in the south and north ends; up to about 42˚ N in the north and below 37˚ N in the south. The errors for the S-wave in the middle of NE Japan are sufficiently small (less than ~0.005 s) compared to the estimated site correction factors of 0.02-0.04 s.

The estimated hypocenter parameters are summarized in Table 2.2. Location differences (δx_j,δy_j,δz_j) range from 0.0006 to 0.2 km. Origin time differences (δt_j) are estimated to be about 0.005 s in magnitude with a maximum of 0.02 s.

We compare the arrival time differences predicted from the best fit model parameters with the observed arrival time differences in Figures 2.4-2.9 and Appendix. As shown in Figure.2.4, the predicted arrival time differences are well matched with the observed ones for event 1. The arrival time

differences for event 5, which show some offsets possibly originating from errors in hypocenter locations and origin times routinely determined are also well explained by the predictions. The other cases shown in Appendix also indicate good fitnesses between the observations and predictions. These consistencies suggest that our simultaneous inversion works well for retrieving the station correction factors as well as hypocenter parameters.

The stability and accuracy of the inversion method to retrieve the hypocenter parameters are tested by performing a Jackknife test. We apply the inversion 80 times to a set of 10 repeating earthquakes randomly selected from the group of 25 events. Figures 2.11 and 2.12 show examples of the statistical analysis applied to the hypocenters determination for 6 events. The other events are shown in the Appendix section. In Table 2.3, the means and standard deviations estimated from the inversion results for all the 25 repeating earthquakes are shown. For the mean, values up to 0.08 km are obtained for δx_j, and δy_j, and values for δz_j are slightly higher up to 0.2 km. δt_j are within about 0.005 s. With respect to the standard deviation, hypocenter parameters δx_j, δy_j, δz_j, and δt_j for each event are of about 0.01 km, 0.02 km, 0.03 km and 0.001 s, in average, respectively. Estimated parameters from this test are in good agreement with those obtained from the inversion of the set of 25 repeating earthquakes (Table 2.2). Travel time changes predicted from these hypocenter parameters are sufficiently small compared with variations of the station correction factors of S-waves we estimated.

2.5. Temporal changes of station correction factors

We conduct inversions for different sets of repeating earthquakes in order to examine if there exists temporal changes of the station correction factors.

2.5.1. Inversion for repeating earthquakes occurring before the Tohoku-Oki earthquake

We apply our inversion method to the arrival time differences of P- and S- waves for repeating earthquakes both of which occurred before the Tohoku-Oki earthquake. We select the repeating earthquakes occurring for the period from 2006 to 2010 in the same manner described in section 2.3. During this period, no significant large earthquake occurred except the 2008 Iwate-Miyagi Nairiku earthquake (Mw 6.9) that is located in the middle of Tohoku region (the epicenter is located at 39.01˚ N and 140.86˚ E with approximately 10 km depth).

We analyze 15 repeating earthquakes, in which both of pairs occurred before the Tohoku-Oki earthquake. Table 2.4 shows the list of repeating earthquakes we analyzed. The inversion results show that no significant change is detected as can be observed in Figure 2.13. In the case of P-wave, values oscillate between -0.003 and 0.003 s, with large values at some stations located at latitudes higher than

42˚ N and smaller than 37˚ N. Such stations show large errors up to 0.02 s as denoted by the error bars in Figure 2.13. On the other hand, for S-wave, almost all the stations show small errors of less than 0.005 s. The station correction factors, which account for the change in the medium velocity, are near to zero at most of the stations along the entire area of NE Japan.

We further analyze the 15 repeating earthquakes by separating them in two groups according to the spatial position of hypocenters. North group consists of the repeating earthquakes located in the north of NE Japan above 38˚ N in latitude (events 1,7,8,9,10 in Table 2.4) and south group consists of those located below 38˚ N in latitude in the south of NE Japan (events 2-6, and 11-15 in Table 2.4). Figures 2.14 and 2.15 show the epicenters of the repeating earthquakes for each group and the estimated station correction factors for the north and south group, respectively. We obtain station correction factors mainly distributing between -0.005 and 0.005 s for P-wave and between -0.002 s and about 0.002 s for S-wave, for both groups of the north and the south, although the north group shows more dispersion in the station correction factors than the south group. Station correction factors for P-wave are more dispersed in the northern and southern ends of NE Japan and the errors are larger. For the S-waves, almost all the values of station correction factors in central NE Japan are close to zero with small errors of less than 0.005 s. No specific spatial pattern of the station correction factors is recognized when applying the inversion method to these two groups.

These results indicate that no velocity change is observed prior to the occurrence of the Tohoku-Oki earthquake.

2.5.2. Inversion for a set of 3 groups with different temporal distribution

Analyses of repeating earthquakes occurring before the Tohoku-Oki earthquake indicate that no significant change occurred before the Mw9.0 event. Since the second event of repeating earthquakes occurred for about 2 years after the Tohoku-Oki earthquake, the seismic velocity changes must have been generated during that period. In the present section, the whole set of 25 repeating earthquakes are divided into 3 groups according to the temporal occurrence of the second event of each pair in order to examine whether or not there is temporal change in seismic velocity changes (i.e., station correction factors). Group 1 consists of the repeating earthquakes in which the second event occurs temporally close to the occurrence of the Tohoku-Oki earthquake (events 1-16 in Table 2.1 and Figure 2.3). Group 2 corresponds to the repeating earthquakes in which the second event occurs temporally separated from the Tohoku-Oki earthquake (events 9-25 in Table 2.1 and Figure 2.3). Finally, Group 3 takes some events from Group 1 and other events from Group 2 (events 1-8 and 17-25 in Table 2.1 and Figure 2.3).

Inversion results for each of the 3 groups are shown in Figure 2.16. Station correction factors up to

0.01 s for the P-waves and 0.04 s for the S-waves are observed. Large values up to 0.04 s for S-waves are observed in the same region of the results for all the set of 25 repeating earthquakes. Moreover, the zone spanning approximately 400 km length in the N-S direction is observed to be almost identical for all of the 3 groups and the whole set of 25 pairs. Figure 2.17 plots examples of the hypocenter locations estimated from each of the 3 groups in different colors. It is also found that hypocenters are relocated to approximately at the same region for each group.

Although temporal resolutions are not high because several repeating earthquakes are belonging to plural groups, these results suggest that there is no significant temporal changes in station correction factors.

2.6. Inversion results for a set of 2 groups with different locations: north and south

To gain an insight into a possible horizontal and depth extent of the seismic velocity change, we divide the set of repeating earthquakes into two groups according to their hypocenter locations: north and south groups. The north group consists of the repeating earthquakes located in the north of NE Japan above 38° N in latitude (14 events indicated in Table 2.5). On the other hand, repeating earthquakes of the south group are those located between 36° N and 38° N in latitude (11 events indicated in Table 2.6).

After applying the inversion method to each of the 2 groups separately, we obtain station correction factors of about 0.005 s for the P-wave and up to 0.04 s for the S-wave, for both groups of the north and the south. For P-wave, there is no clear spatial pattern in station correction factors for both north and south group (Figure 2.18). For S-wave, we find a specific distribution of high values according to the epicenters of the repeating earthquakes. As shown in Figure 2.18, with respect to the region immediately west from the large slip area of the Tohoku-Oki earthquake, larger values (up to 0.04 s) of the north group are shifted to the south: large values are mostly located between 37° N and 39° N in latitude. For the south group, large values (~0.04 s) are shifted to the north from about 37-38°N and extending up to 40° N in latitude. Large values appear distributed in a north-south elongated zone in the middle of NE Japan.

The hypocenter parameters obtained from the north and south groups are almost in the same range with those calculated from all the 25 events (Tables 2.5 and 2.6). Location differences range mostly from 0.001~0.05 km in δx_j and δy_j, and 0.05~0.1 km in δz_j, and the origin time differences (δt_j) are from 0.001~0.006 s. These findings allow us to infer spatial and depth extension of the anomaly where seismic velocity change occurred.

2.7. Region where seismic velocity is changed

The spatial shift of the station correction factors for S-wave obtained in the previous section strongly suggests that an anomaly where seismic velocity change occurred extends to a certain depth. This is because the direct waves traveling in deep regions appear in a distant area behind a common region.

First, we estimate the horizontal extent of the anomaly. Station correction factors at the stations locating on the anomaly must have large values for both of the north and south groups. Since the errors of station correction factors are about 0.005 s as shown in Figure 2.10 and Table 2.2 (for whole set of 25 repeating earthquakes) and Figure 2.13 (for the repeating earthquakes before the Tohoku-Oki earthquake), we suppose that the anomaly is located at the area with the station correction factor having high values, which is set to be >0.015 s in the present study, for both of the north and south groups. This defines the anomaly shown by the black dashed curve in Figure 2.19. This anomaly is located in the back bone of NE Japan with an N-S direction between about 36.5˚ N and 39˚ N.

Next, we estimate the depth extent of the anomaly. Figure 2.19 shows the station correction factors along the profiles X-X' and Y-Y', which pass almost the center of the high values of station correction factors from the north and south groups of repeating earthquakes, respectively. Amplitude of the station correction factors of S-wave along these profiles are shown in the lower panels in Figure 2.19. It is clearly seen that large values (up to about 0.04 s) are found in a main zone between 150 and 300 km along the profile of the north group. For the profile of the south group, the area where the amplitude of the station correction factors reaches their maximum values is wider. The larger values of about 0.035 s are observed between 200 and 350 km along this profile.

To infer the vertical extent of the anomaly, we calculate the ray paths of S-waves from the hypocenters to stations using travel time tables from JMA. Since plural repeating earthquakes are used for the inversions, we set the hypocenter to be the middle of the repeating earthquakes belonging to each group. We fix the horizontal extent of anomaly as shown in Figure 2.19 and the anomaly vertically extends beneath itself. We change the maximum depth of anomaly from 15 km to 30 km every 5 km (Figure 2.20) and seismic velocity changes from 0.06 % to 0.09 % every 0.01%. We first calculate travel times from the source to the receivers along the profiles when the medium has no velocity change. Then, we calculate travel times by changing the seismic velocity in the anomaly. The seismic rays and the location of the anomaly are illustrated in Figure 2.20. As the depth of the anomaly increases, travel time delays appear farther behind the anomaly. For example, for the depth of anomaly of 30 km, the time delays are observed at up to about 120 km away from the anomaly. Increasing the velocity change of the anomaly increases the amplitude of time delays (Figure 2.20). Velocity changes of 0.09 % introduce time delays of 0.05 s in maximum. This process allows us to estimate the travel

time differences due to the velocity change in the medium defined by the anomaly by comparing the predicted values with the observed station correction factors as shown in Figure 2.21.

In the case of the north group, if an anomaly extends deep in 30 km, travel time delays come to be detected at the receivers beyond 350 km. This does not fit the observed station correction factors. On the other hand, an anomaly with a depth of 20 km or less does not fit the observations. Therefore, vertical extent of the anomaly come to be 25 km. The velocity change is estimated to be about 0.08% from the amplitude of observed station factors. This best model is shown as blue lines in Figure 2.21; the fit between observed (black line) and modeled time differences (blue line) is good for the case of the north group.

By fixing the depth of the anomaly at 25 km we calculate the time differences for the profile Y-Y' (south group). Velocity change is set to be 0.06% to fit the amplitude of station correction factor. Large station correction factors are well reproduced in the northern region behind the anomaly. The lack of similitude between the observed station factors (black line) and modeled one (blue line) found in the southern region may be caused by strong velocity changes and/or complex inhomogeneous changes. We further calculate travel time differences along another profile as shown in Figure 2.21 (profile X-X''). The observed station correction factors and the predicted travel time differences of S-wave are shown with ray paths from the source to stations. By examining different values of velocity changes, we find that the observed values are well explained by a velocity change of 0.08 %.

Our simple model of the anomaly with a constant velocity change and with constant vertical extent may explain overall characteristics of the spatial changes of station correction factors along the profiles. The discrepancies found may be corrected by considering more complex distribution of the anomaly. Also, more data (repeating earthquakes) distributed at different latitudes sampling the medium from different positions may improve the fitting between modeled time differences and observed station correction factors.

Based on these modeling of S-waves travel time differences, we conclude that the anomaly of S-wave velocity change with average amplitude of 0.06-0.08 % extends down to 25 km in the center of NE Japan, immediately west from the large slip area of the Tohoku-Oki earthquake.

2.8. Summary

We developed a new inversion method for simultaneously estimating hypocenter parameters and station correction factors that are related to the seismic velocity changes along the ray path inherent to each station. We applied the method to a set of 25 repeating earthquakes occurring before and after the Tohoku-Oki earthquake, and obtained station correction factors of about 0.005 s for the P-wave and up

to 0.04 s for the S-wave that are observed in a wide area west from the fault zone of the Tohoku-Oki earthquake. Our tests using different sets of repeating earthquakes and a Jackknife test show that the sources are relocated to at almost the same positions. Analyses of another set of 15 repeating earthquakes occurring before the Tohoku-Oki earthquake show no significant velocity change prior to the occurrence of the Tohoku-Oki earthquake.

We further divide the set of repeating earthquakes into the north and south groups, based on the hypocenter locations. The inversion results show interesting spatial shifts of the S-wave station correction factors between the two groups. Assuming that the anomaly generating the travel time differences extends down into the crust, we determined horizontal and vertical extents of the anomaly. The results show that the anomaly is located in the back bone of NE Japan between 36˚N and 39˚N in latitude. The vertical extent of the anomaly is estimated to be 25 km. S-wave velocity decrease in the anomaly is estimated to be about 0.1% (0.06-0.08%).

Table 2.1. Date, latitude, longitude, depth and magnitude for each event of the set of 25 repeating earthquakes used in this study.

Event number and date			Longitude	Latitude	Depth	Mw
No.	Before	After	N (deg)	E (deg)	(km)	
1	19 Nov 2010	24 Oct 2011	142.104	39.634	48.3	4.0
2	30 Nov 2007	10 Sept 2011	140.696	36.472	52.9	4.7
3	19 Nov 2010	26 May 2011	142.104	39.634	48.3	4.0
4	22 Jun 2008	15 Mar 2011	140.948	36.635	49.2	4.2
5	09 Aug 2010	16 Apr 2011	142.107	39.636	47.6	3.9
6	13 Aug 2008	23 Mar 2011	140.681	36.428	52.3	3.8
7	18 Jan 2009	02 Feb 2012	140.572	36.52	56.5	3.9
8	31 Dec 2009	16 Dec 2011	142.207	39.102	43.2	3.8
9	31 Dec 2009	24 Apr 2012	142.207	39.102	43.2	3.8
10	09 Aug 2010	01 May 2012	142.107	39.636	47.6	3.9
11	09 Aug 2010	04 Feb 2012	142.107	39.636	47.6	3.9
12	18 Jan 2009	02 Feb 2012	140.572	36.52	56.5	3.9
13	31 Dec 2009	17 Sep 2012	142.207	39.102	43.2	3.8
14	09 Aug 2010	02 Aug 2012	142.107	39.636	47.6	3.9
15	14 Jul 2009	18 Nov 2012	141.673	38.176	50.6	3.7
16	31 Dec 2009	17 Sept 2012	142.207	39.102	43.2	3.8
17	04 Jan 2009	10 Aug 2012	141.199	37.059	50.1	3.7
18	09 Aug 2010	02 Aug 2012	142.107	39.636	47.6	3.9
19	26 Dec 2004	01 Aug 2012	141.06	37.192	53.7	3.7
20	23 Oct 2006	22 Jul 2012	140.018	36.191	52.2	3.7
21	17 Jun 2009	08 Oct 2013	141.831	39.758	58.1	3.9
22	15 Mar 2009	03 Sept 2013	142.494	40.257	34.1	3.7
23	18 Jan 2009	30 Jul 2013	140.572	36.52	56.5	3.9
24	04 Jan 2009	04 Apr 2013	141.199	37.059	50.1	3.7
25	01 Sep 2009	21 Mar 2013	141.343	37.16	48.3	3.9

Table 2.2. Hypocenter parameters determined from the inversion of all the sets of 25 repeating earthquakes.

Event	δx (km)	δy (km)	δz (km)	δt (s)
1	0.0527	0.0562	-0.0762	-0.0053
2	-0.0174	-0.0006	0.0351	-0.0013
3	0.0648	0.0685	-0.0850	-0.0071
4	0.0075	-0.0164	0.1042	-0.0077
5	0.0234	-0.0230	0.0167	0.0034
6	-0.0388	-0.0190	0.1040	-0.0008
7	0.0023	-0.0072	0.0500	-0.0055
8	0.0124	0.0358	-0.0729	0.0000
9	0.0380	0.0389	-0.0718	-0.0019
10	0.0055	-0.0070	-0.0005	0.0014
11	0.0352	0.0398	-0.0420	-0.0092
12	-0.0007	-0.0236	0.0601	-0.0030
13	0.0411	0.0681	-0.1424	-0.0007
14	0.0366	0.0390	-0.0913	-0.0010
15	-0.0061	0.0207	-0.2399	0.0237
16	0.0266	0.0521	-0.1091	-0.0001
17	0.0186	0.0153	-0.0951	0.0052
18	0.0313	0.0304	-0.1241	0.0072
19	0.0243	0.0720	-0.2112	0.0088
20	0.0043	-0.0018	-0.0320	0.0011
21	0.0026	0.0150	-0.0053	-0.0018
22	0.0505	0.0735	-0.1617	-0.0051
23	-0.0241	-0.0295	0.0494	0.0024
24	0.0056	0.0047	0.0042	-0.0043
25	-0.0894	-0.0956	0.2444	-0.0004

Table 2.3. Mean value μ and standard deviation σ of hypocenter parameters determined from the Jackknife test.

Event	μ[δx] (km)	σ[δx] (km)	μ[δy] (km)	σ[δy] (km)	μ[δz] (km)	σ[δz] (km)	μ[δt] (s)	σ[δt] (s)
1	0.048	0.009	0.053	0.015	-0.068	0.027	-0.0053	0.0016
2	-0.025	0.010	-0.010	0.014	0.058	0.037	-0.0014	0.0015
3	0.061	0.010	0.064	0.018	-0.071	0.033	-0.0077	0.0018
4	0.007	0.009	-0.017	0.011	0.106	0.030	-0.0078	0.0017
5	0.023	0.010	-0.025	0.017	0.024	0.027	0.0030	0.0016
6	-0.038	0.013	-0.017	0.014	0.099	0.035	-0.0011	0.0016
7	0.002	0.009	-0.005	0.013	0.042	0.032	-0.0050	0.0014
8	0.010	0.007	0.036	0.012	-0.070	0.023	-0.0002	0.0016
9	0.034	0.007	0.037	0.010	-0.064	0.018	-0.0022	0.0014
10	0.008	0.009	-0.001	0.015	-0.009	0.027	0.0010	0.0017
11	0.035	0.010	0.037	0.016	-0.037	0.028	-0.0090	0.0014
12	-0.001	0.011	-0.022	0.015	0.055	0.039	-0.0025	0.0016
13	0.038	0.008	0.063	0.011	-0.129	0.018	-0.0011	0.0015
14	0.035	0.010	0.038	0.014	-0.086	0.026	-0.0013	0.0015
15	-0.006	0.009	0.022	0.013	-0.227	0.026	0.0219	0.0010
16	0.026	0.007	0.048	0.011	-0.102	0.018	0.0000	0.0015
17	0.017	0.012	0.015	0.016	-0.094	0.040	0.0052	0.0018
18	0.027	0.010	0.026	0.017	-0.111	0.027	0.0067	0.0016
19	0.027	0.014	0.075	0.018	-0.208	0.039	0.0075	0.0018
20	0.005	0.014	-0.002	0.012	-0.029	0.036	0.0008	0.0018
21	-0.001	0.012	0.013	0.017	0.000	0.033	-0.0018	0.0016
22	0.044	0.009	0.069	0.009	-0.148	0.023	-0.0050	0.0016
23	-0.025	0.009	-0.030	0.011	0.053	0.030	0.0021	0.0017
24	0.003	0.011	0.002	0.015	0.012	0.035	-0.0042	0.0017
25	-0.087	0.011	-0.093	0.015	0.238	0.037	-0.0005	0.0020

Table 2.4. Date, latitude, longitude, depth and magnitude for each repeating earthquake occurring before the Tohoku-Oki earthquake.

Event number and date			Longitude	Latitude	Depth	Mw
No.	Before	After	N (deg)	E (deg)	(km)	
1	15 Dec 2007	09 Aug 2010	142.100	39.636	47.6	3.9
2	16 Oct 2009	26 Oct 2010	140.596	36.457	55.7	3.8
3	25 Sep 2008	26 Oct 2010	142.596	36.457	55.7	3.8
4	09 Jan 2008	26 Oct 2010	140.596	36.457	55.7	3.8
5	18 Jan 2009	07 Mar 2011	140.571	36.523	58.0	3.9
6	18 Jan 2009	15 Nov 2006	140.566	36.523	57.7	3.9
7	09 Aug 2010	15 Dec 2007	142.103	39.637	47.9	3.7
8	17 Dec 2008	25 Nov 2010	142.458	40.119	34.6	4.0
9	29 May 2007	19 Nov 2010	142.104	39.634	48.3	4.0
10	14 May 2008	06 Oct 2010	142.010	41.492	62.6	4.1
11	16 Oct 2009	26 Oct 2010	140.596	36.457	55.7	3.8
12	28 Sep 2008	16 Oct 2010	141.033	36.397	47.2	3.8
13	14 Dec 2006	07 Jul 2010	140.089	36.021	62.5	3.8
14	13 Aug 2008	07 May 2010	140.688	36.430	53.0	3.9
15	22 Sep 2006	14 Jan 2010	141.113	36.375	47.8	3.7

Table 2.5. Hypocenter parameters determined from the inversion of the repeating earthquakes of the north group.

Event	δx (km)	δy (km)	δz (km)	δt (s)
1	0.0360	0.0610	-0.1300	-0.0054
3	-0.0300	-0.0330	0.0990	-0.0100
5	-0.0008	-0.0073	0.0750	0.0010
8	-0.0104	0.0063	-0.0140	-0.0012
9	0.0160	0.0132	-0.0860	-0.0072
10	0.0141	0.0139	-0.0080	-0.0022
11	-0.0094	0.0104	0.0072	-0.0021
13	-0.0060	-0.0630	0.0983	0.0041
14	0.0148	0.0027	0.0401	-0.0050
15	0.0197	0.0033	0.0559	-0.0060
16	0.0227	0.0506	-0.1000	-0.0006
18	0.0078	0.0330	-0.0662	0.0000
22	0.0387	0.0395	-0.3233	0.0236
21	0.0034	0.0310	-0.1010	0.0065

Table 2.6. Hypocenter parameters determined from the inversion of the repeating earthquakes of the south group.

Event	δx(km)	δy (km)	δz (km)	δt (s)
24	-0.0193	-0.0367	0.0575	0.0023
19	0.0013	-0.0220	-0.0040	0.0043
17	-0.0190	-0.0390	0.0650	-0.0011
25	-0.0970	-0.0136	0.0347	-0.0028
12	0.0052	-0.0410	0.0790	-0.0018
4	0.0191	-0.0343	0.1120	-0.0060
2	-0.0260	-0.0240	0.0510	0.0015
7	0.0120	-0.0230	0.0670	-0.0040
23	-0.0200	-0.0480	0.0870	0.0010
6	-0.0280	-0.0310	0.1220	-0.0010
20	-0.0020	-0.0240	0.0220	0.0006

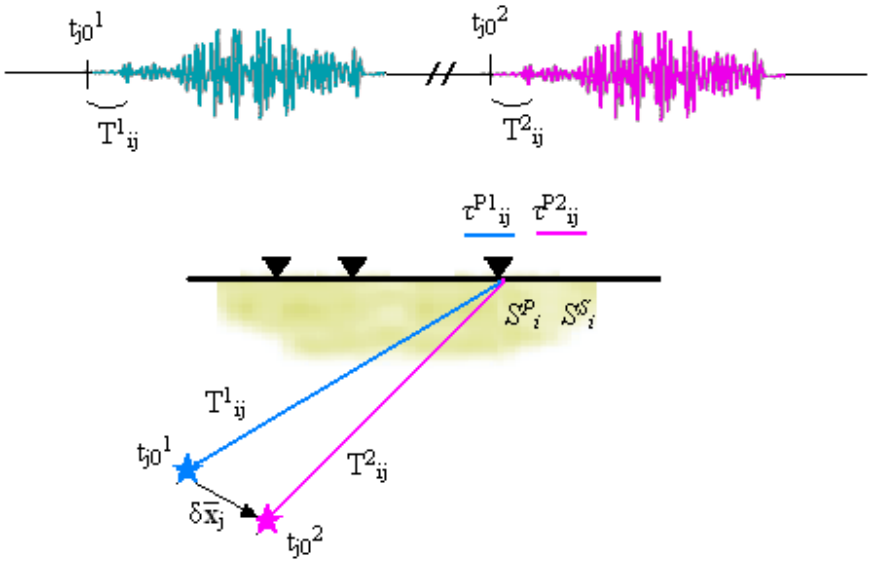

Figure 2.1. Schematic representation of travel times, hypocenters, and station correction factors of a repeating earthquake. Events occurring before and after the main earthquake are denoted by blue and pink colors, respectively. Each waveform is referenced to an origin time, $t_{j0}{}^1$ and $t_{j0}{}^2$, respectively. The measured arrival times (of direct P- or S-waves) $\tau^{P1}{}_{ij}$ and $\tau^{P2}{}_{ij}$ are related to the travel times $T^1{}_{ij}$, $T^2{}_{ij}$ and the station correction factors $S^P{}_i$ and $S^S{}_i$ .Yellow area beneath the stations (inverted triangles) represent the medium that change seismic velocity after the main earthquake.

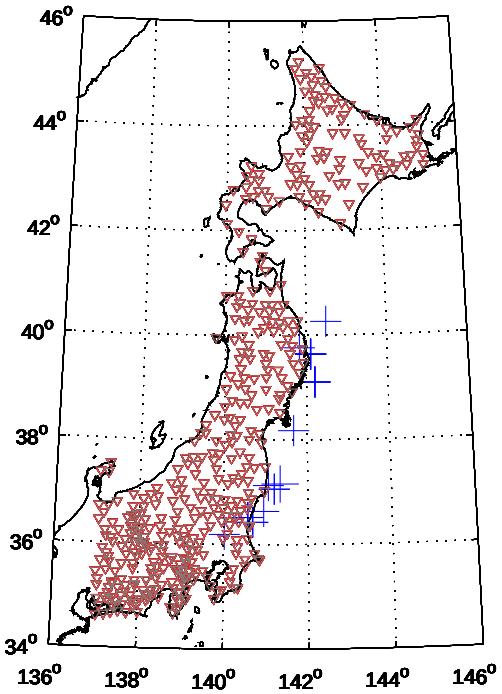

Figure 2.2. Location map of the repeating earthquakes (blue crosses) and Hi-net stations (inverted triangles) used in this study.

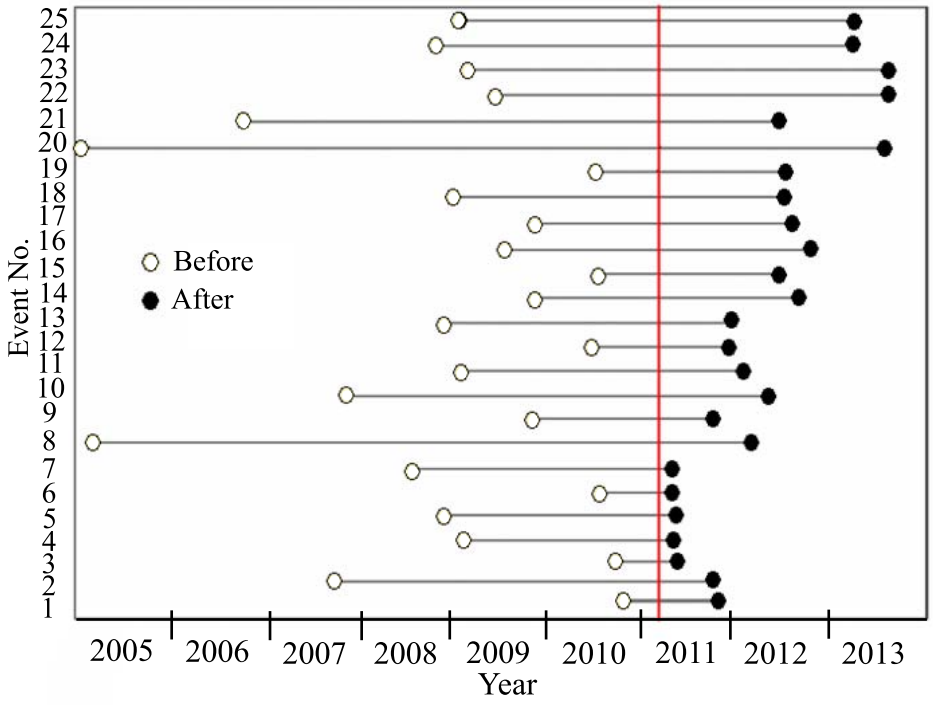

Figure 2.3. Timeline for the set of 25 repeating earthquakes used in this study. The number of the event is indicated in the vertical axis and the horizontal axis represents the year starting from 2005. Vertical red line shows the occurrence of the Tohoku-Oki earthquake on March 2011. Each repeating earthquake consists of two events occurring before (white circles) and after (black circles) the Mw 9.0 event.

(a)

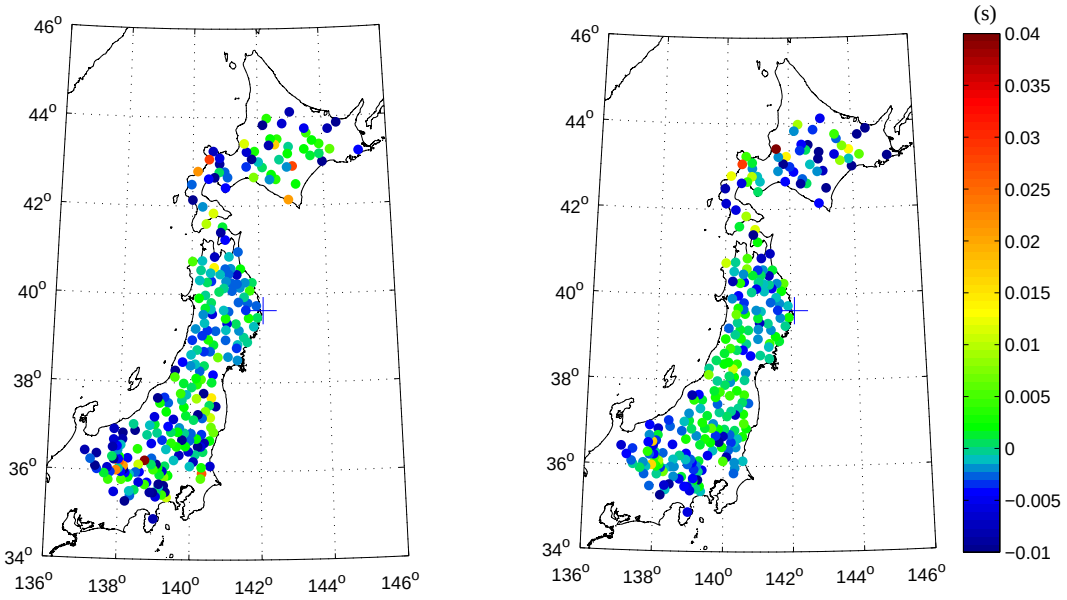

(b)

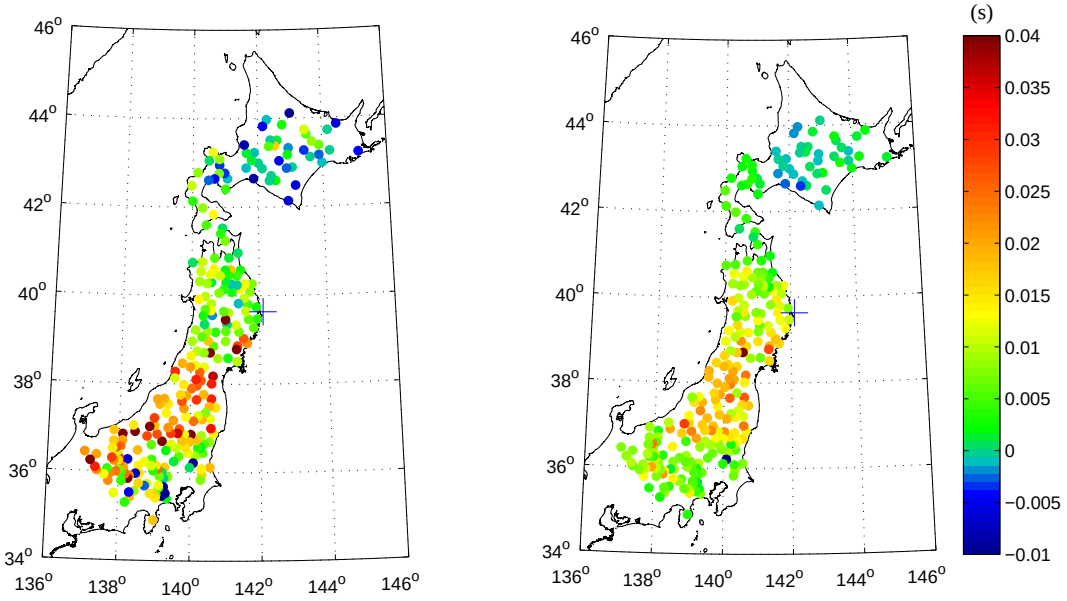

Figure 2.4. Observed (left panels) and predicted arrival time differences (right panels) of (a) P-waves and (b) the S-waves for event 1. Color scale indicates arrival time difference in seconds. Crosses show the location of the repeating earthquake source.

(a)

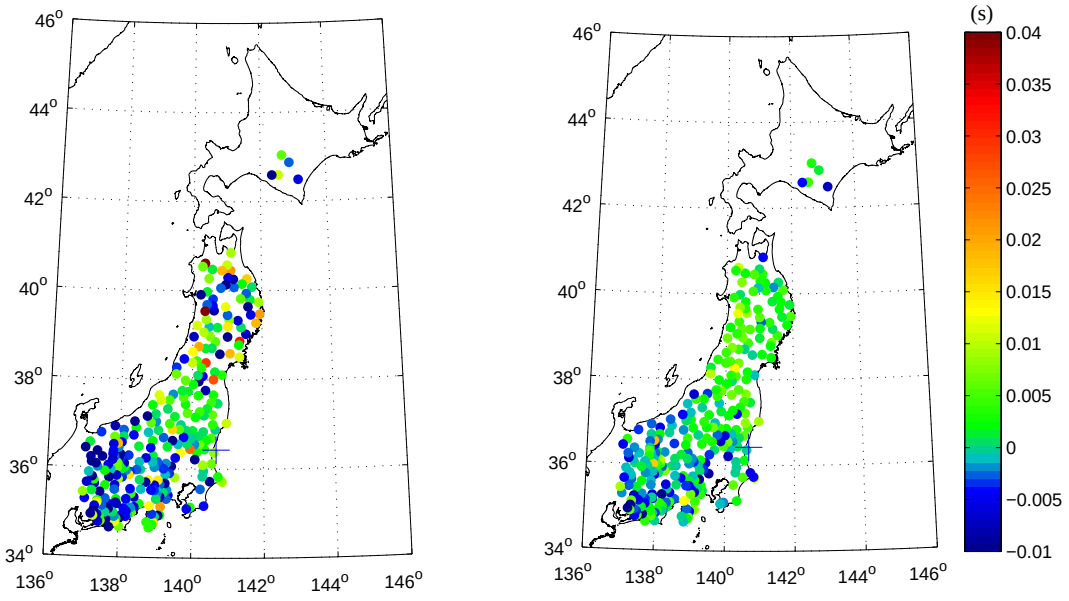

(b)

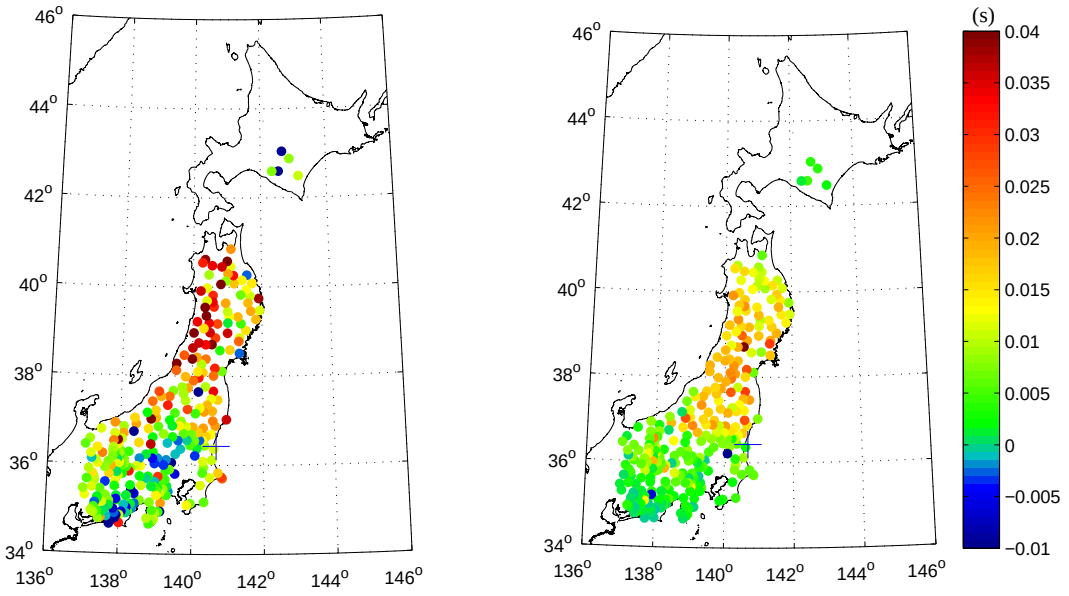

Figure 2.5. Same as Figure 2.4 but for event 2.

(a)

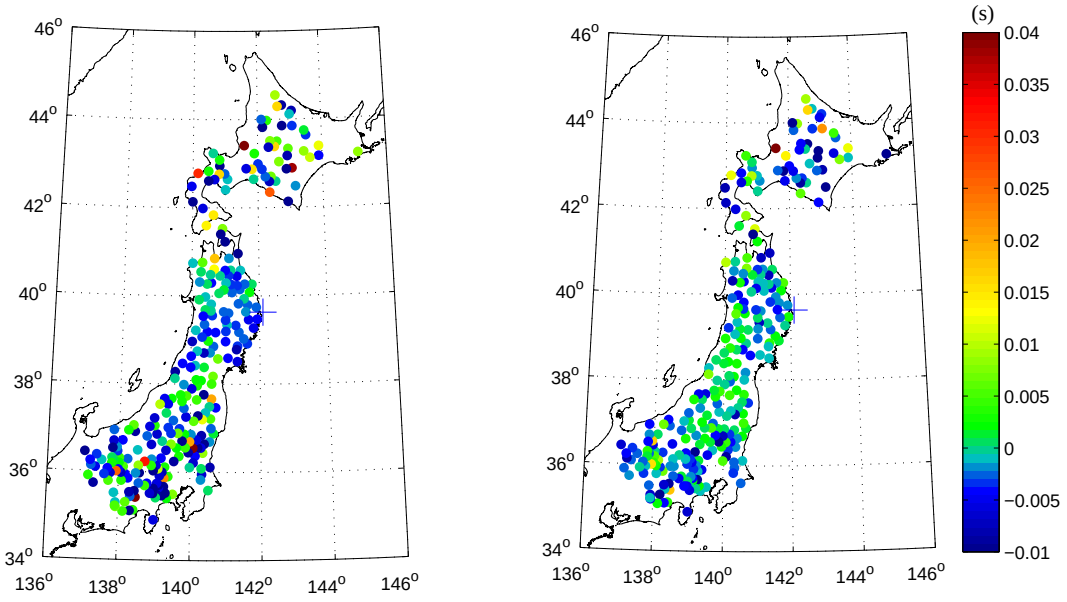

(b)

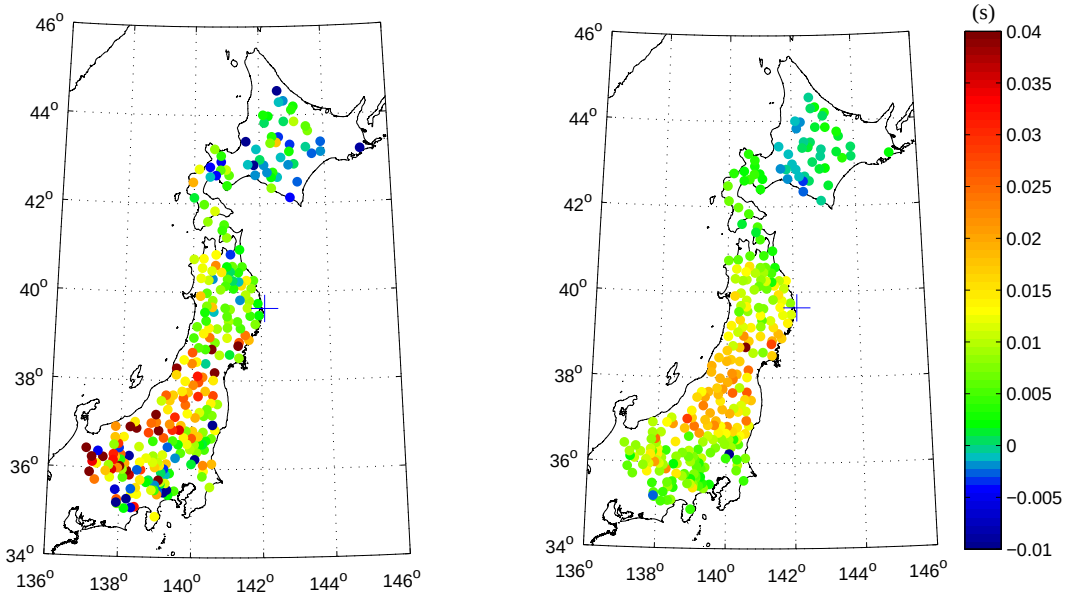

Figure 2.6. Same as Figure 2.4 but for event 3.

(a)

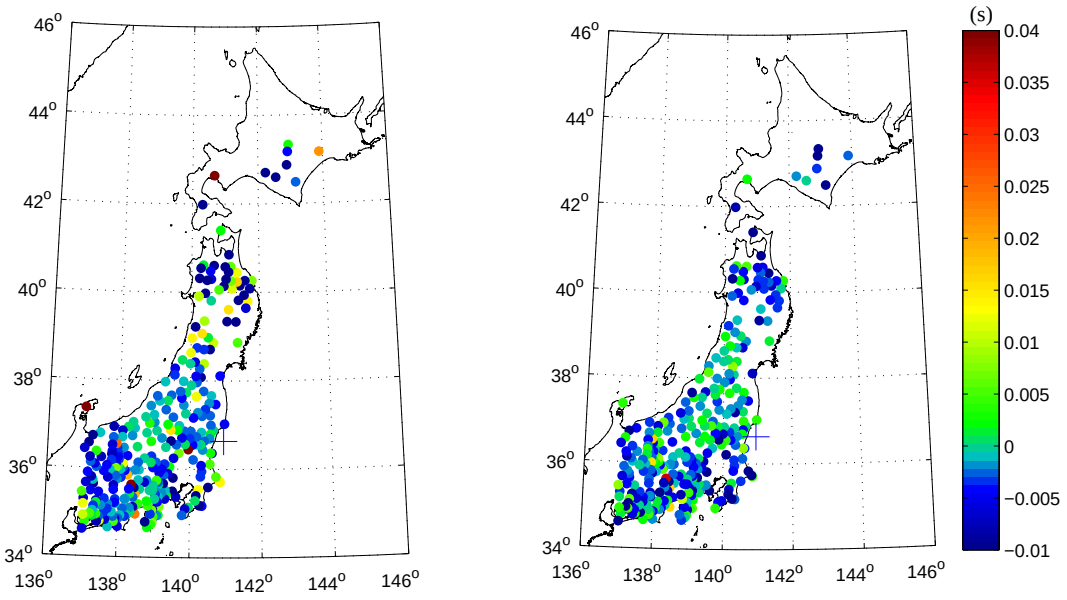

(b)

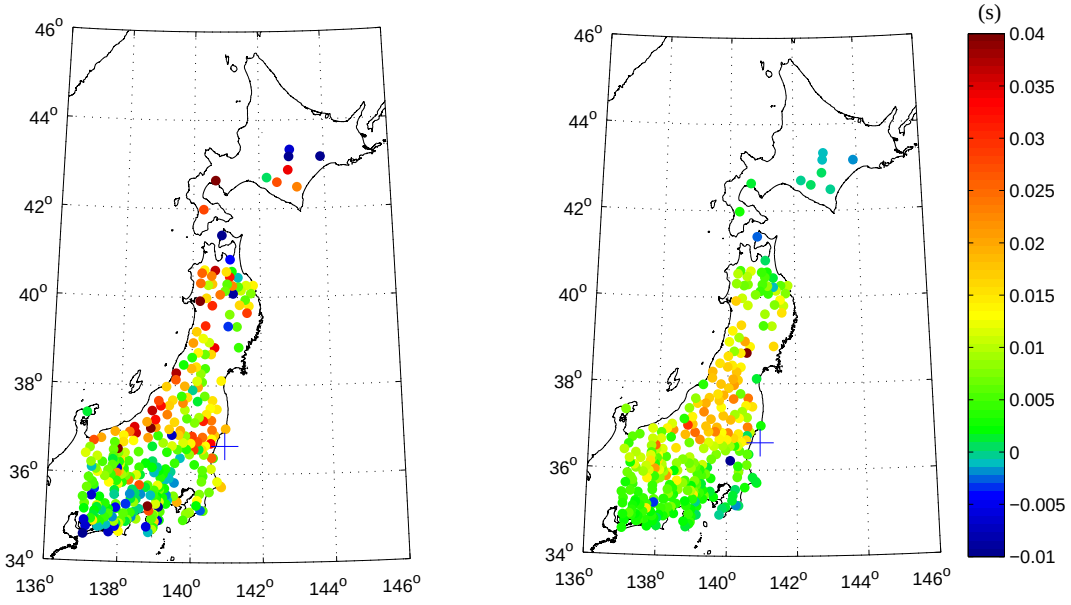

Figure 2.7. Same as Figure 2.4 but for event 4.

(a)

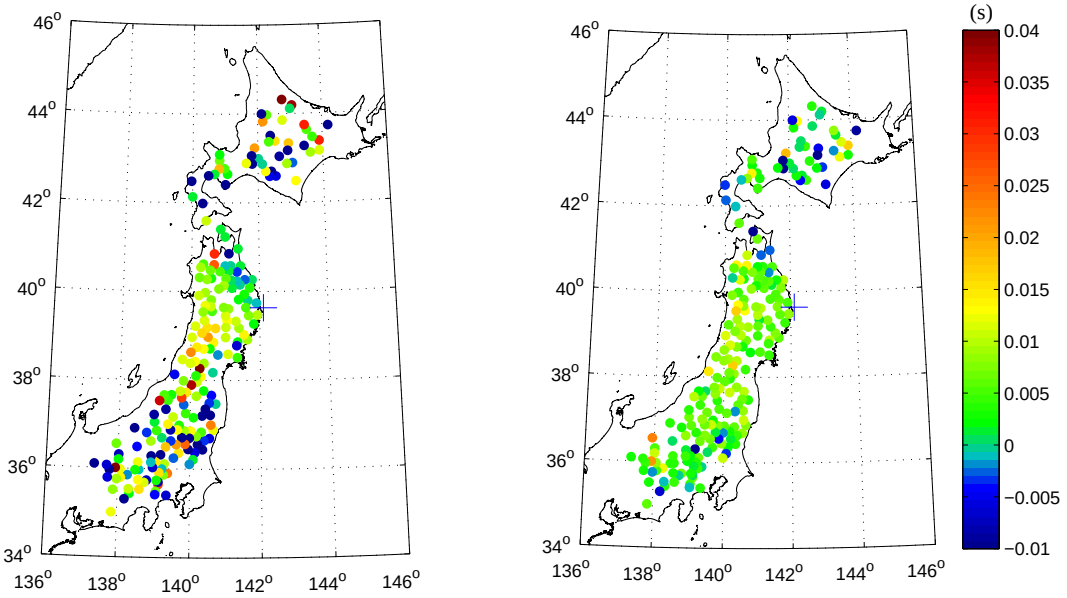

(b)

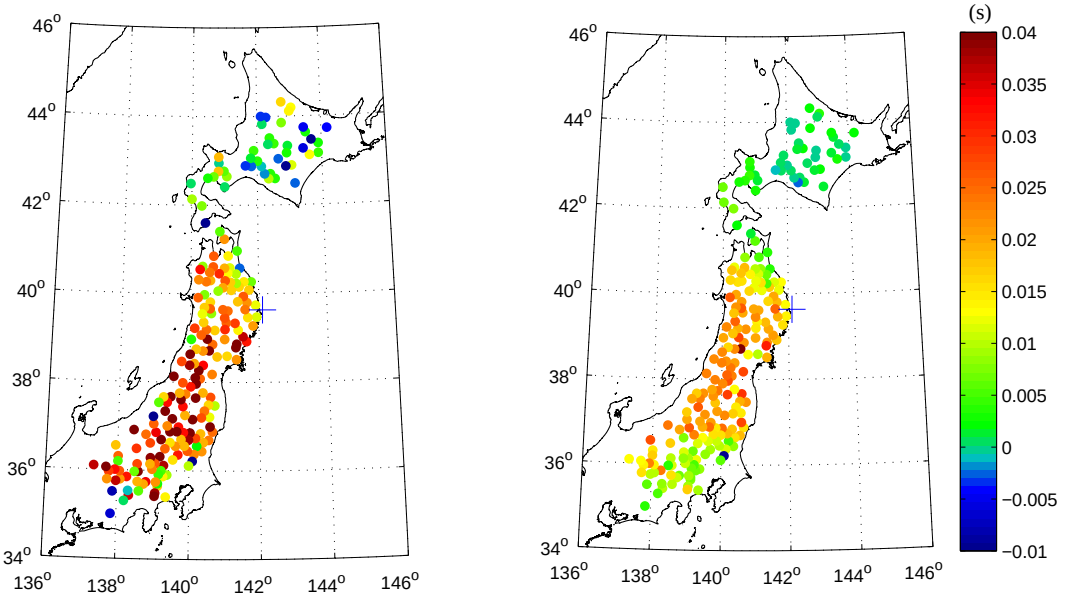

Figure 2.8. Same as Figure 2.4 but for event 5.

(a)

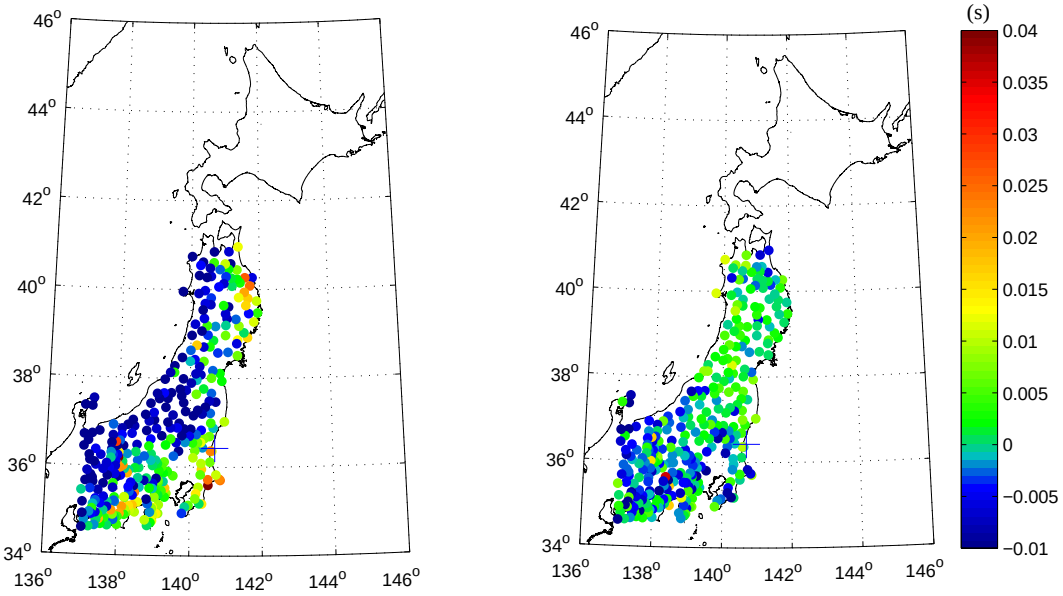

(b)

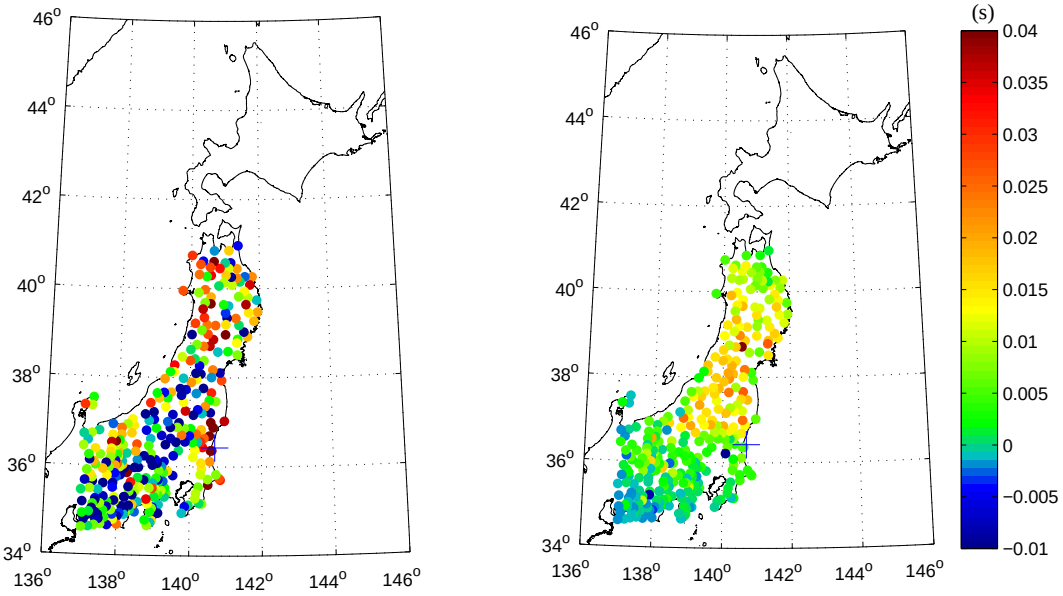

Figure 2.9. Same as Figure 2.4 but for event 6.

(a)

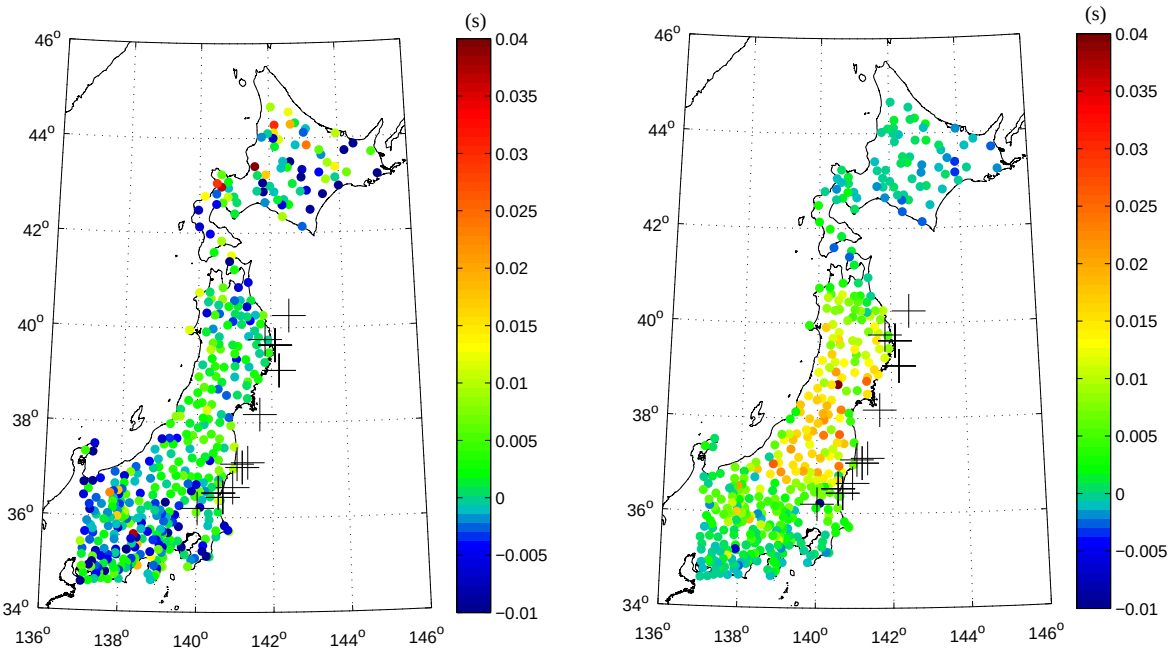

(b)

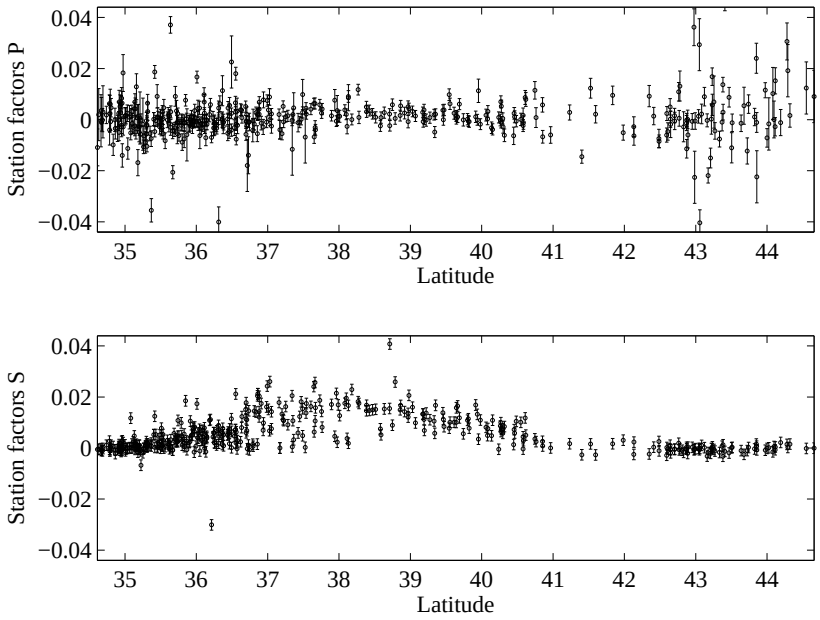

Figure 2.10. (a) Station correction factors estimated from the set of 25 events for P-wave (left) and S-wave (right). Color scale shows time difference in seconds and black crosses shows the locations of repeating earthquakes. (b) Plot of the station correction factors vs. latitude for the P- and S-waves with error bars.

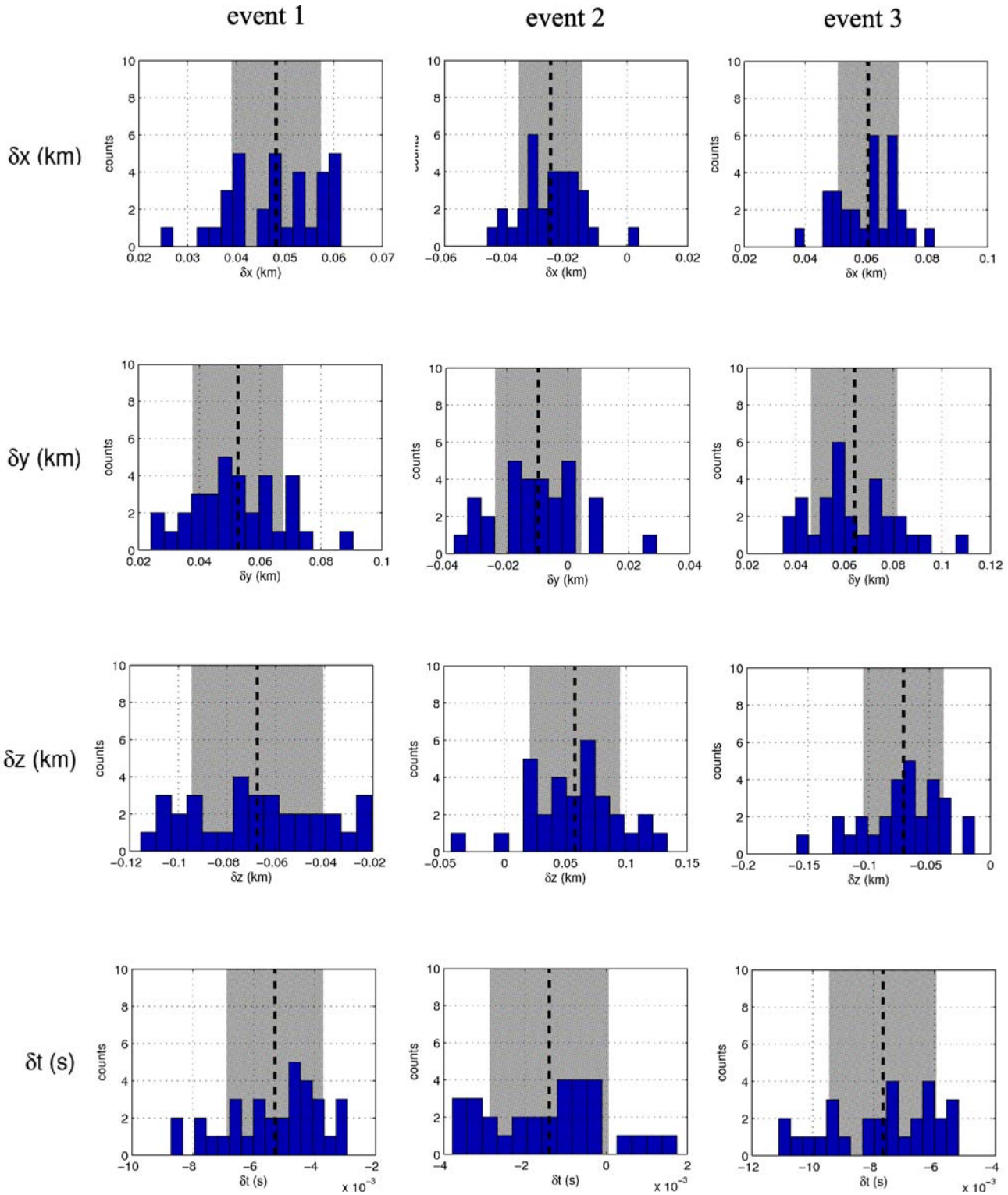

Figure 2.11. Histograms of hypocenter parameters estimated from the Jackknife test applied to a set of 10 repeating earthquakes selected randomly from the set of all 25 repeating earthquakes. Panels in each row correspond to the four hypocenter parameters δx_j, δy_j, δz_j, and δt_j, respectively. Dashed lines indicate the mean and shaded zone the standard deviation. Figure shows the case of events 1, 2, and 3.

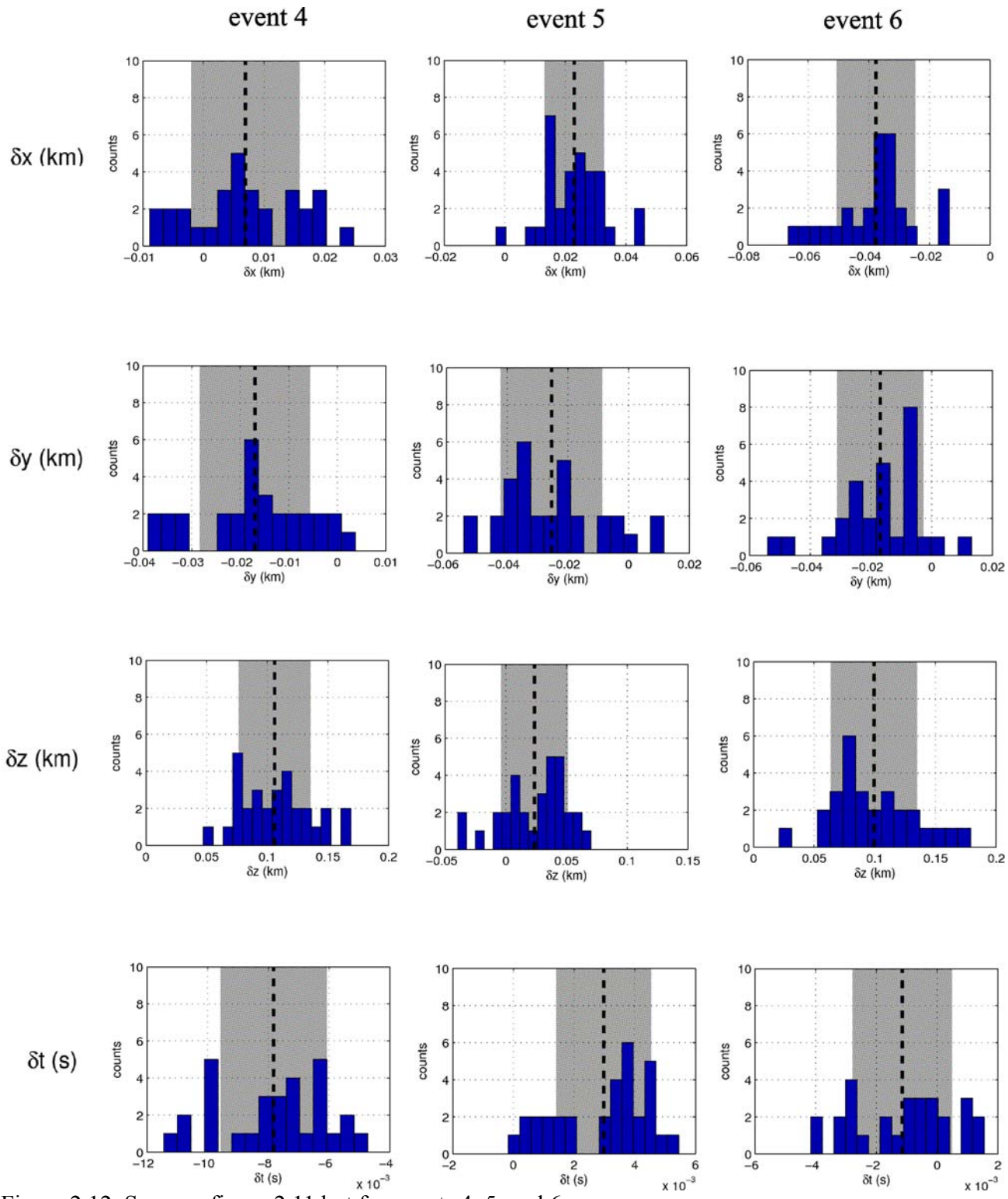

Figure 2.12. Same as figure 2.11 but for events 4, 5, and 6.

(a)

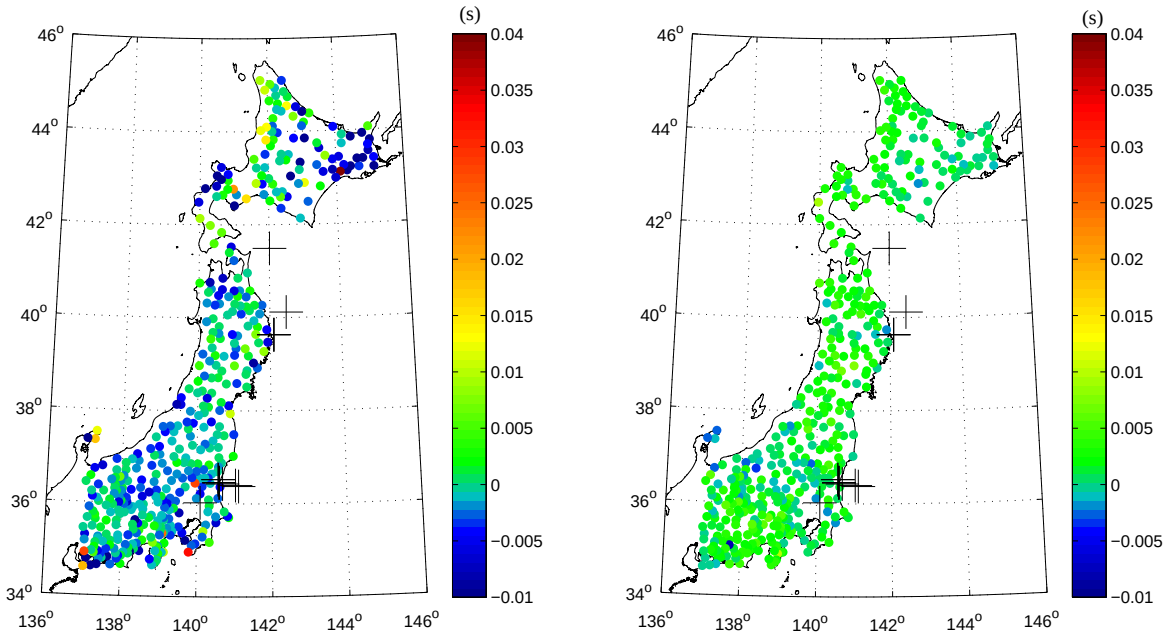

(b)

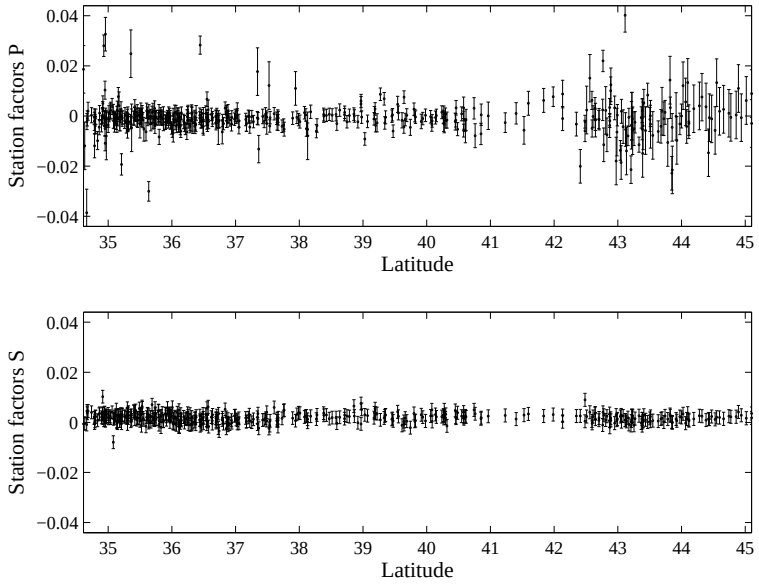

Figure 2.13. (a) Station correction factors estimated from the set of 15 events occurring before the Tohoku-Oki earthquake for P-wave (left) and S-wave (right). Color scale shows time difference in seconds and black crosses shows the locations of repeating earthquakes. (b) Plot of the station correction factors vs. latitude for the P- and S-waves with error bars.

(a)

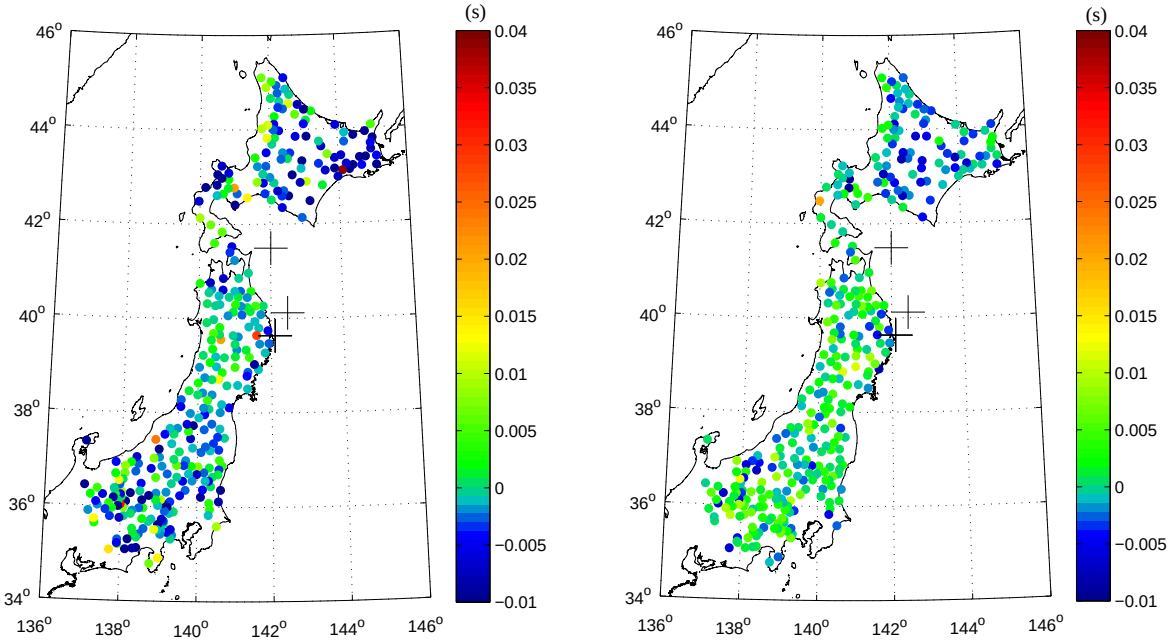

(b)

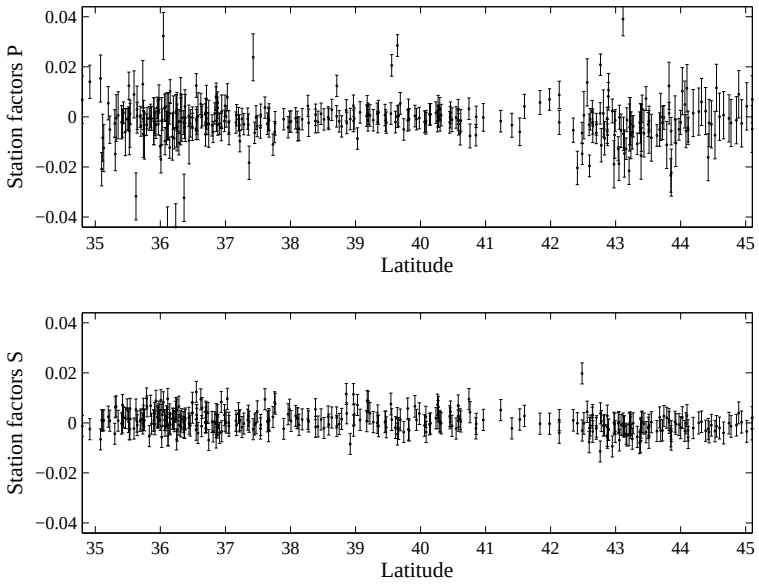

Figure 2.14. (a) Station correction factors estimated from the north group of the set of 15 events occurring before the Tohoku-Oki earthquake for P-wave (left) and S-wave (right). Color scale shows time difference in seconds and black crosses shows the locations of repeating earthquakes. (b) Plot of the station correction factors vs. latitude for the P- and S-waves with error bars.

(a)

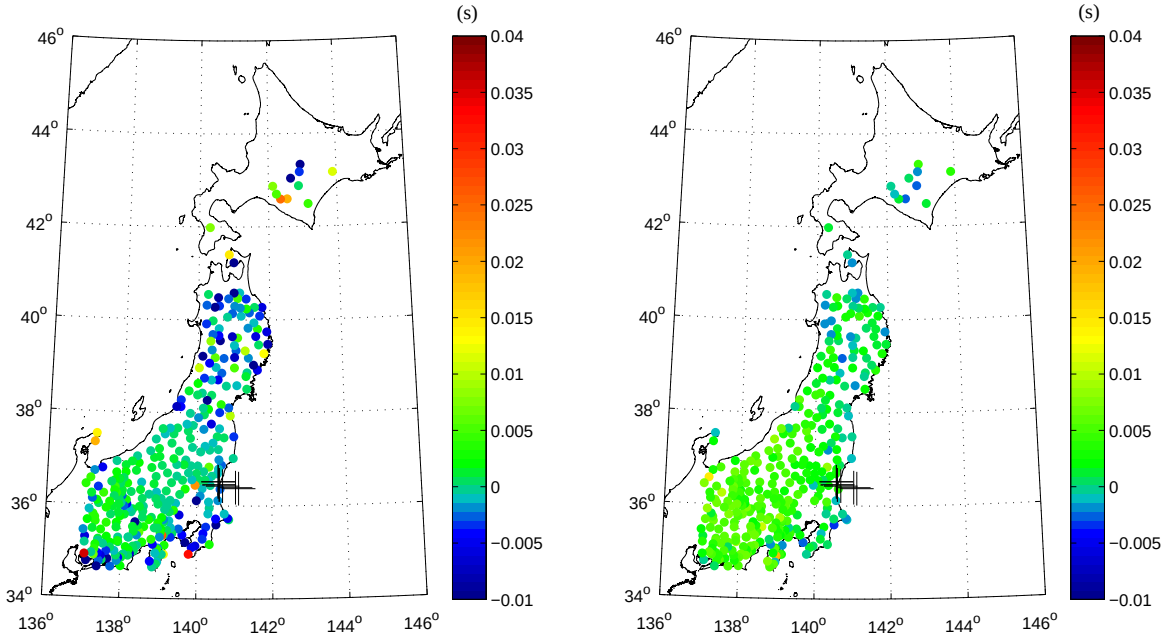

(b)

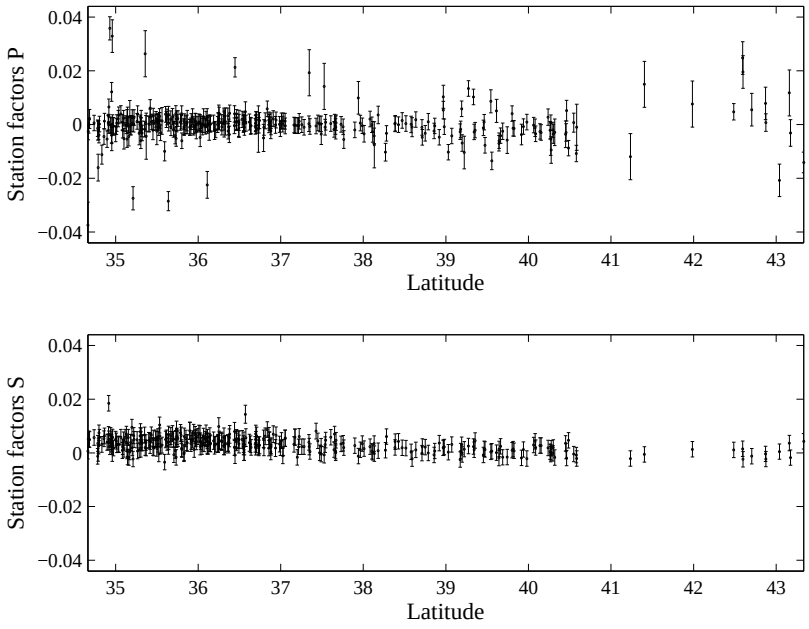

Figure 2.15. (a) Station correction factors estimated from the south group of the set of 15 events occurring before the Tohoku-Oki earthquake for P-wave (left) and S-wave (right). Color scale shows time difference in seconds and black crosses shows the locations of repeating earthquakes. (b) Plot of the station correction factors vs. latitude for the P- and S-waves with error bars.

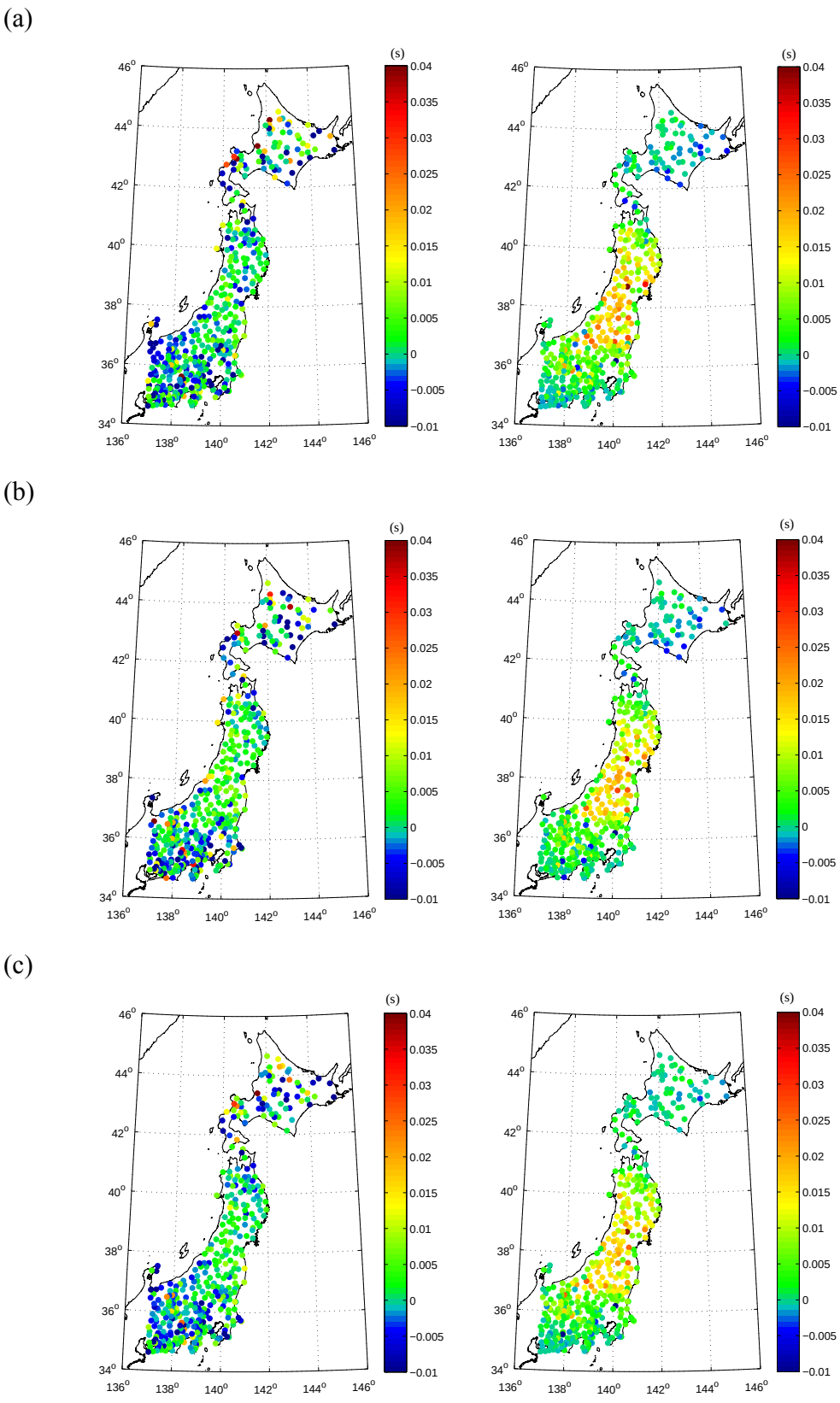

Figure 2.16. Station correction factors obtained from the inversion of the 3 groups for P-wave (left) and S-wave (right). Groups 1, 2 and 3 are shown in (a), (b) and (c), respectively.

(a)

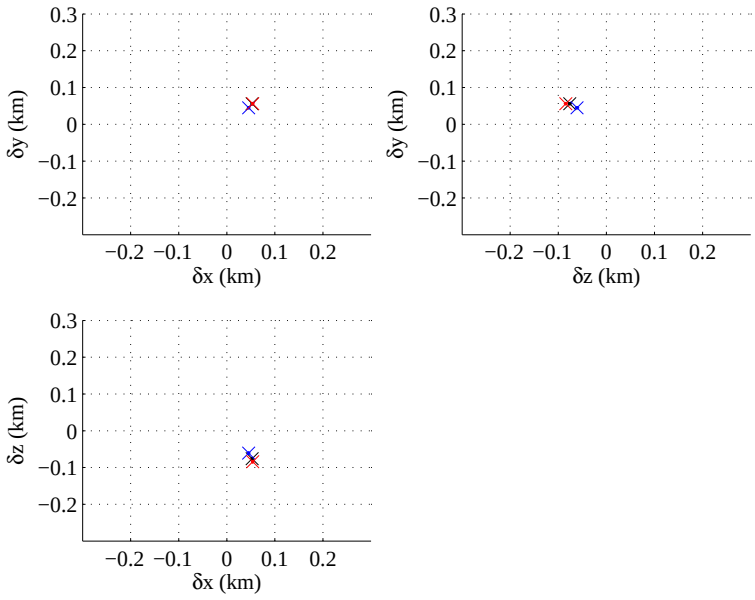

(b)

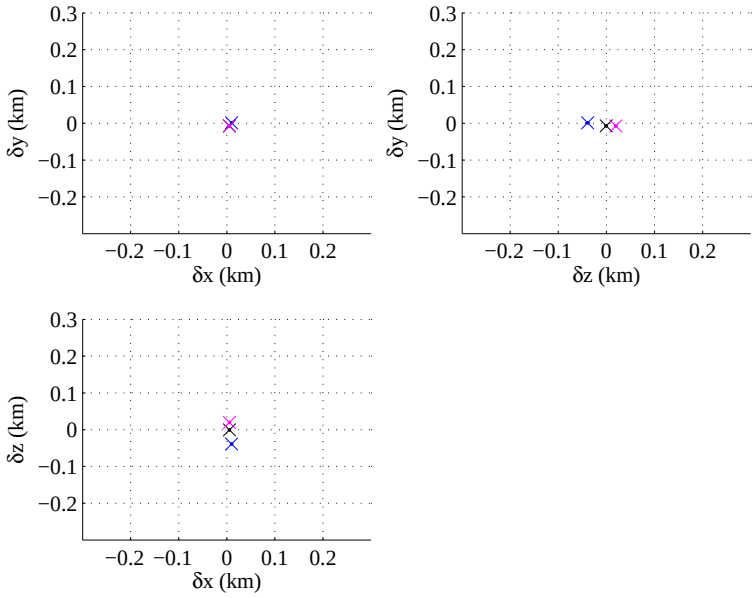

Figure 2.17. Hypocenter parameters estimated after the inversion for the set of three groups and the set of all the 25 repeating earthquakes. The results for events 1 (a) and 10 (b) are shown. Colors represent the results for each of the groups of 1 (blue), 2 (red), 3 (pink) and the set of all 25 repeating earthquakes (black).

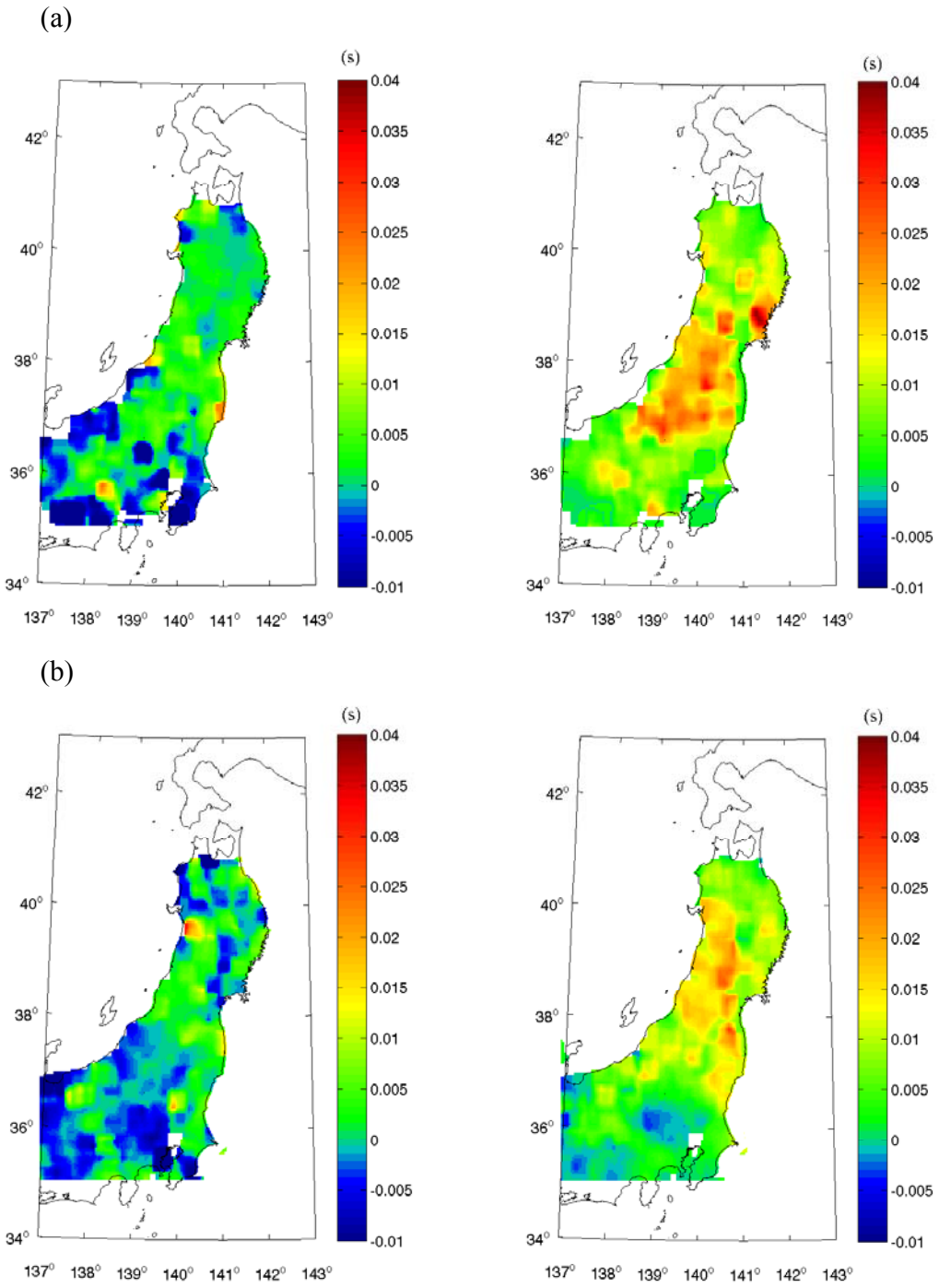

Figure 2.18. Station correction factors estimated from the set of repeating earthquakes occurring in the north (a) and south (b). Left and right panels show results for P- and S-waves, respectively. Color scales indicate station correction factors in seconds.

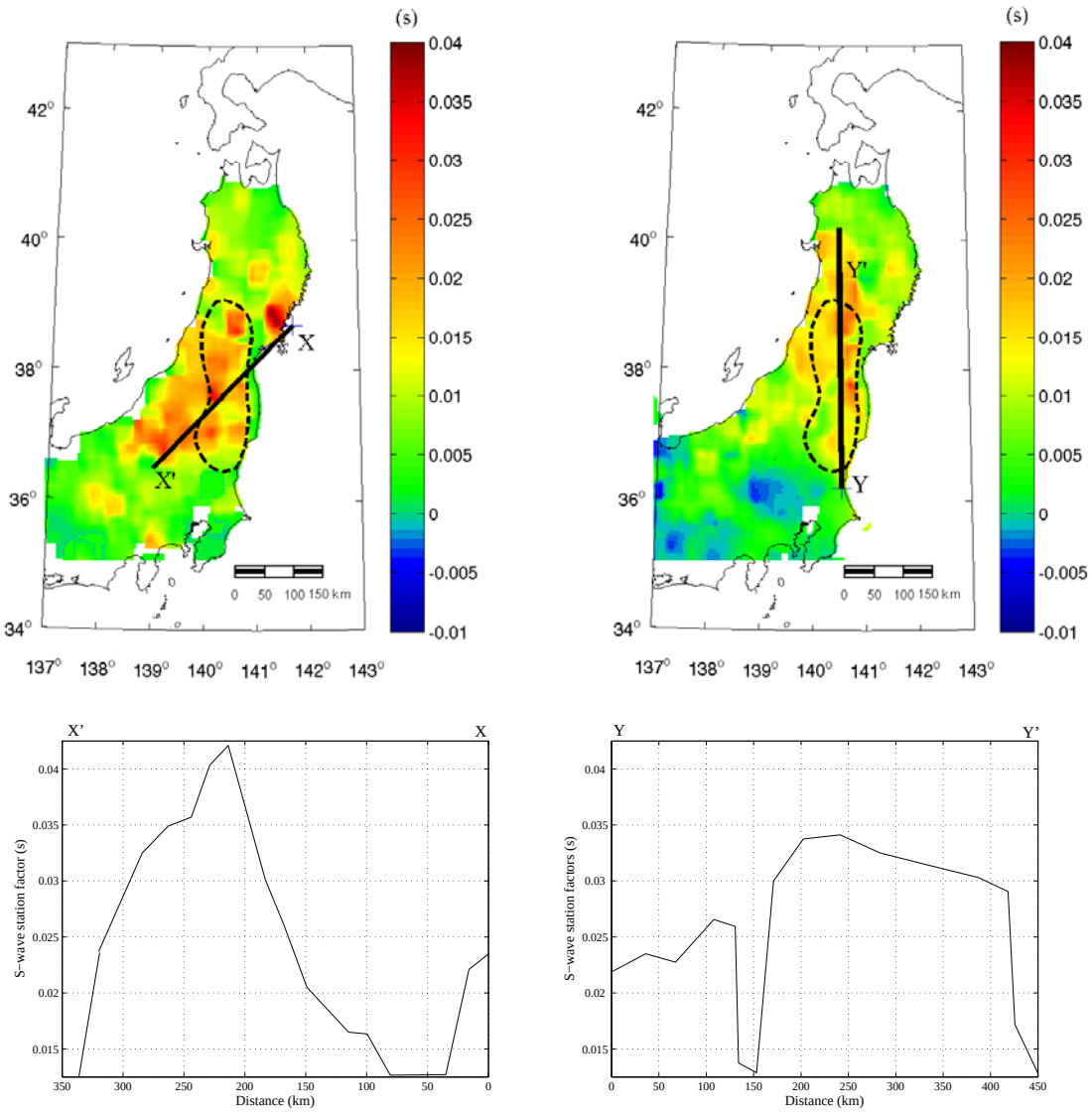

Figure 2.19. S-wave station correction factors along the X-X' and Y-Y' profiles (black lines). The estimated anomaly of velocity change is indicated by black dashed curve in the upper panels. Lower panels show the observed S-wave station correction factors along the profiles.

(a)

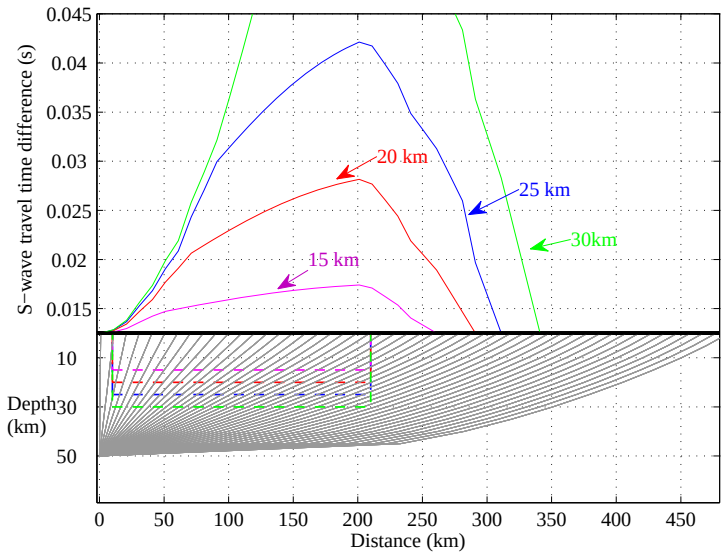

(b)

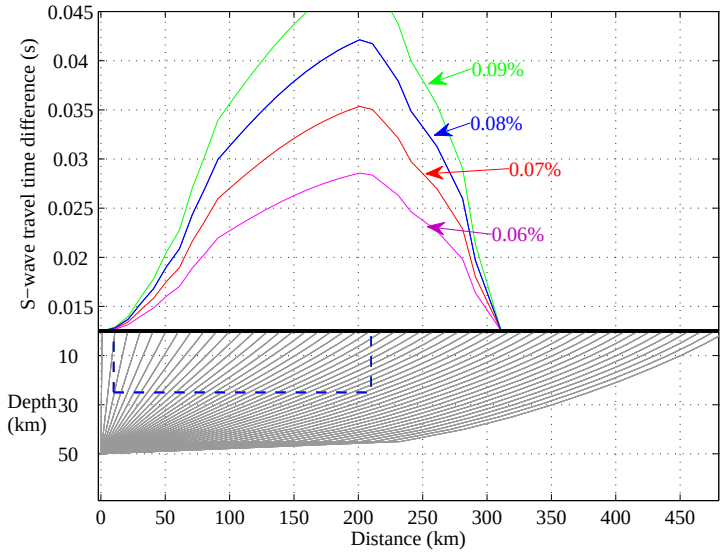

Figure 2.20. Predicted travel time differences for different combinations of depth (a) and velocity change (b) of the anomaly. Each solid color line corresponds to time differences in seconds. Dashed lines in the lower part indicate the location of the anomaly. Direct S-wave rays are shown by gray lines.

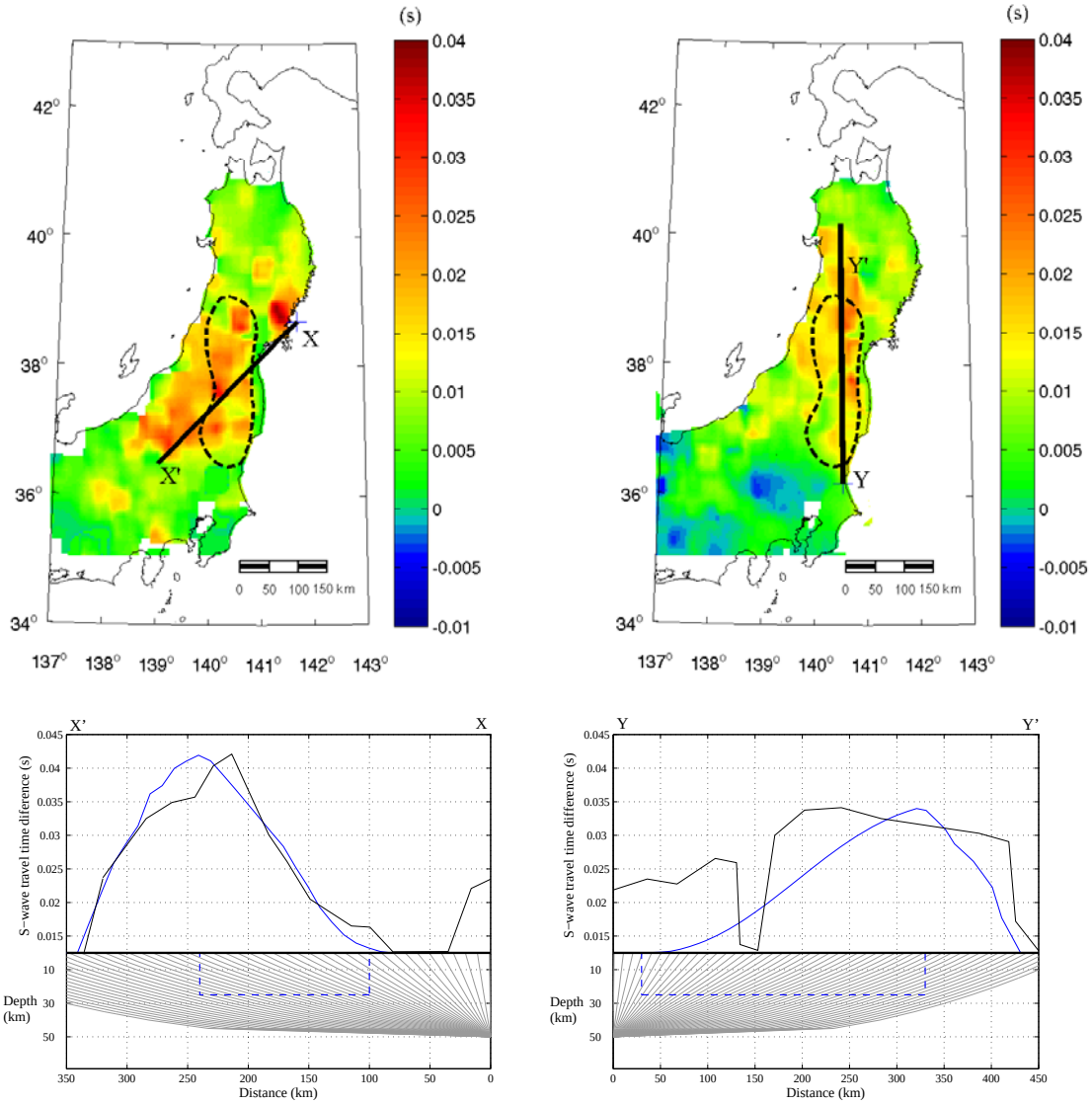

Figure 2.21. S-wave station correction factors along the X-X' and Y-Y' profiles (black lines). The estimated anomaly of velocity change is indicated by black dashed curve in the upper panels. Blue crosses indicate the location of hypocenters sources for each group. Lower panels show the observed S-wave station correction factors along the profiles (black lines) and the best model (blue lines). North group (left) and south group (right) are plotted in the lower panels with ray paths.

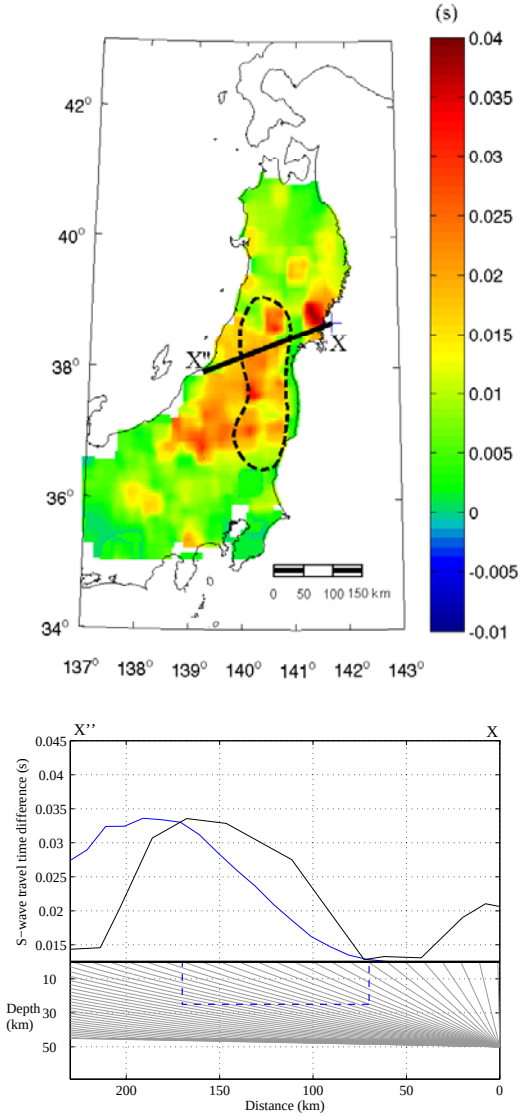

Figure 2.21 (continued). S-wave station correction factors along the X-X'' profile (black line). The estimated anomaly of velocity change is indicated by black dashed curve in the upper panel. Blue cross indicate the location of hypocenter source. Lower panel shows the observed S-wave station correction factor along the profile (black line) and the best model (blue line).

3. Analyses of direct body waves and coda waves of repeating earthquakes recorded by KiK-net network

In the previous section, we estimated a velocity change of about 0.1% extending down to 25 km in the middle of NE Japan, immediately west from the main fault of the Tohoku-Oki earthquake. On the other hand, S-waves propagating between borehole and ground surface that are retrieved from cross-correlation analyses indicate large seismic velocity reductions up to 5-10 % [Nakata and Snieder, 2012; Okada and Takagi, 2013]. Previous studies using Rayleigh waves retrieved from ambient noises [Minato et al., 2012; Brenguier et al., 2014] and S-coda waves at 1-2 Hz indicate different amount of velocity changes. It is not clear how these previous studies are linked to our results, because the amount of velocity changes are very different and spatial distributions of anomaly are not matched in both horizontal and vertical directions. These differences should be carefully discussed by examining the properties of seismic waves we analyzed and those used in the previous studies.

In order to understand where and how the seismic waves analyzed in the previous studies as well as the present study propagate, we simultaneously analyze seismograms recorded on the ground surface and at the bottom of boreholes of KiK-net seismic stations. By measuring arrival time differences of body waves from the repeating earthquakes recorded by the two sensors located at the borehole and ground surface, we examine the regions where the seismic waves sample. We also measure seismic velocity changes from S-coda analyses of KiK-net seismic data.

3.1. Data

We use acceleration data recorded by the KiK-net seismic network. The sensors of KiK-net network are installed at the bottom of a borehole and ground surface which allows us to compare waveforms recorded by this vertical array. Since the waveforms given by this seismic network are triggered records of strong motion seismometers, the number of available seismograms is smaller compared to those analyzed in the previous section from Hi-net seismic network.

A set of 6 repeating earthquakes with magnitudes ranging between 3.9 and 4.0 and depths from 48 km to 58 km are used (Table 3.1). Figure 3.1 shows the location of repeating earthquakes and KiK-net stations used in this study. Figure 3.2 shows EW-component recorded at the borehole and the ground surface by stations of KiK-net network. Waveforms recorded at borehole and ground surface before the Tohoku-Oki earthquake look very similar to those after the earthquake at this frequency band (1-2 Hz). Figure 3.1 shows the waveforms of event 1, and the other events are plotted in the Appendix.

3.2. Arrival time differences of direct P- and S-waves

We measure arrival time differences, $\Delta\tau$, by applying the cross-spectrum method described in section 2.2 to seismograms recorded at boreholes and ground surface. Arrival time differences of P- and S-waves are estimated at each station for the 6 pairs of repeating earthquakes, and then the origin time is corrected by using the inversion results obtained in the previous chapter to estimate travel time difference before and after the Tohoku-Oki earthquake. Then we calculate averages of arrival time differences for the borehole and ground surface sensors at each station. When only one data is available at a station, we do not use the data of the station.

Travel time differences are shown in Figure 3.3. Travel time differences of P-wave are distributed in the range between -0.01 and 0.01 s. Travel time differences in the south (e.g., Ibaraki Prefecture) tend to be slightly larger those in the north (e.g., Iwate Prefecture). Relatively high values of up to 0.03 s are observed at some stations in the south of NE Japan (Fukushima Prefecture). On the other hand, S-waves show values ranging mainly from 0.01 to 0.04 s. Large travel time differences of up to 0.04 s are observed at some stations in the coast of Iwate and Miyagi Prefectures. In the southern area (Fukushima and Ibaraki Prefectures), large travel time differences of about 0.02 s - 0.04 s are widely observed for S-waves. It is recognized that the spatial distributions of travel time differences obtained from the borehole and ground surface sensors are similar to each other.

3.3. Seismic velocity changes estimated from S-coda

Seismic velocity changes are estimated by measuring the phase shift between the two waveforms using the moving window technique presented by Poupinet et al. (1984). When the seismic velocity of the medium decreases (or increases) uniformly in space, S-coda are delayed (or advanced) linearly with lapse time. This is because coda waves travel larger distance, being proportional to the lapse time. Hence, seismic velocity change is estimated from a relation $\Delta v/v=-\Delta t/t$, where t is the lapse time from the origin time. We may estimate the velocity changes by fitting a straight line to the observed Δt throughout the S-coda.

We align the two seismograms of the first and second events to the P-wave arrivals. We set a 3.5 s time window every 1.5 s from the arrivals of direct S-waves for 35 s throughout the S-coda. At each time window, the coherence and phase differences are estimated from cross-spectrum of the S-coda of the first and second events. We estimate time differences, Δt, from the phase differences between the first and second events. The data with a coherence higher than 0.8 is used in the following analyses.

Examples of the moving window cross-spectrum analysis are shown in Figures 3.4 and 3.5. These figures show the waveforms recorded at stations IBRH19 and TCGH09 of KiK-net seismic network for event 2. Seismograms recorded before the Tohoku-Oki earthquake are very similar to those after the earthquake. At station IBRH19 (Figure 3.4), the coherence are close to 1 for about 40 s from the beginning of the S-coda. Station TCGH09 shows high coherence of more than 0.8 for the first 20 s and decreases gradually to about 0.5 at later times. Figure 3.5 shows the waveforms recorded after the Tohoku-Oki earthquake are gradually delayed with respect to the waveform recorded before the Mw 9.0 event as the lapse time increases. We calculate time difference for a time window of 3 s every 1.5 s, and fit a straight line to the time difference with coherence higher than 0.8 against lapse time. As a result, for example, at station IBRH19, small velocity changes of about 0.026% and 0.0058 % are detected at the borehole and ground surface, respectively. At station TCGH09, larger velocity changes of 0.14% and 0.13% are estimated for the records of the borehole and ground surface.

We measure velocity changes from S-coda recorded for each of the 6 sets of repeating earthquakes. S-wave velocity changes are estimated separately for the records of the borehole and ground surface. We estimate the averages of velocity change when two or more data are available. The estimated velocity changes are mainly ranging from 0.01 to 0.2 % (Figure 3.6). In the north of NE Japan, small velocity changes of about 0-0.05% are observed in the northern and central area (Aomori Prefecture and northern area of Iwate Prefecture). Higher values of up to 0.2% are recognized in the southern inland of Iwate Prefecture and along the coast. In the south (Fukushima and Ibaraki Prefectures), large values of velocity decreases up to 0.2% are observed at stations located in the southern area of Kanto-region (around 140˚E in longitude). It is noted that such spatial distributions of velocity changes are almost the same for the borehole and ground surface.

3.4. Comparison of the results obtained from ground surface and borehole data

Figure 3.7 compares the travel time differences of P- and S-wave. Most of travel time differences of P-wave range from -0.02 s to 0.018 s while those of S-wave from -0.01 s to about 0.04 s. As travel time difference of P-wave increases, that of S-wave roughly increases. Also, travel time difference of S-waves is about 0.02-0.03 s larger than those for the P-wave.

As shown in Figure 3.8 for the P- and S-wave, it is evident that the results obtained from the borehole sensor and those from the ground surface sensor are very similar. Most of the data show almost same values as the correlation coefficient is estimated to be 0.87. This result suggests that the seismic waves recorded at boreholes and on the ground surface we analyzed mostly propagate in the same regions.

We use not only the onsets of P- and S-waves but also the coda waves following the initial onsets to measure travel time differences, because cross-spectrum analyses need to set a time window for the target waves. Seismic waves captured within a short time window consist of the direct and scattered, reflected, and/or refracted waves that propagate in the medium close to the ray paths from the source to station. Hence, we may discuss the regions where the seismic waves we analyzed sample. For example, if the seismic waves we analyzed propagate mainly in shallow medium where large seismic velocity reductions are observed [e.g., Nakata and Snieder, 2011], larger travel time differences could be estimated for the case using a long time window. Figures 3.9 and 3.10 compare the results obtained from a time window of 5 s length with those from a time window of 2.5 s. Figures 3.9 and 3.10 indicate the results for the borehole sensor and the ground surface, respectively. High values of correlation coefficient of about 0.9 are observed for the borehole results and of near to 0.87 for the ground surface case. These results show no significant differences between the results from the borehole and ground surface for both P- and S-waves. We interpret that seismic waves coming into the time window we used are not dominated by reverberation at subsurface but includes the waves sampling deeper region beneath the stations.

Figure 3.11 compares seismic velocity changes estimated from S-coda recorded by the borehole sensors with those recorded by the ground surface ones. Although the data are scattered, the velocity changes estimated from borehole sensors are positively correlated with those from ground surface. This represents that S-coda recorded on the ground surface sample the same region where the S-coda at depth of about 100 m. Hence we infer that S-coda recorded at borehole and ground surface propagates in the same region.

3.5. Summary

We analyzed seismograms recorded by sensors set at boreholes with depths of about 100 m and on the ground surface. From the analyses of 6 pairs of repeating earthquakes recorded at about 60 stations located on the eastern coast of NE Japan, we obtain the following results.

Direct P- and S-wave analyses show travel time differences of up to 0.01 s for the P-waves and 0.04 s for the S-waves. S-coda analyses indicate velocity changes of up to about 0.2%. There is no significant change between the results obtained from the ground surface and borehole sensors. These results strongly suggest that the waves are sampling the same region at ground surface and borehole.

Travel time differences estimated by using a time window with a length of 5 s are almost the same to those obtained by using time window of 2.5 s for both of the boreholes and ground surface sensors. This consistency implies that the seismic waves we analyzed in given time windows do not dominantly

consist of reverberations in the subsurface, but include the waves coming from deeper zones.

Table 3.1. Date, latitude, longitude, depth and magnitude for the set of 6 repeating earthquakes.

Event number and date			Longitude	Latitude	Depth	Mw
No.	Before	After	N (deg)	E (deg)	(km)	
1	19 Nov 2010	24 Oct 2011	142.104	39.634	48.3	4.0
2	18 Jan 2009	02 Feb 2012	140.572	36.520	56.5	3.9
3	09 Aug 2010	04 Feb 2012	142.107	39.636	47.6	3.9
4	17 Jun 2009	08 Oct 2013	141.831	39.758	58.1	3.9
5	18 Jan 2009	30 Jul 2013	140.572	36.520	56.5	3.9
6	01 Sep 2009	21 Mar 2013	141.343	37.160	48.3	3.9

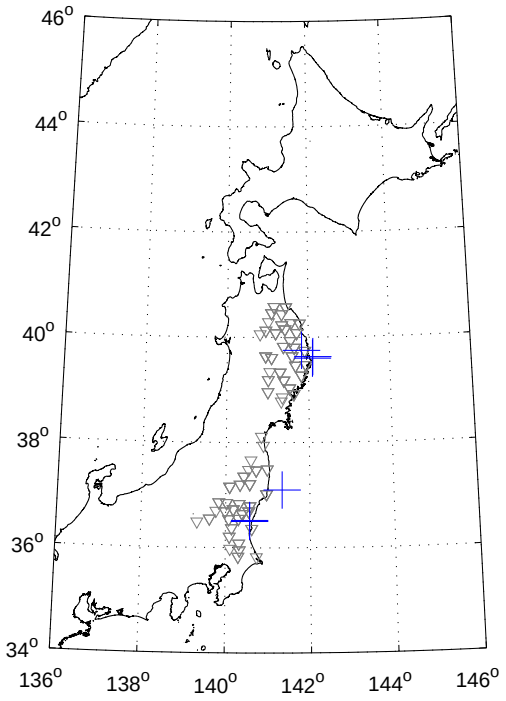

Figure 3.1. Map showing the location of the repeating earthquakes (crosses) and stations of KiK-net seismic network (inverted triangles) used in this study.

(a)

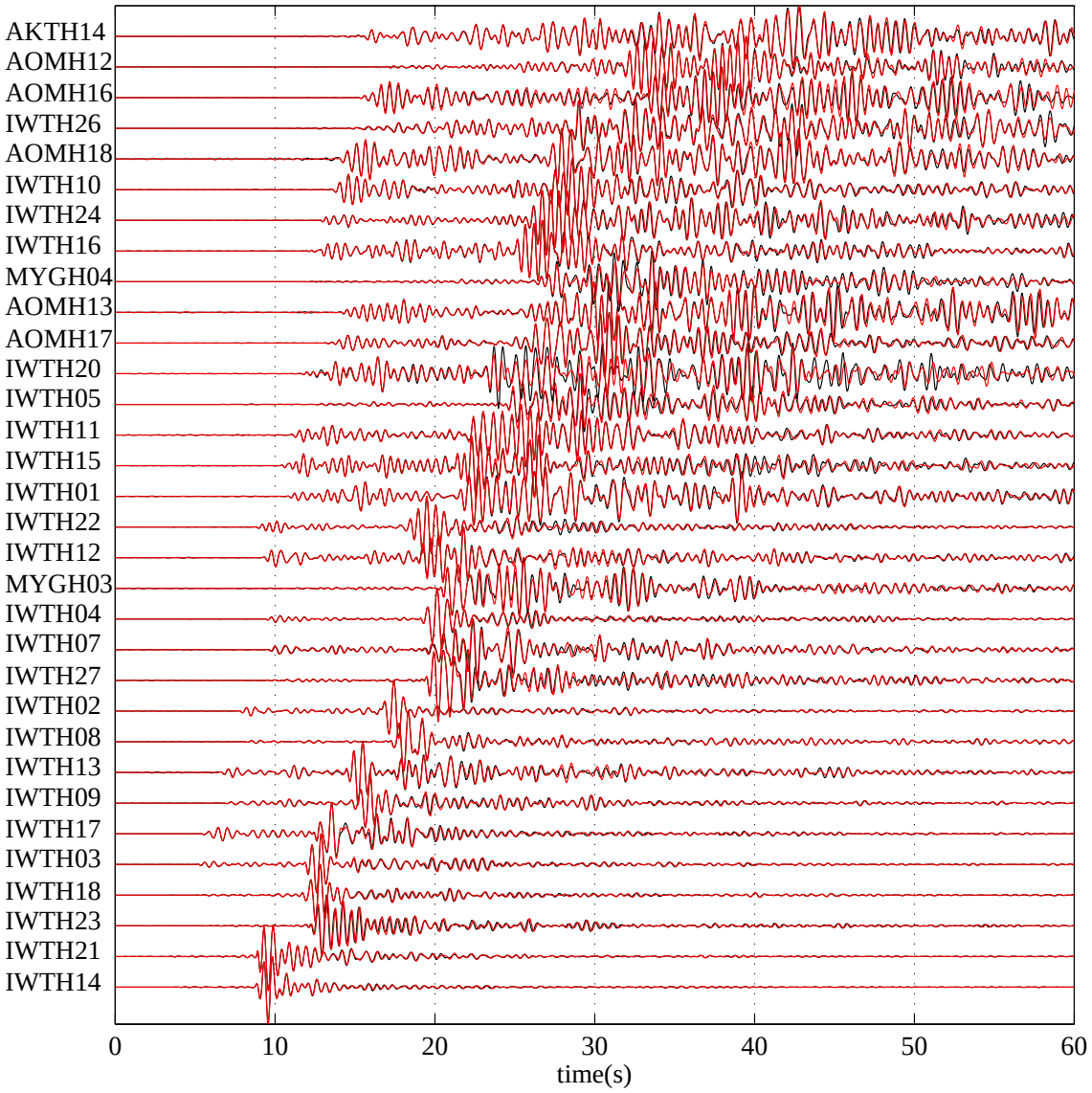

Figure 3.2. (a) Example of waveforms of event 1 recorded at the borehole sensor of KiK-net seismic network. Station code is indicated in the left. Black and red lines correspond to the waveforms recorded before and after the Tohoku-Oki earthquake, respectively.

(b)

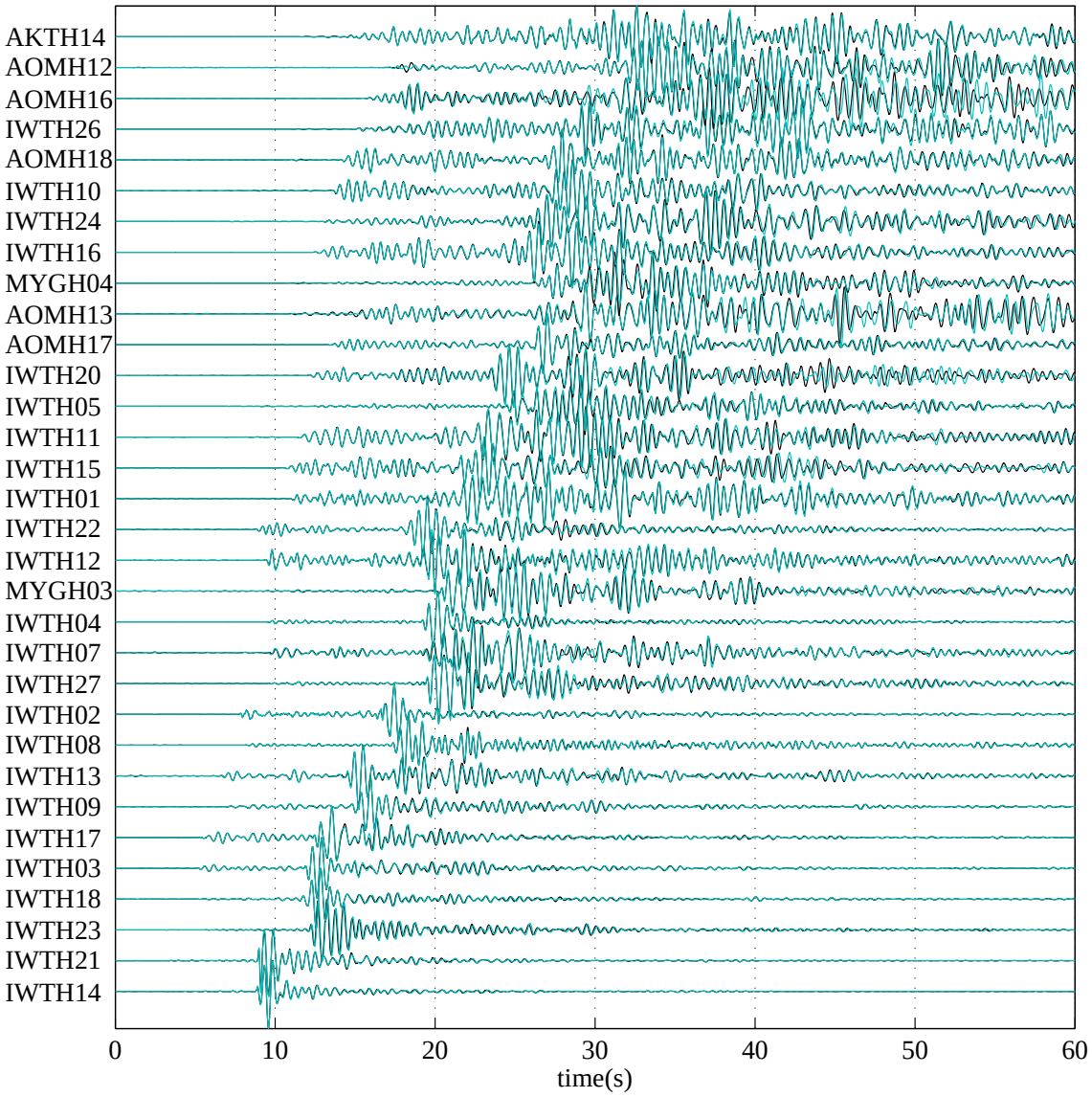

Figure 3.2. (b) Example of waveforms of event 1 recorded at the ground surface sensor of KiK-net seismic network. Station code is indicated in the left. Black and red lines correspond to the waveforms recorded before and after the Tohoku-Oki earthquake, respectively.

(a)

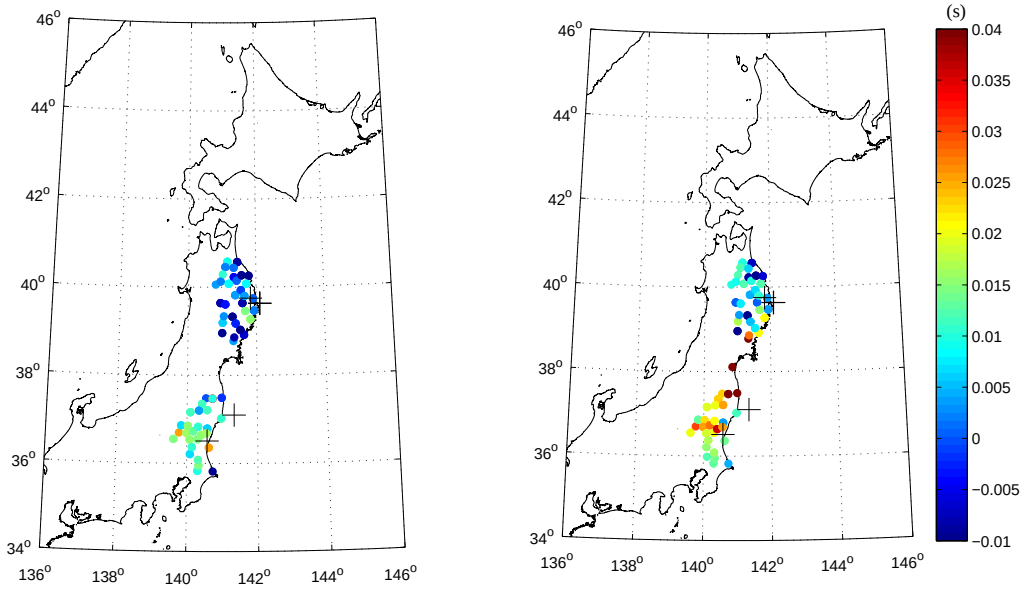

(b)

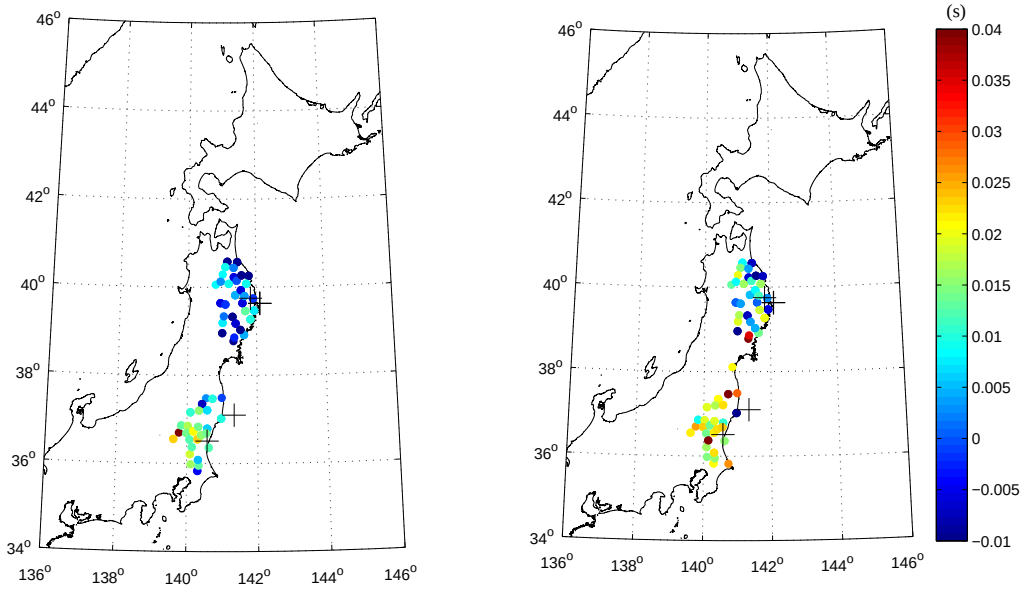

Figure 3.3. Spatial distributions of travel time differences obtained from (a) borehole and (b) ground surface seismograms. Left panels show the results for P-wave and right panels indicate those for the S-wave. Color scale indicates travel time differences in seconds and black crosses shows the epicenters of the repeating earthquakes.

(a)

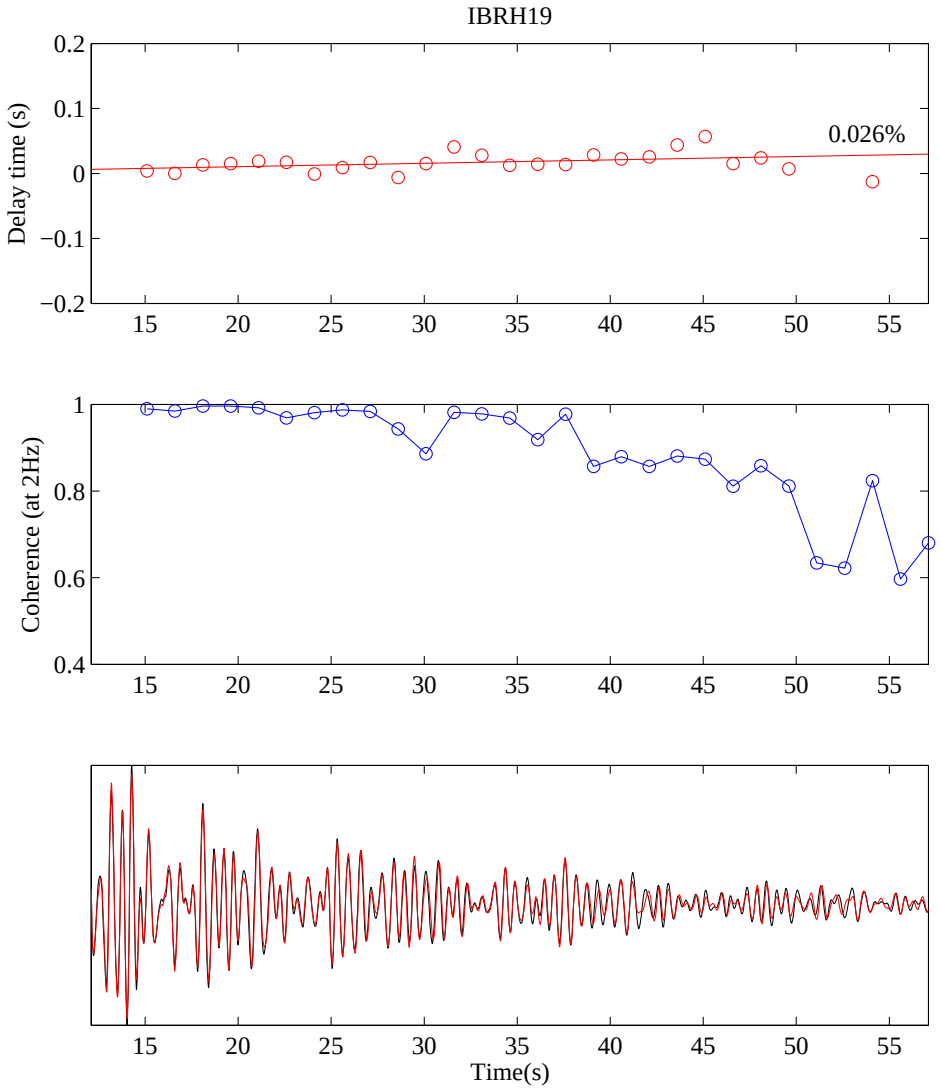

Figure 3.4. (a) Example of moving window analysis applied to the S-coda of the waveform recorded at the borehole sensor of station IBRH19 of the KiK-net seismic network for event 2. Station code is indicated in the upper part. Top, middle and bottom panels show the delay time with the best fitting line, coherence estimated at 2 Hz, and the waveform before (black) and after (red) the Tohoku-Oki earthquake, respectively, against the lapse time from the S-wave onset. Estimated velocity change is indicated in the right of the top panel. Red circles in the top panel show calculated delay times in each window with coherence of >0.08. Blue circles in the middle panel show the coherence estimated in each time window.

(b)

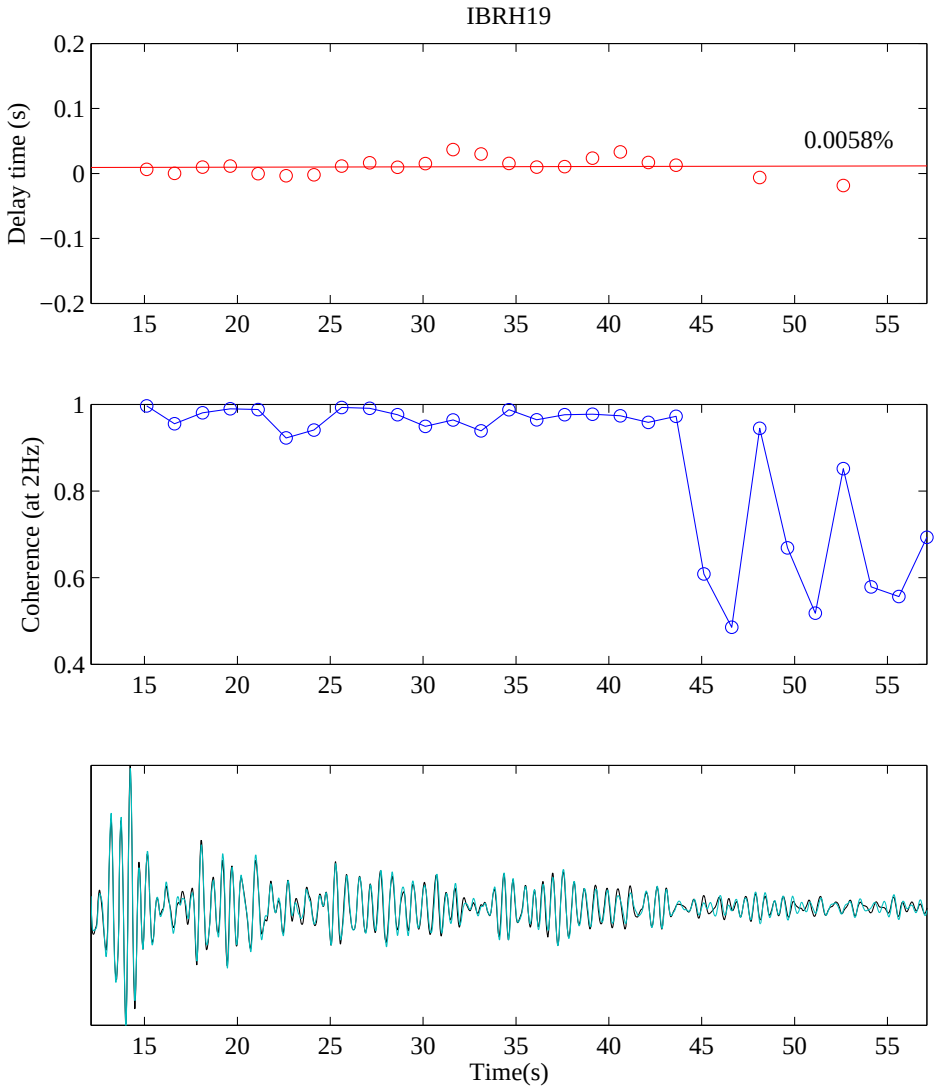

Figure 3.4. (b) Example of moving window analysis applied to the S-coda of the waveform recorded at the ground surface sensor of station IBRH19 of the KiK-net seismic network for event 2. Station code is indicated in the upper part. Top, middle and bottom panels show the delay time with the best fitting line, coherence estimated at 2 Hz, and the waveform before (black) and after (blue) the Tohoku-Oki earthquake, respectively, against the lapse time from the S-wave onset. Estimated velocity change is indicated in the right of the top panel. Red circles in the top panel show calculated delay times in each window with coherence of >0.08. Blue circles in the middle panel show the coherence estimated in each time window.

(a)

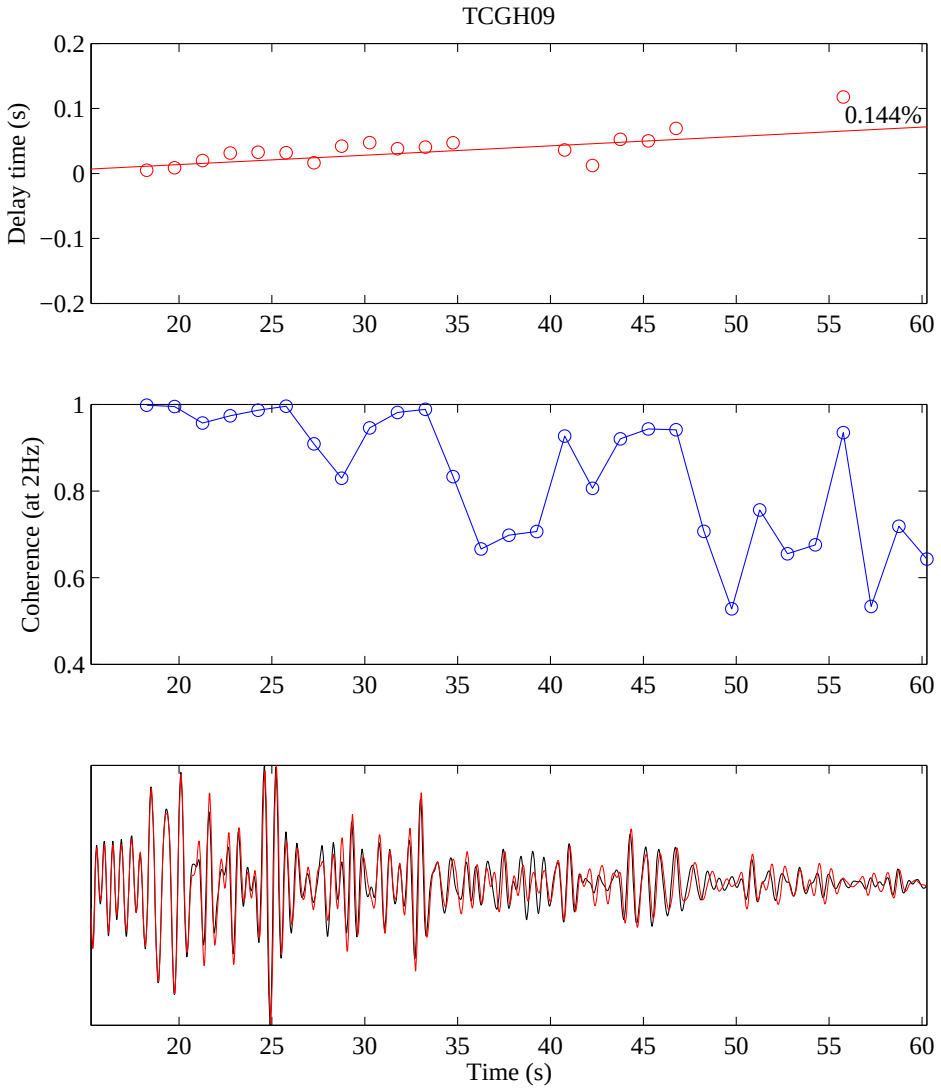

Figure 3.5. (a) Example of moving window analysis applied to the S-coda of the waveform recorded at the borehole sensor of station TCGH09 of the KiK-net seismic network for event 2. Station code is indicated in the upper part. Top, middle and bottom panels show the delay time with the best fitting line, coherence estimated at 2 Hz, and the waveform before (black) and after (red) the Tohoku-Oki earthquake, respectively, against the lapse time from the S-wave onset. Estimated velocity change is indicated in the right of the top panel. Red circles in the top panel show calculated delay times in each window with coherence of >0.08. Blue circles in the middle panel show the coherence estimated in each time window.

(b)

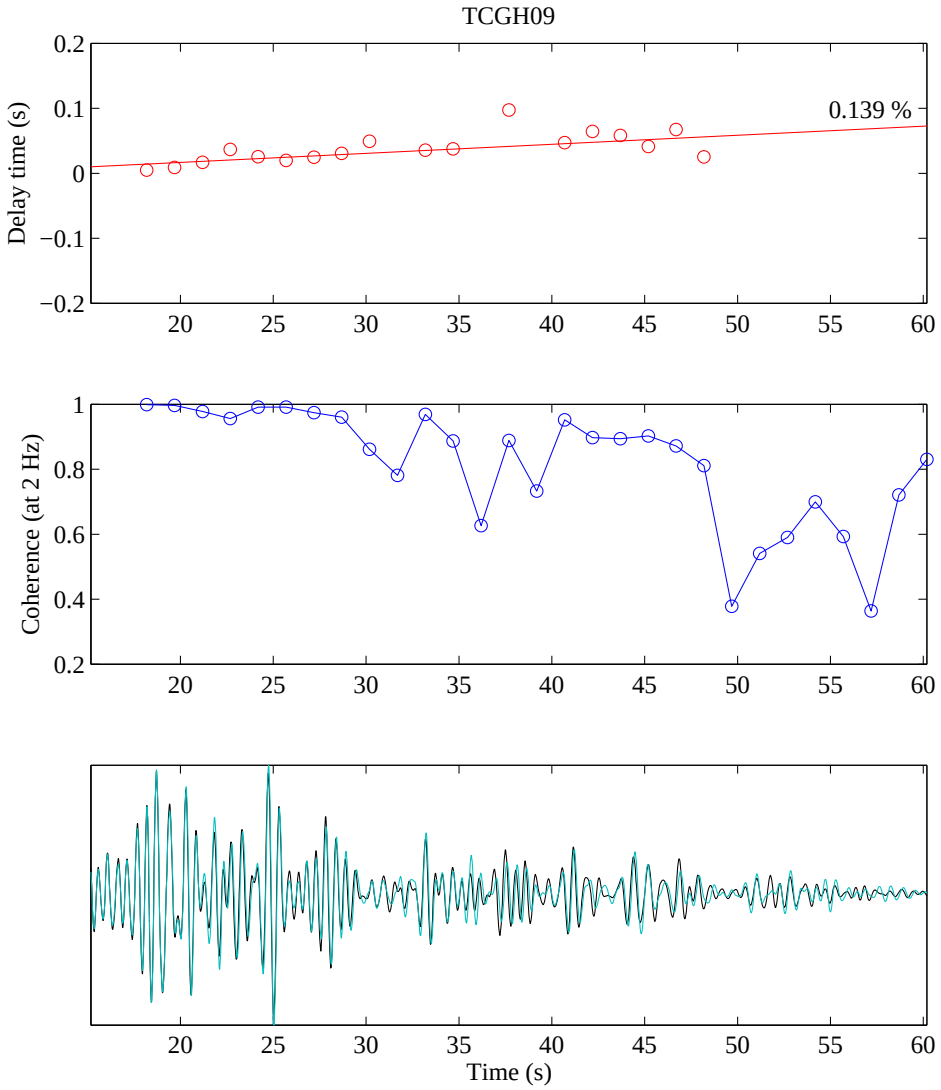

Figure 3.5. (b) Example of moving window analysis applied to the S-coda of the waveform recorded at the ground surface sensor of station TCGH09 of the KiK-net seismic network for event 2. Station code is indicated in the upper part. Top, middle and bottom panels show the delay time with the best fitting line, coherence estimated at 2 Hz, and the waveform before (black) and after (red) the Tohoku-Oki earthquake, respectively, against the lapse time from the S-wave onset. Estimated velocity change is indicated in the right of the top panel. Red circles in the top panel show calculated delay times in each window with coherence of >0.08. Blue circles in the middle panel show the coherence estimated in each time window.

(a)

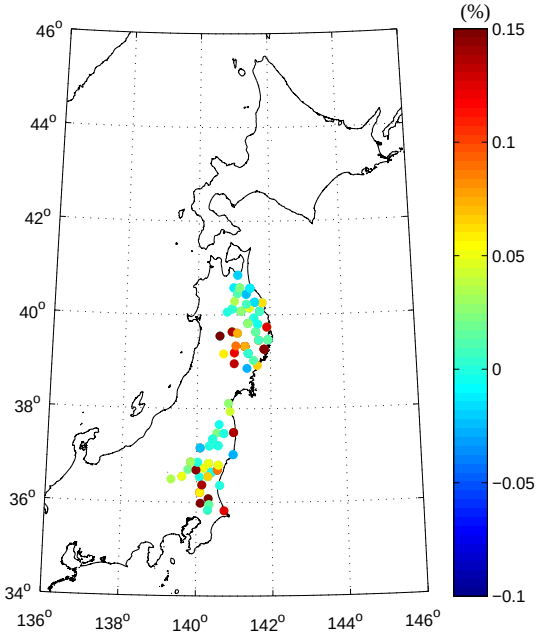

(b)

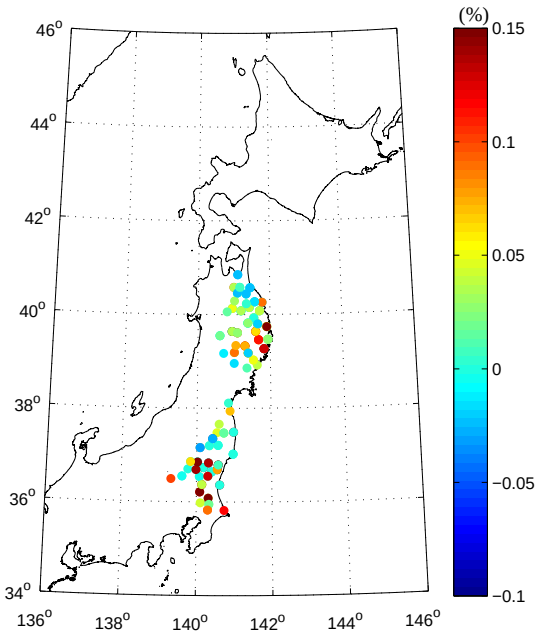

Figure 3.6. Spatial distribution of velocity changes estimated from S-coda wave analysis. (a) Borehole and (b) ground surface results. Color scales indicate the velocity change (%).

(a)

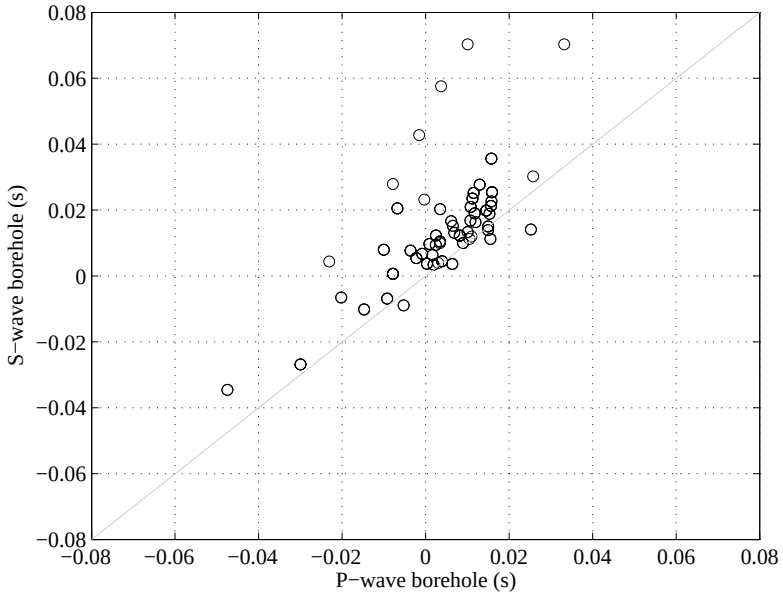

(b)

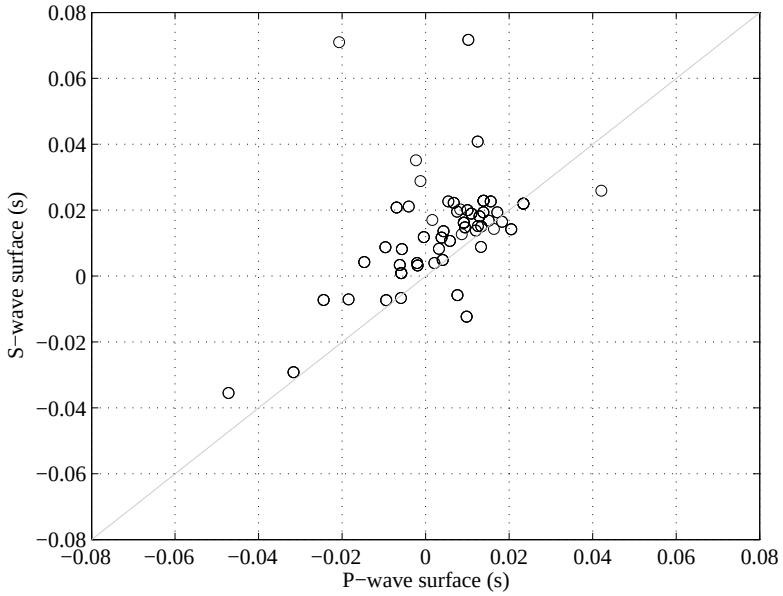

Figure 3.7. Comparison between P- and S-wave time differences for the results obtained from the borehole sensor (a), and the ground surface sensor (b) of the KiK-net seismic network.

(a)

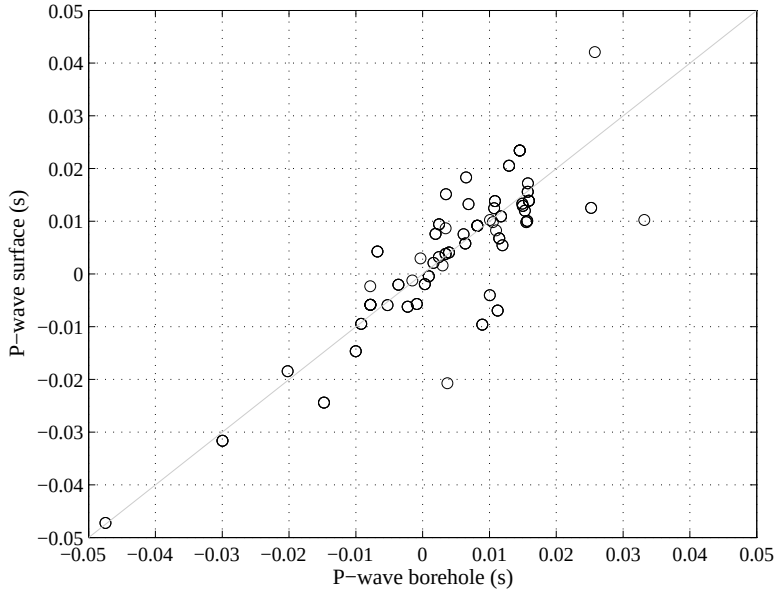

(b)

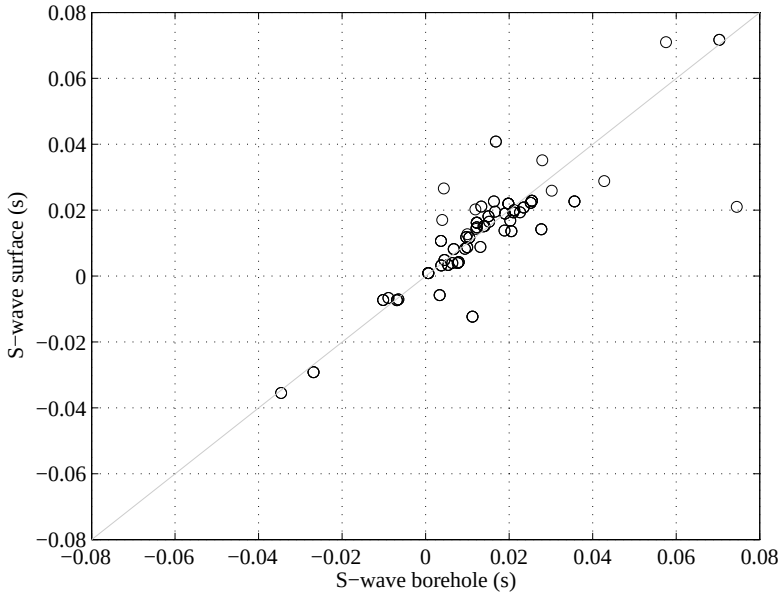

Figure 3.8. Comparison between borehole and ground surface time differences estimated from the direct P-wave (a) and S-wave (b) analyses. Correlation coefficients for P- and S-wave are (a) 0.85 and (b) 0.87, respectively.

(a)

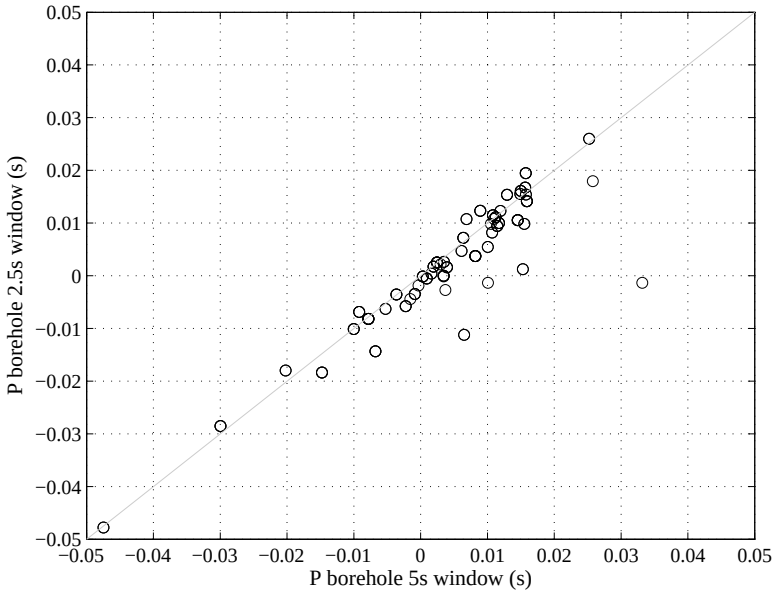

(b)

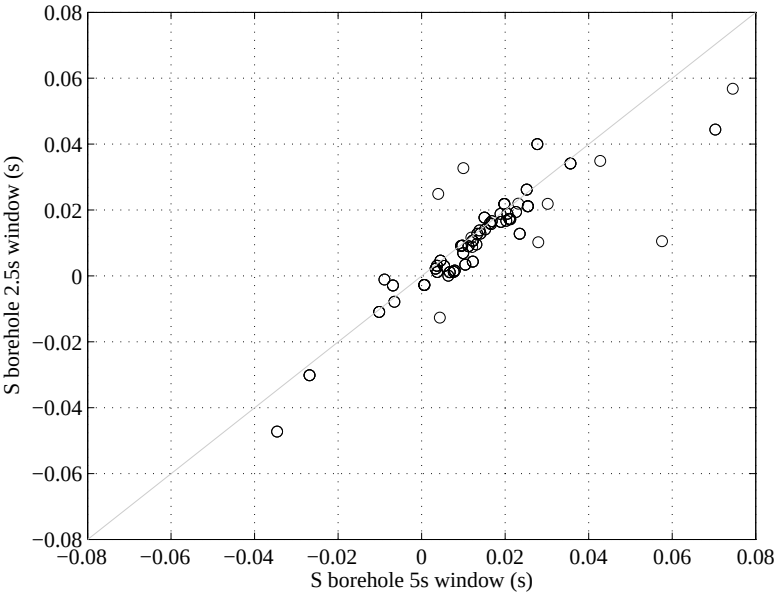

Figure 3.9. Comparison between time differences estimated by using a 5 s length time window and those obtained by using a 2.5 s length time window. Results from seismograms of borehole sensors are shown for (a) P-wave and (b) S-wave. Correlation coefficients are (a) 0.93 and (b) 0.89.

(a)

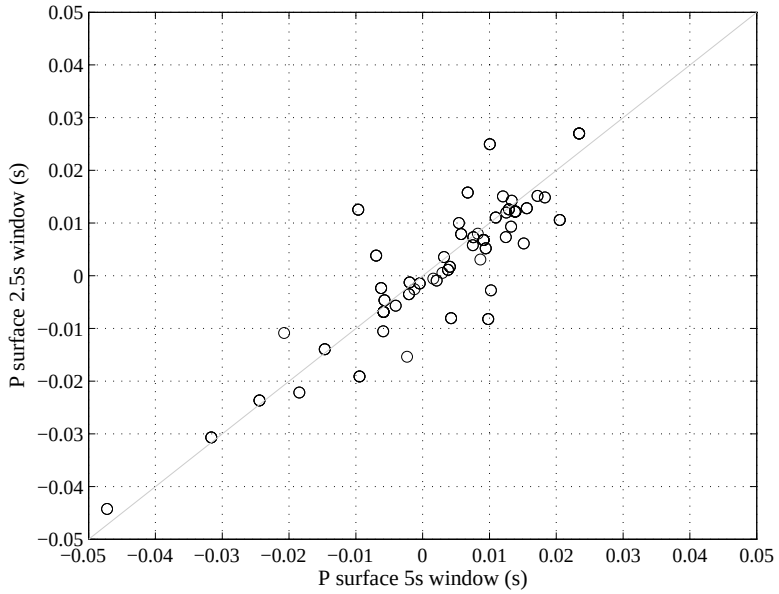

(b)

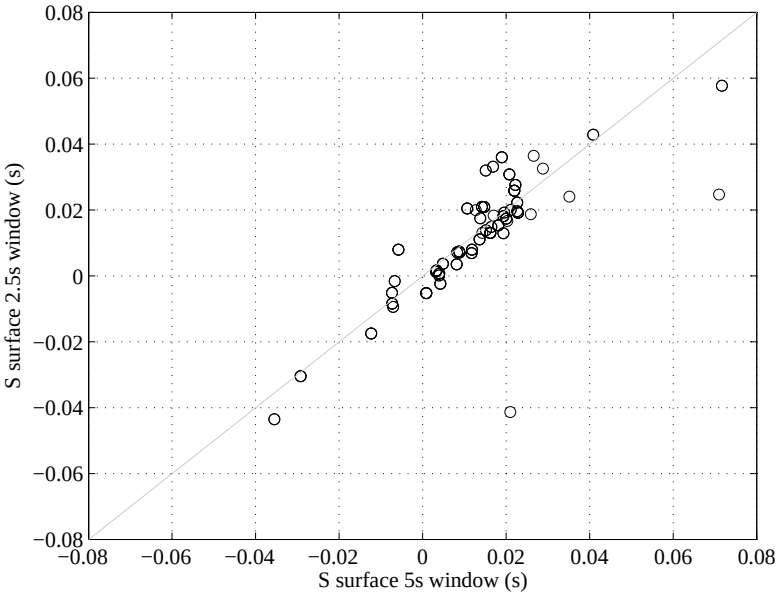

Figure 3.10. Comparison between time differences estimated by using a 5 s length time window and those obtained by using a 2.5 s length time window. Results from seismograms of ground surface are shown for (a) P-wave and (b) S-wave. Correlation coefficients are (a) 0.87 and (b) 0.84.

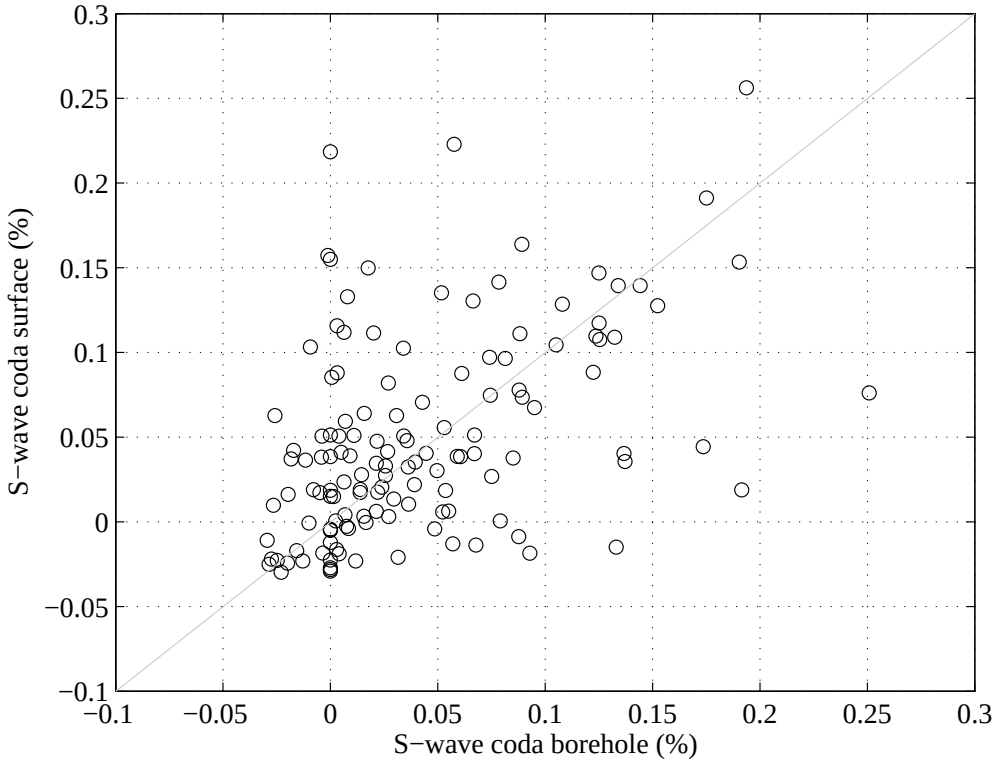

Figure 3.11. Comparison between velocity changes estimated from the borehole sensor and those from the ground surface sensor of KiK-net.

4. Discussion

4.1. Comparison with strong motion and strain changes

According to Schaff and Beroza (2004), large velocity changes in S-waves and small ones in P-waves are attributed to the opening or enlargement of cracks filled with fluid in shallow media at the sites that are subject to strong motions. This mechanism may explain the case of the Tohoku-Oki earthquake. Hence, we compare the station correction factors we estimated with the peak ground acceleration (PGA) reported by K-net seismic network (Figure 4.1). In this figure, we use the station correction factors determined from 25 pairs of repeating earthquakes. Contrary to large accelerations observed along the eastern coast of NE Japan, the estimated large station correction factors are widely observed, especially immediately west from the fault zone of the Tohoku-Oki earthquake. Spatial distributions of the station correction factors estimated from the analyses by using the north and south groups of repeating earthquakes are not matched with the distributions of PGA. We conclude that the spatial distribution of acceleration is not the same as the station correction factors for the S-waves, as indicated by the correlation between them (Figure 4.1 (b)).

We further compare our results with the areal strain amplitudes, because very large strain changes ($>10^{-6}$) are observed in NE Japan associated with the Tohoku-Oki earthquake and seismic velocity changes are expected to occur as even tidal motions of as low as 10^{-8} strain generate the velocity changes in the shallow medium [e.g., Takano et al., 2014]. Figure 4.2 shows relations of the areal strain amplitude directly calculated from the displacement data of GSNN [Ohta pers.com.] and the observed station correction factors of S-wave. Their correlations are poor, thus indicating that the changes in strain may not be the main cause of the estimated station correction factors.

4.2 Comparison with seismic velocity changes previously reported

Seismic velocity changes have been already examined from the analyses of the borehole and ground surface sensors of KiK-net stations [e.g. Nakata & Snieder 2011; Takagi & Okada 2012], seismic interferometry analyses of ambient noises at 0.1-0.9 Hz [Brenguier et al. 2014], and multi-time window analyses of S-coda at 1-2 Hz using Hi-net data [Nishimura et al., 2013]. In this section, we compare the region where seismic velocity changes we detected with the results from these previous studies. Figure 4.3 summarizes spatial distributions of the seismic velocity changes.

By retrieving the direct S-wave propagating in the subsurface down to a few hundred meters depth from interferometric analysis of vertical arrays of KiK-net seismic network, Takagi & Okada (2012)

estimated velocity changes of up to 10% in the frequency band of 4-16 Hz. They observed large velocity decreases along the Pacific coast (Figure 4.3 (a)). From a high correlation between spatial distribution of velocity changes and PGA, they interpreted that the main factor generating the observed velocity change is strong ground motion. Also, they show a clear correlation between the dynamic strain change and travel time shift. These results are based on the body waves propagating from the borehole sensors at depths of about 100 m to the ground surface sensor, which are retrieved by calculating cross-correlation functions of S-coda of regional earthquakes. Hence, the seismic velocity changes in these studies are attributed to the medium located at depths shallower than about 100 m. Figure 4.3 (d) shows the results estimated from direct S-waves in this work. The spatial distributions are poorly correlated to the results of subsurface velocity change in Figure 4.3 (a).

Recently, Brenguier et al. (2014) analyzed Rayleigh waves retrieved from ambient noise analyses in the frequency band of 0.1-0.9 Hz to estimate the crustal seismic velocity changes due to the Tohoku-Oki earthquake. Since they analyzed long-period waves of about 1-10 s, their measurements may capture averaged S-wave velocity changes at depths from the ground surface to about 10 km [Brenguier et al. 2014]. The spatial distribution of velocity change is shown in Figure 4.3 (b). They observed that the velocity drops are not correlated with the intensity of ground shaking or with the coseismic deformation of the Tohoku-Oki earthquake. They interpreted the observed seismic wave velocity reductions as related to mechanical weakening of the pressurized crust due to the dynamic stress originated from the passing of the seismic waves of the Tohoku-Oki earthquake.

Nishimura et al. (2013) estimated velocity changes from moving time window analyses of S-coda using records of Hi-net seismic network. They detected velocity decreases of about 0.4% at 1-2 Hz in the middle of Tohoku region as shown in Figure 4.3 (c). Large values of velocity decrease are distributed in an N-S direction in the middle of NE Japan, mainly between 37^{o}N and 40^{o}N in latitude.

Horizontal spatial distributions of the seismic velocity changes we detected seem to be correlated with the regions detected from S-coda (1-2 Hz) [Nishimura et al., 2013] and Rayleigh waves (0.1-0.9 Hz) [Brenguier et al., 2014]. For all the three cases, large velocity decreases are observed in the N-S direction in the middle of the NE Japan, and are not observed in the east coast in NE Japan where large strong-motions are observed. Although there are several discrepancy between them (for example, the large velocity decrease at Mt.Fuji in Figure 4.3(b)), high similitude of spatial distributions suggests that the velocity changes detected are not limited to the shallow subsurface [e.g. Nakata & Snieder 2011; Takagi & Okada 2012].

Here, we summarize the observed results on the seismic velocity changes associated with the Tohoku-Oki earthquake.

(1) Wide area of NE Japan shows velocity decrease of up to 10 % in the subsurface at depths of a few hundred meters. This is observed from analyses of the seismic waves propagating from the borehole sensor to the ground surface of KiK-net data that are retrieved from seismic interferometry analyses [Nakata & Snieder 2011; Takagi & Okada 2012].

(2) Analyses of Rayleigh waves retrieved from ambient noise in the frequency band 0.1-0.9 Hz indicate velocity decreases up to 0.12% that are spatially correlated with the volcanic front. S-wave velocity changes are inferred to occur at depths between the ground surface and about 10 km depth [Brenguier et al., 2014]. The velocity decreases are not correlated with the intensity of strong-motions or co-seismic deformation.

(3) Seismic velocity changes estimated from S-coda at 1-2 Hz show large velocity decreases of about 0.4% located in the middle of Tohoku region [Nishimura et al., 2013].

(4) Analyses of arrival time differences of direct P- and S-waves from repeating earthquakes indicate the anomaly of seismic velocity changes extending down to 25 km depth beneath the middle of NE Japan in latitudes ranging between 37^{o}N and 40^{o}N [this study].

(5) Travel time differences of direct P- and S-waves observed on the ground surface and those at boreholes are almost same, even when different time window lengths are used. This means that the direct P-waves we analyzed are not formed by reverberation in the subsurface but consist of seismic waves that are incident from deeper regions [this study].

(6) Seismic velocity decrease estimated from S-coda recorded at the ground surface and borehole sensors show similar results. This indicates that the S-coda consist mainly of shear waves coming from deep regions and not from the reverberation in the subsurface [this study].

4.3. Structural changes associated with the Tohoku-Oki earthquake

We summarized in the previous section seismic velocity changes associated with the Tohoku-Oki earthquake detected from analyses of different seismic waves retrieved from different methods. Here, we present three different conceptual models of structural changes beneath NE Japan that are inferred from these previous studies as well as ours, and explain the different observations by considering propagation processes of the seismic waves that are analyzed in previous studies and this work.

The first model is introduced from the evidence that velocity changes of up to 10% are detected in subsurface at a few hundreds of meters down and between the two sensors of the KiK-net seismic network (observation (1) in the previous section). This is Model I in Fig. 4.4, which describes the velocity changes occurring only in the subsurface at depths less than a few hundred meters. We examine whether or not this structural model may explain the other observations by considering

possible wave propagation processes. Our results indicate that seismic velocity changes detected by ground surface and borehole sensors are almost the same for direct P- and S-waves as well as S-coda (observations (5) and (6)). This implies that the waves captured at depths of a few hundred meters sample the same region of the waves observed on the ground surface. Small velocity changes of S-coda (up to about 0.4 % of observations (3) and (6)) may be explained by considering S-coda that consists of not only the reverberations in the subsurface but also the scattered waves in deeper region where smaller velocity changes are expected. If S-coda consists mainly of reverberations in the subsurface, the spatial distribution of seismic velocity changes detected by S-coda [Nishimura et al., 2013] comes to be similar to those by KiK-net data analyses [Nakata & Snieder 2011; Takagi & Okada 2012]. But, they are not matched (observations (1) and (3)). Moreover, as confirmed from the analyses performed by changing the window length between 5 s and 2.5 s in the measurement of the arrival time differences of P- and S-waves, the waves contributing to the time window are not dominated by reverberations and reflections in the subsurface, because such reverberations and reflections could increase the velocity changes as the length of time window increases. Spatial distribution of velocity changes estimated from Rayleigh wave at 0.1-0.9 Hz (observation (2)) also differs from observation (1). Therefore, Model I may not explain the velocity changes detected by analyses of S-coda and Rayleigh waves retrieved from ambient noises.

The second model consists of the subsurface with velocity changes up to 10% in a few hundred meters and the zone down to approximately 10 km in the upper crust where velocity decrease of about 0.1 % occurred. This Model II is depicted schematically in Figure 4.4. Since Model I cannot explain the observed results of S-coda and Rayleigh waves (observations (2) and (3)), we extend seismic velocity changes into deeper region as proposed by Brenguier et al. (2014). Velocity changes at deep zones do not affect the seismic wave propagating from the borehole to the ground surface, therefore Model II can explain the observation (1). As the spatial pattern of velocity changes inferred by Nishimura et al. (2013) are well correlated with those obtained by Brenguier et al. (2014) (observations (2) and (3)), the velocity drops of about 0.12 % are well explained by this model by considering that the S-coda are scattered waves sampling upper crust. This is consistent with observation (6) in which S-coda is not caused by reverberations in the subsurface. However, the velocity changes of Model II are limited down to approximately 10 km; therefore observation (4) is not explained.

The third model takes into account the anomaly extending down to ~25 km as depicted in Figure 4.4. Model III consists of the subsurface with velocity changes of up to 10 %, the upper crust with 0.1% velocity decrease, and the anomaly extending down to 25 km. As same as Model II, this model can explain the observations from KiK-net data analyses (observations (5) and (6)). Also, the observed

velocity changes detected from Rayleigh waves (observation (2)) are well explained because Model II includes velocity changes in the upper crust. Velocity changes detected from S-coda (observation (3)) can be predicted even if S-coda samples in the deeper zones down to 25 km because the amount of velocity changes are almost same in the upper and lower crust. Our results (observations (5) and (6)) that P- and S- waves recorded by borehole (and ground surface sensors) consist of body waves from deeper zones and not from the subsurface also support this model.

From these considerations, we conclude that Model III is the most appropriate model of the structural changes associated with the Tohoku-Oki earthquake. The anomaly extending down to ~25 km located in the middle of NE Japan, immediately west from the fault of Tohoku-Oki earthquake suggest that the occurrence of the Tohoku-Oki earthquake damaged not only the subsurface but also the medium down to the lower crust.

4.4. Velocity changes in the lower crust

Seismic velocity changes due to a large earthquake have been often attributed to the damage in the subsurface down to a few hundred meters by strong ground motions [Rubinstein & Beroza, 2005; Rubinstein et al., 2007; Takagi & Okada 2012] for these decades. Such velocity reduction must occur at the site where large strong motions are observed, as the KiK-net data analyses retrieve the direct body waves propagating between borehole and ground surface sensors. On the other hand, several studies suggested velocity changes at deep regions down to about 10 km from observed positive correlations between the seismic velocity changes and crustal deformations detected by GNSS [Brenguier et al. 2008]. However, it had not been easy to clarify whether or not the velocity changes at deep region occur because large earthquakes accompany strong motions close to the seismic source. Hence, seismic wave velocity change extending to deeper zones is still under investigation. Recently, Rivet et al. (2014) analyzed slow slip events that occurred in 2009 and 2010 in Guerrero, Mexico. They calculated cross-correlation functions from ambient noises to retrieve Rayleigh waves for the period from 4 s to 27 s and detected subtle velocity variations. Since the slow slip events did not generate strong ground motions at all, there must have been no damage in the subsurface [Rivet et al. 2011]. Their analyses indicate velocity decreases of up to about 0.03 % that extends from 10 km down to 30 km deep with no velocity change in the upper 10 km. The authors estimated that velocity changes maximize at periods longer than 12 s and attributed the observed changes to transient deformation (strain rate) at depth.

Their observation may be matched with our results that, after a big earthquake such as the Tohoku-Oki earthquake (Mw 9.0), medium changes may extends to a few tens of km into the lower crust, and such changes are detectable from analyses of seismic waves. Also, Brenguier et al. (2014) suggest that

dynamic stress associated with the seismic waves emitted by the Tohoku-Oki earthquake has been suggested as the main cause of the observed large velocity reductions at depths down to 10 km. The observed velocity reductions delineate the regions where pressurized volcanic fluids are present, hence the authors infer that volcanic fluids reduce the effective pressure in the crust and thus increase the sensitivity of seismic velocity to stress changes. Our results and observations from Nishimura et al. (2013) at a similar frequency band (1-2 Hz) correlate with spatial distribution of velocity changes estimated by Brenguier et al. (2014). This implies that dynamic stress may be an important factor to understand the medium changes in the crust. But, rock properties at such depths are not fully understood with respect to velocity changes. Also, examples of studies showing velocity changes at such depths are quite limited (only two). Hence, further investigation is necessary to better understand the mechanism generating the velocity changes in the medium at depths down to a few tens of kilometers in the Earth's crust.

(a)

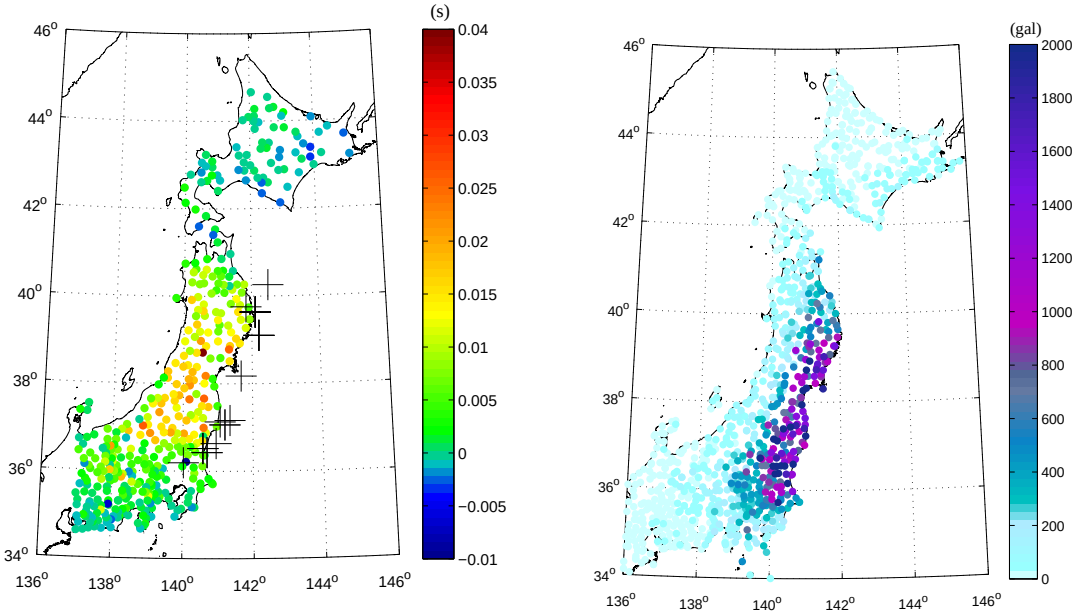

(b)

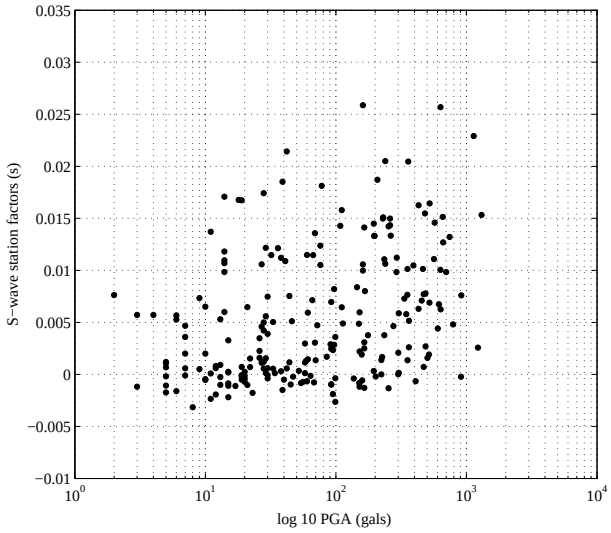

Figure 4.1. Comparison of the S-wave station correction factors with the PGA acceleration from K-net seismic network. (a) Spatial distribution of the station correction factors (left panel) and PGA (right panel), units are in seconds and gal, respectively. (b) Amplitude of the S-wave station factors plotted against the PGA for stations at approximately the same location.

(a)

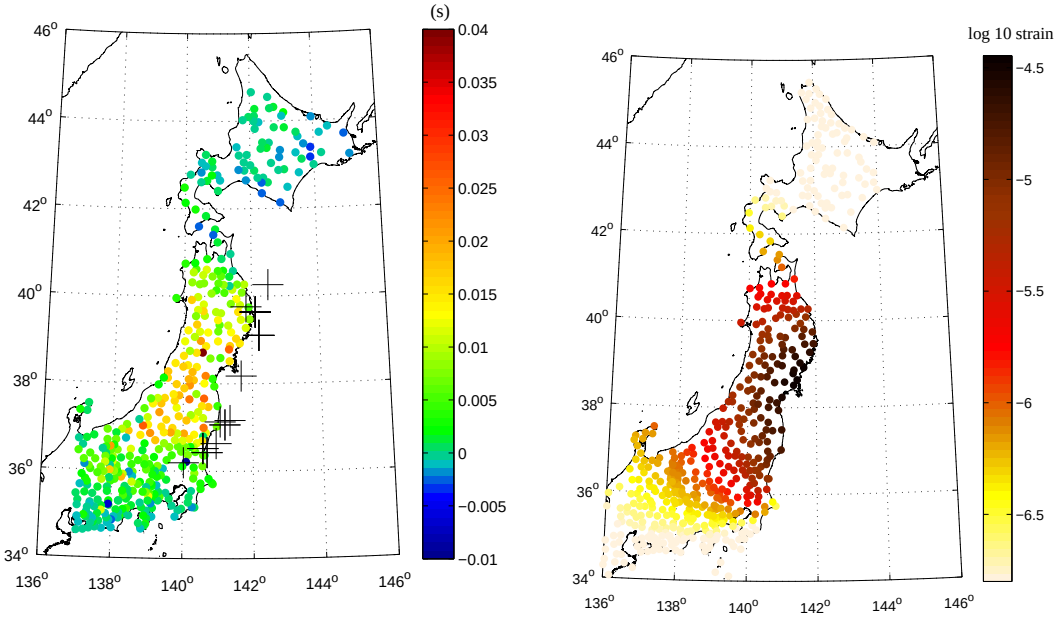

(b)

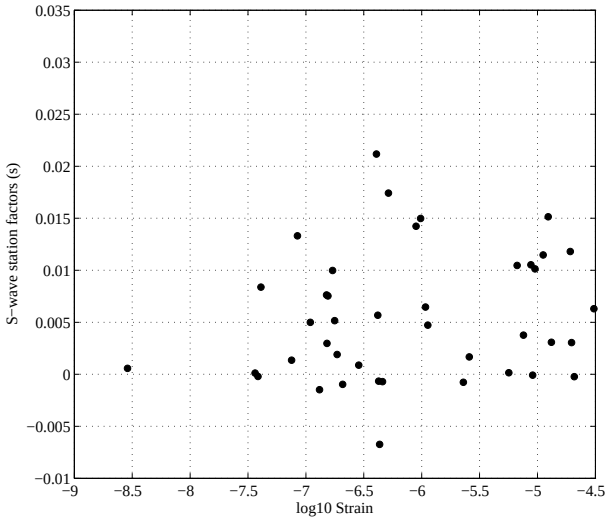

Figure 4.2. Comparison of the S-wave station correction factors with the areal strain (Ohta, pers. com.). (a) Station correction factors (left panel) are in seconds and strain (right panel) are indicated in logarithmic scale. (b) Amplitude of the S-wave station correction factors plotted against the areal strain for stations at approximately the same location.

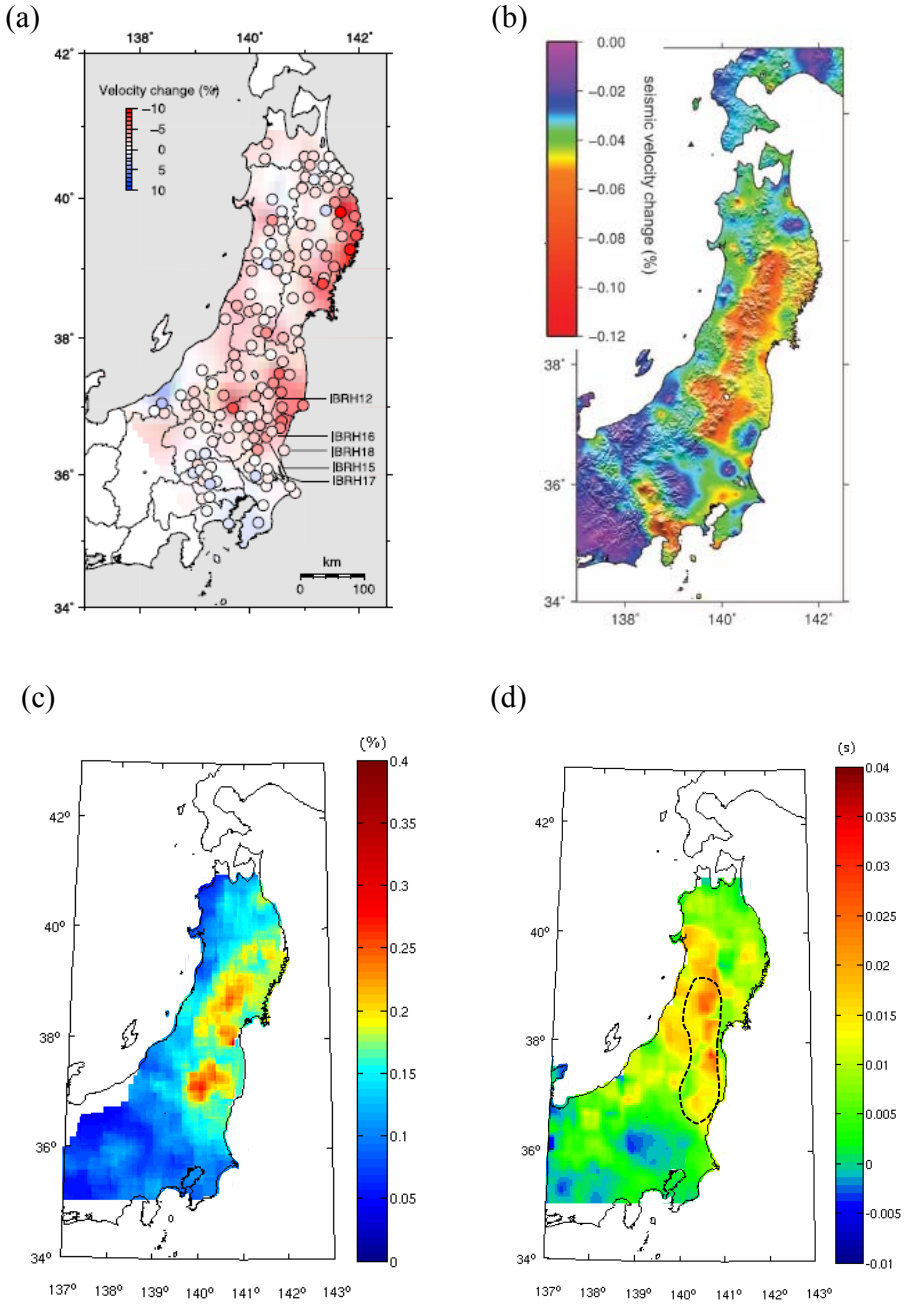

Figure 4.3. (a) Velocity changes of subsurface before and after the Tohoku-Oki earthquake (Takagi & Okada 2012). (b) Crustal velocity changes estimated from Rayleigh waves at 0.1-0.9 Hz (Brenguier et al. 2014). (c) Spatial distribution of velocity changes from S-coda at 1-2 Hz (Nishimura et al., 2013). (d) Arrival time differences of S-waves station correction factors corresponding to the set of repeating earthquakes of the south group analyzed in this work. The black dashed curve shows the location of the anomaly of velocity change.

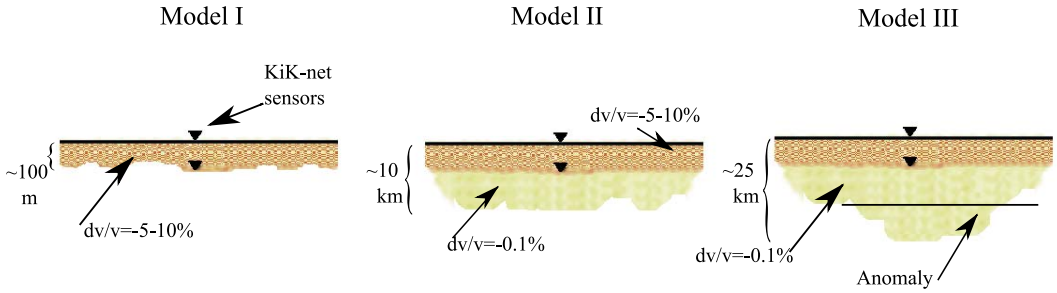

Figure 4.4. Schematic illustrations of structural changes in the crust of NE Japan associated with the occurrence of the Tohoku-Oki. Inverted triangles represent the ground surface and borehole sensors of the KiK-net seismic network. Seismic velocity change up to 10% at subsurface is represented by brown color and velocity drops of about 0.1% in the crust by yellow color. The location of the anomaly is indicated below the black solid line of Model III. See the text for more details.

5. Conclusions

We have examined seismic velocity changes of the structure beneath NE Japan associated with the occurrence of the Tohoku-Oki earthquake (Mw9.0) on March 11, 2011. To clarify the regions of seismic velocity changes, we analyzed repeating earthquakes that occurred at almost same locations before and after this earthquake.

First, since the earthquake's strong motion significantly decreased seismic velocity of the medium beneath seismic stations, we developed a new inversion method to simultaneously determine relative locations and origin times of the pairs of repeating earthquakes and station correction factors of travel times for P- and S-waves. From analyses of Hi-net data for 25 pairs of repeating earthquakes occurring at depth of about 50 km beneath the coast lines of NE Japan, we obtained the following main results:

1. Arrival time delays up to 0.01 s and 0.04 s for direct P- and S-waves, respectively, were detected from cross-spectrum analyses of waveform data of repeating earthquakes at the frequency of 1-2 Hz. The observed delays of S-wave are widely distributed in central NE Japan while those of P-wave are smaller than the S-wave. The location differences of hypocenter parameters ranges from 0.0006 to 0.2 km and origin time differences are estimated to be from 0.0005 s to 0.02 s.
2. Station correction factors estimated from analyses of a set of 15 repeating earthquakes occurring before the Tohoku-Oki earthquake are quite small, which suggests no significant temporal changes. Repeating earthquakes occurring before and after the Tohoku-Oki earthquake were divided according to different temporal distribution, and the results from these different groups show no significant temporal change in spatial distribution.
3. The 25 pairs of repeating earthquakes were divided into 2 groups according to the locations of the hypocenter. By applying the inversion method to each group, we inferred an anomaly located in the backbone of central Tohoku, west from the large slip area of the Tohoku-Oki earthquake. Forward modeling of direct S-wave ray tracing clarified that the anomaly extends down to 25 km with an average velocity change of about 0.1%.

To understand the observed temporal changes of seismic wave velocity and the wave propagation processes, we analyzed both of the seismograms recorded by borehole and ground surface sensors of KiK-net. We analyzed waveforms at 1-2 Hz for a set of 6 repeating earthquakes located in NE Japan. We obtained the following main results:

1. Travel time differences of about 0.01 s and up to 0.04 s were detected at the borehole and ground surface sensors for direct P- and S-waves, respectively.

2. Moving time window analyses applied to S-coda of repeating earthquakes indicate velocity changes up to 0.2% at some stations in NE Japan.
3. The observed travel time differences obtained from analyses of the seismograms recorded by borehole and ground surface sensors are almost same to each other. Also, the velocity changes measured from the borehole sensor are roughly same to those from the ground surface. These results suggest that the velocity changes are not limited to the subsurface.
4. We analyzed direct waves by using time windows with two different lengths and concluded that waves we analyzed are not formed only by reverberations at the subsurface but consist of body waves sampling deeper regions in the medium.

We compared our results with strong-motions and strains caused by the Tohoku-Oki earthquake and the velocity changes reported in previous studies. Considering consistency of the spatial distributions and amplitude of velocity changes as well as seismic wave propagation processes clarified in chapter 3, we present a structural model in order to explain the different spatial patterns and amount of the velocity changes due to the Tohoku-Oki earthquake. A structural model consisting of a velocity change up to 10% in subsurface and an anomaly of velocity change (~0.1 %) extending down to 25 km explain the results from this work and previous studies that detected seismic wave velocity changes associated with the occurrence of the Tohoku-Oki earthquake (Mw 9.0) in NE Japan.

We succeeded in showing the existence of seismic velocity changes extending down to the upper and lower crust from detailed analyses of the waveform data of repeating earthquakes. This new finding of the velocity changes in the crust, which have not yet been well investigated except for the case associated with slow slip events at Mexico [Rivet et al., 2011, 2014], can give us a new evidence that should be considered to understand the structural changes associated with large earthquakes and medium properties in the crust.

References:

Anggono, T., T. Nishimura, H. Sato, H. Ueda, and M. Ukawa (2012), Spatio-temporal changes in seismic velocity associated with the 2000 activity of Miyakejima volcano as inferred from cross-correlation analyses of ambient noise, *J. Vocanol. Geotherm. Res., 247-248*, 93-107. doi:10.1016/j.jvolgeores.2012.08.001.

Brenguier, F., M. Campillo, C. Hadziioannou, N.M. Shapiro, R.M Nadeau, and E. Larose (2008), Postseismic relaxation along the San Andreas fault at Parkfield from continuous seismological observations, *Science*, *321*, 1478-1481, doi:10.1126/science.1160943.

Brenguier, F., N.M. Shapiro, M. Campillo, V. Ferrazzini, Z. Duputel, O. Coutant, and A. Nercessian (2008), Towards forecasting volcanic eruptions using seismic noise, *Nat. Geosci.*, *1*, 126-130.doi:10.1038/ngeo104.

Brenguier, F., M. Campillo, T. Takeda, Y. Aoki, N.M. Shapiro, X. Briand, K. Emoto, and H. Miyake, (2014), Mapping pressurized volcanic fluids from induced crustal seismic velocity drops, *Science*, *345*, 80-82, doi:10.1126/science.1254073.

Campillo, M. and A. Paul, (2003), Long-range correlations in the diffuse seismic coda, *Science, 299*, 547-549, doi: 10.1126lscience.1078551.

Cheng, X., F. Niu, and B. Wang (2010), Coseismic velocity change in the rupture zone of the 2008 Mw 7.9 Wenchuan earthquake observed from ambient seismic noise, *Bull. Seismol. Soc. Am., 100* (5B), 2539-2550, doi: 10.1785/0120090329.

Dolbilkina, N.A., V.I. Myachkin, A.M. Palyonov, and V.B. Preobrazensky (1979), The study of time variations of elastic-wave parameters: results and problems, *Phys. Earth Planet. Inter., 18*, 319-325, doi:10.1016/0031-9201(79)90068-2.

Douglas, A. (1967), Joint epicenter determination, *Nature*, *215*, 47-48,doi:10.1038/215047a0.

Furumura, T., S. Takemura, S. Noguchi, T. Takemoto, T. Maeda, K. Iwaki, and S. Padhy (2011), Strong ground motions from the 2011 off-the Pacific-Coast-of-Tohoku, Japan (Mw=9.0) earthquake obtained from a dense nationwide seismic network, *Landslides, 8*, 333-338,doi:10.1007/s10346-011-0279-3.

Gret, A., R. Snieder, R.C. Aster, P.R. Kyle (2005), Monitoring rapid temporal changes in a volcano with coda wave interferometry. *Geophys. Res. Lett.*, *32*, L06304,doi:10.29/2004GL021143.

Hobiger, M., U. Wegler, K. Shiomi, and H. Nakahara (2012), Coseismic and postseismic elastic wave velocity variations caused by the 2008 Iwate-Miyagi Nairiku earthquake, Japan, *J. Geophys. Res.*, *117B09313*, doi:10.1029/2012JB009402.

Ichikawa, M., and E. Mochizuki (1971), Travel time tables for local earthquakes in and near Japan (in Japanese), *Pap. Meteorol. Geophys.*, *22*, 229-290, doi:10.2467/mripapers1950.22.3-4_229.

Igarashi, T., T. Matsuzawa, N. Umino, and A. Hasegawa (2001), Spatial distribution of focal mechanism for interpolate and intraplate earthquakes associated with the subducting Pacific plate beneath the northeastern Japan arc: A triple-planed deep seismic zone, *J. Geophys. Res.*, *106*, 2177-2191, doi:10.1029/2000JB900386.

Igarashi, T., T. Matsuzawa, and A. Hasegawa (2003), Repeating earthquakes and interplate aseismic slip in the northeastern Japan subduction zone, *J. Geophys. Res.*,*108*,2249, doi:10.1029/2002JB001920.

Iinuma, T., M. Ohzono Y. Ohta and S. Miura (2011), Coseismic slip distribution of the 2011 off the Pacific coast of Tohoku Earthquake (M9.0) estimated based on GPS data-Was the asperity in Miyagi-Oki ruptured?, *Earth Planets Space*, *63,* 7, 643-648.doi: 10.5047/eps.2011.06.013.

Kanamori, H., and G.. Fuis (1976), Variation of P-wave velocity before and after the Galway Lake earthquake (ML=5.2) and the Goat Mountain earthquakes (ML=4.7) in the Mojave desert, *Bull. Seismol. Soc. Am*. *66*, 2017-2037.

Koketsu, K. et al., (2011), A unified source model for the 2011 Tohoku earthquake, *Earth planet. Sci. Lett.*, *310* (3-4), 480-487, doi:10.1016/j.epsl.2011.09.009.

Mainsant, G., E. Larose, C. Bronnimann, D. Jongmans, C. Michoud, and M. Jaboyedoff (2012), Ambient seismic noise monitoring of a clay landslide: Toward failure prediction, *J. Geophys. Res.*, *117*, F01030,doi:10.1029/2011JF002154.

Meier, U., N.M. Shapiro, and F. Brenguier (2010), Detecting seasonal variations in seismic velocities within Los Angeles basin from correlations of ambient seismic noise, *Geophys. J. Int. 181*, 985-996, doi:10.1111/j.1365-246X.2010.04550.x.

Meunier, J., F. Huguet, and P. Meynier (2001), Reservoir monitoring using permanent sources and vertical receiver antennae: The Cere-la-Ronde case study, *Leading Edge, 20*, 622, doi:10.1190/1.1439008.

Minato, S., T. Tsuji, S. Ohmi, and T. Matsuoka (2012), Monitoring seismic velocity change caused by the 2011 Tohoku-Oki earthquake using ambient noise records, *Geophys. Res. Lett.*, *39*, L03909,doi:10.1029/2012GL051405.

Nakahara, H. (2014), Auto correlation analysis of coda waves from local earthquakes for detecting temporal changes in shallow subsurface structures: the 2011 Tohoku-Oki, Japan earthquake, *Pure Appl. Geophys*. doi:10.1007/s00024-014-0849-0.

Nakata, N. and R. Snieder (2011), Near-surface weakening in Japan after the 2011 Tohoku-Oki earthquake, *Geophys. Res. Lett.*, *38*, L17302, doi:10.1029/2011GL048800.

Nakata, N., and R. Snieder (2012), Estimating near-surface shear wave velocities in Japan by applying seismic interferometry to KiK-net data, *J.Geophys. Res.*, *117*, B01308, doi:10.1029/2011JB008595.

Nishimura, T., N. Uchida, H. Sato, M. Ohtake, S. Tanaka, and H. Hamaguchi (2000), Temporal changes of the crustal structure associated with the M6.1 eartqhuake on Semptember 3, 1998, and the volcanic activity of Mount Iwate, Japan, *Geophys. Res. Lett.*, *27* (2), 269-272, doi:10.1029/1999GL005439.

Nishimura, T., S. Tanaka, H. Yamawaki, H. Yamamoto, T. Sano, M. Sato, H. Nakahara, N. Uchida, S. Hori, and H. Sato (2005), Temporal changes in seismic velocity of the crust around Iwate volcano , Japan, as inferred from analyses of repeated active seismic experiment data from 1998 to 2003, *Earth Planets Space*, *57*, 491-505,doi:10.1186/BF03352583.

Nishimura, T., Y. Ohta, H. Nakahara, and T. Takeda (2013), Seismic velocity changes associated with the 2011 off the Pacific coast of Tohoku earthquake, M9.0, as inferred from correlation analyses of repeating earthquakes, *submitted to Geophys. J. Int*.

Okada, Y., K. Kasahara, S. Hori, K. Obara, S. Sekiguchi, H. Fujiwara, and A. Yamamoto (2004), Recent progress of seismic observation networks in Japan-Hi-net, F-net, K-net and KiK-net-, *Earth Planets Space*, *56*, 15-28.

Obermann, A., T. Planes, E. Larose, C. Sens-Schonfelder, and M. Campillo (2013). Depth sensitivity of seismic coda waves to velocity perturbations in an elastic heterogeneous medium, *Geophys. J. Int., 194*, 372-382,doi:10.1093/gji/ggt043.

Ozawa, S., T. Nishimura, H. Munekane, H. Suito, T. Kobayashi, M. Tobita, and T. Imakiire (2012), Preceding, coseismic and postseismic slips of the 2011 Tohoku earthquake, Japan, *J. Geophys. Res.*, *117* (B07404), doi:10.1029/2011JB009120.

Poupinet, G., W.L. Ellsworth, and J. Frechet (1984), Monitoring velocity variations in the crust using earthquake doublets: An application to the Calaveras Fault, California, *J. Geophys. Res.*, *89* (B7), 5719-5731, doi:10.1029/JB089iB07p05719.

Pujol, J. (1992), Joint hypocentral location in media with lateral velocity variations and interpretation of the station corrections, *Phys. Earth Planet. Inter.*, *75*, 7-24,doi:10.1016/0031-9201(92)90114-B.

Pujol, J., (2000), Joint event location - The JHD technique and applications to data from local seismic networks, in *Advances in Seismic Event Location*, ed. Thurber, C.H. and Rabinowitz, N. 163-204, Kluwer, Academic Publishers, Dordrecht/Boston/London,doi:10.1007/978-94-015-9536-0_7.

Ratdomopurbo, A., and G.. Poupinet (1995). Monitoring a temporal change of seismic velocity in a volcano: Application to the 1992 eruption of Mt.Merapi (Indonesia). *Geophys. Res. Lett.*, *22*, 775-778, doi:10.1029/95GL00302.

Rivet, D., M. Campillo, N.M. Shapiro, V. Cruz-Atienza, M. Radiguet, N. Cotte, and V. Kostoglodov (2011), Seismic evidence of nonlinear crustal deformation during a large slow slip event in Mexico, *Geophys. Res. Lett.*, *38*, L08308, doi:10.1029/2011GL047151.

Rivet, D., M. Campillo, M. Radiguet, D. Zigone, V. Cruz-Atienza, N.M. Shapiro, V. Kostoglodov, N. Cotte, G.. Cougoulat, A. Wapersdorf, and E. Daub (2014), Seismic velocity changes, strain rate and non-volcanic tremors during the 2009-2010 slow slip event in Guerrero, Mexico, *Geophys. J. Int.196,* 447-460, doi:10.1093/gji/ggt374.

Rubinstein, J.L., and G.C. Beroza (2005), Nonlinear strong motion in the ML 5.4 Chittenden earthquake: Evidence that preexisting damage increase susceptibility to further damage, *Geophys. Res. Lett., 31*, L23614, doi:10.1029/2004GL021357.

Rubinstein J.L., and G.C. Beroza (2004), Evidence for widespread nonlinear strong ground motion in the Mw 6.9 Loma Prieta earthquake, *Bull. Seismol. Soc. Am*. *94*(5), 1595-1608, doi 10.1785/012004009.

Rubinstein, J. L., N. Uchida, and G.C. Beroza (2007), Seismic velocity reductions caused by the 2003 Tokachi-Oki earthquake, *J.Geophys. Res.*, *112*, B05315, doi:10.1029/2006JB004440.

Savarensky, E.F. (1968), On the prediction of earthquakes, *Tectonophysics, 6*, 17-27, doi:10.1016/0040-1951(68)90023-1.

Sawazaki, K., H. Sato, H. Nakahara, and T. Nishimura (2009), Time-lapse changes of seismic velocity in the shallow ground caused by strong ground motion shock of the 2000 Western-Tottori earthquake, Japan, as revealed from coda deconvolution analysis, *Bull. Seismol. Soc. Am., 99* (1), 352-366, doi: 10.1785/0120080058.

Sawazaki K., and R. Snieder (2013), Time-lapse changes of P- and S-wave velocities and shear wave splitting in the first year after the 2011 Tohoku earthquake, Japan: shallow subsurface, *Geophys. J. Int.193,* 238-251, doi:10.1093/gji/ggs080.

Schaff, D.P., and G.C. Beroza (2004), Coseismic and postseismic velocity changes measured by repeating earthquakes, *J. Geophys. Res., 109*, B10302, doi. 10.1029/2004JB003011.

Schaff, D.P. (2012), Placing an upper bound on preseismic velocity changes measured by ambient noise monitoring for the 2004 Mw 6.0 Parkfield earthquake (California), *Bull. Seismol. Soc. Am*. *102(4)*, 1400-1416, doi 10.1785/0120110342.

Takagi, R., and T. Okada, (2012), Temporal change in shear velocity and polarization anisotropy related to the 2011 M9.0 Tohoku-Oki earthquake examined using KiK-net vertical array data, *Geophys. Res. Lett.*, *39*, L09310, doi:10.1029/2012GL051342.

Takahashi, H. (2011), Static strain and stress changes in eastern Japan due to the 2011 off the Pacific coast of Tohoku Earthquake, as derived from GPS data, *Earth Planets Space, 63*, 741-744.

Takano T., T. Nishimura, H. Nakahara, Y. Ohta, and S. Tanaka (2014), Seismic velocity changes caused by the Earth tide: Ambient noise correlation analyses of small-array data, *Geophys. Res. Lett.*, *14*, 6131-6136, doi:10.1002/2014GL060690.

Wegler, U., B.G. Luhr, R. Snieder, and A. Ratdomopurbo (2006), Increase of shear wave velocity before the 1998 eruption of Merapi volcano (Indonesia), *Geophys. Res. Lett.*, *33*, L09303, doi:10.1029/2006GL025928.

Wegler, U., and C. Sens-Schonfelder (2007), Fault zone monitoring with passive image interferometry, *Geophys. J. Int.,168* , 1029-1033, doi:10.1111/j.1365-246X.2006.03284.x.

Wegler, U., H. Nakahara, C. Sens-Schonfelder, M. Korn, and K. Shiomi, (2009), Sudden drop of seismic velocity after the 2004 Mw 6.6 mid-Niigata earthquake, Japan, observed with Passive Image Interferometry, *J. Geophys. Res. 114*, B06305, doi: 10.1029/2008JB005869.

Wu, C., and Z. Peng, (2011), Temporal changes of site response during the 2011 Mw 9.0 off the Pacific coast of Tohoku Earthquake, *Earth Planets Space*, *63*, 791-795, doi:10.5047/eps.2011.06.011.

Wyss, M. (1975), Precursors to the Garm Earthquake of March 1969, *J. Geophys. Res., 80*, 2926-2930, doi:10.1029/JB08i020p02926.

Yamamura , K., O. Sano, H. Utada, Y. Takei, S. Nakao, and Y. Fukao (2003), Long-term observation of in situ seismic velocity and attenuation, *J. Geophys. Res. 108* (B6), 2317, doi:10.1029/2002JB002005.

Zaccarelli, L., D. Pandolfi, F. Bianco, G.. Saccorotti, C.J. Bean, and E. Del Pezzo (2009), Temporal changes in seismic wave propagation towards the end of the 2002 Mt Etna eruption, *Geophys. J. Int.,178* , 1779-1788, doi:10.1111/j.1365-246X.2009.04219.x.

Appendix

Appendix.A1

Figures A1.1-A1.19 show the observed and predicted arrival time differences estimated from the inversion of the pairs of 25 repeating earthquakes for the P- and S-waves. Results of events 7 to 25 are shown.

(a)

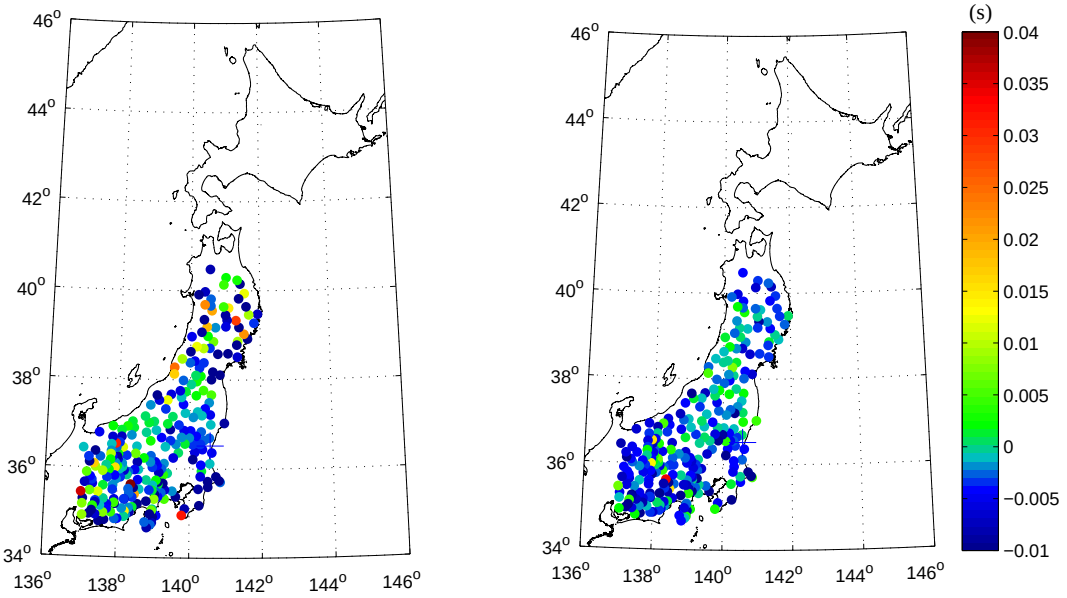

(b)

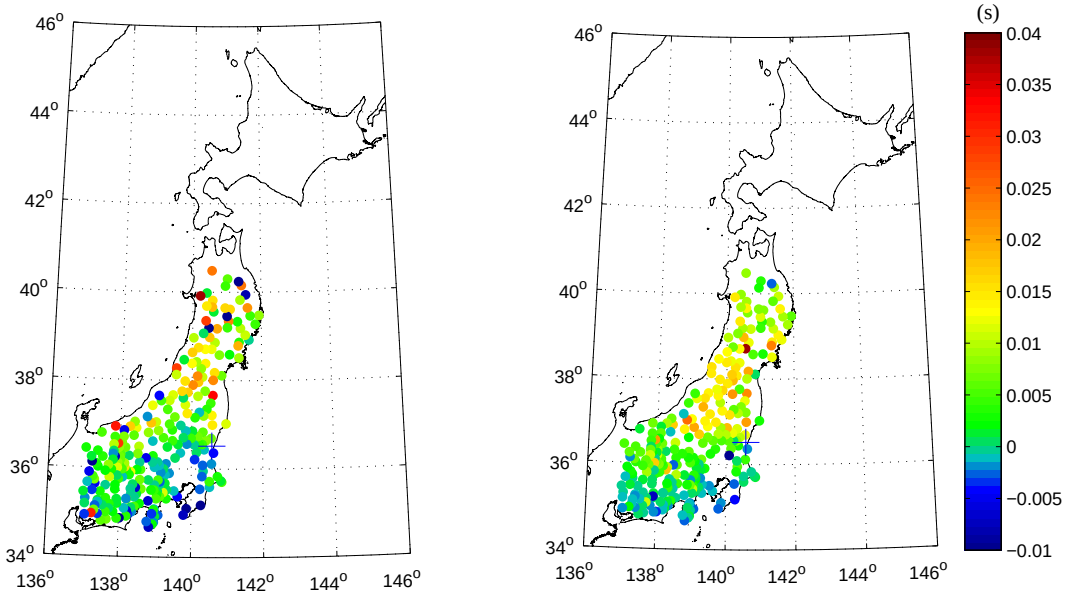

Figure A1.1. Observed (left panels) and predicted arrival time differences (right panels) of (a) P-waves and (b) S-waves for event 7. Color scale indicates arrival time difference in seconds. Crosses show the location of the repeating earthquake source.

(a)

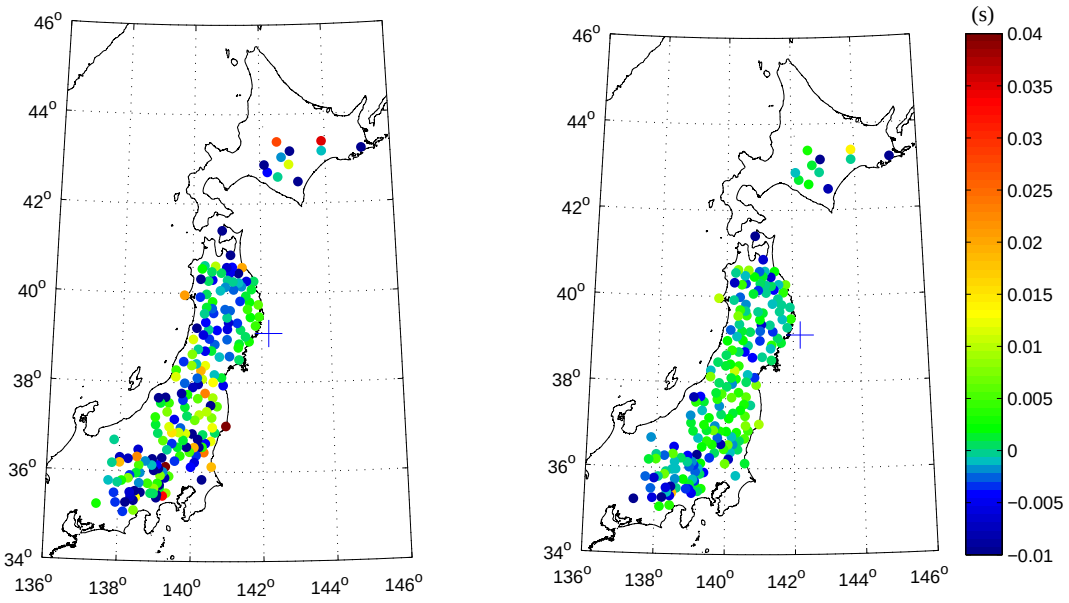

(b)

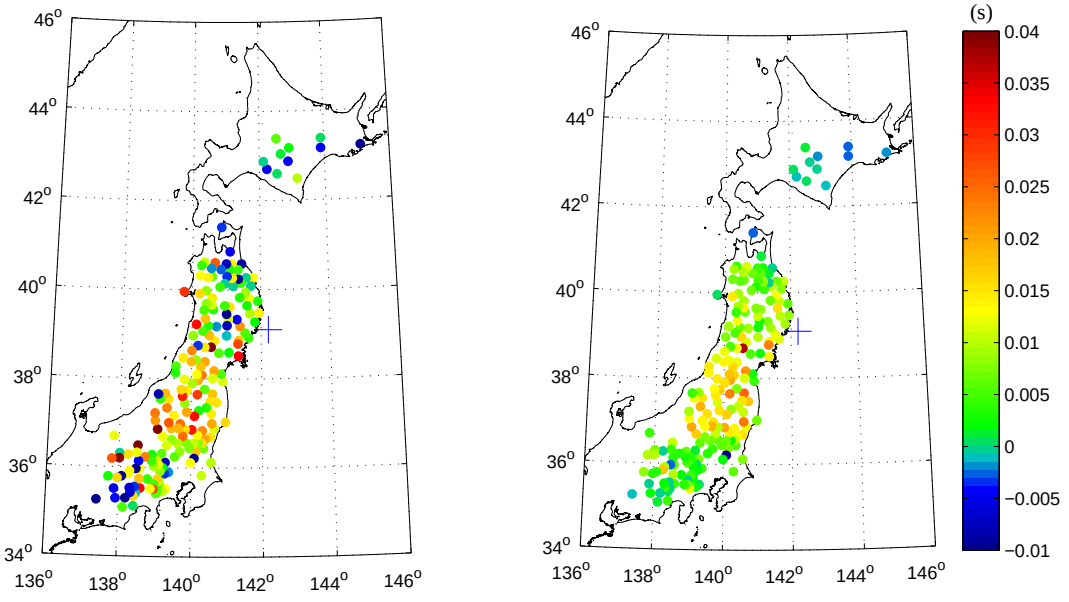

Figure A1.2. Same as Figure A1.1 but for event 8.

(a)

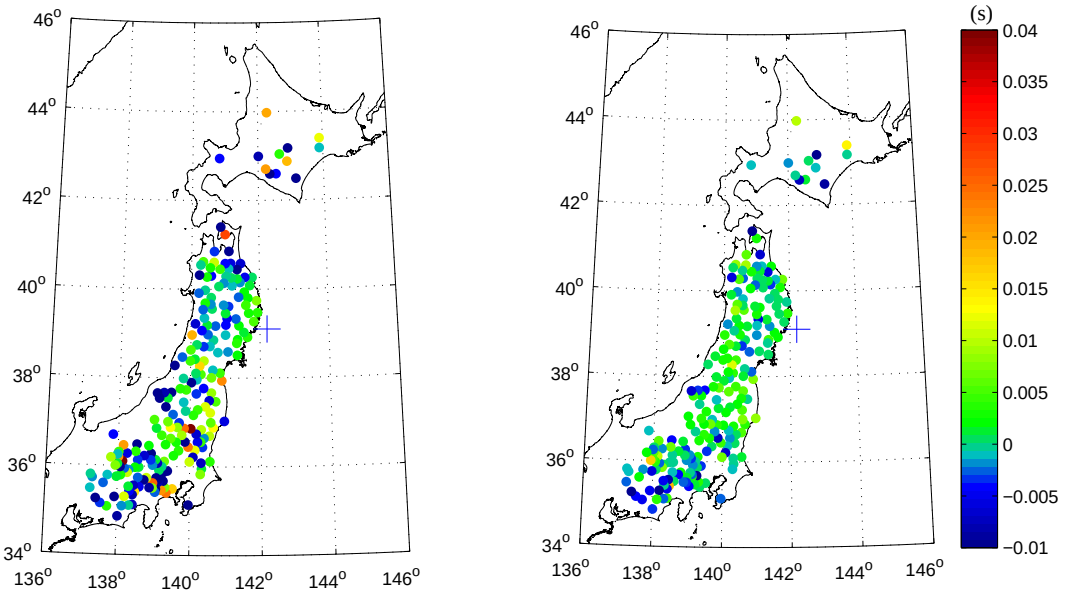

(b)

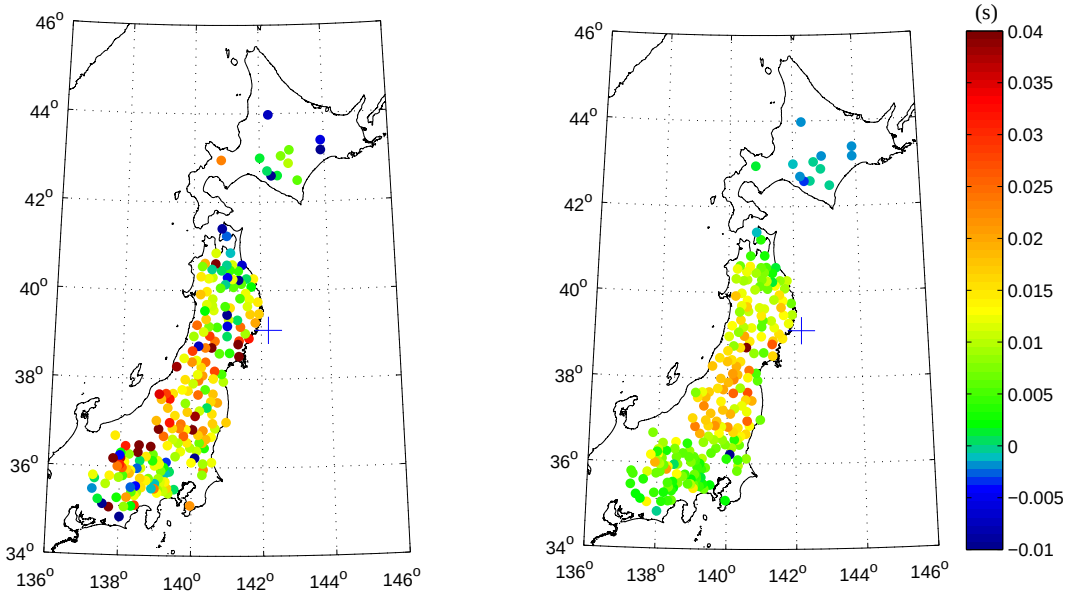

Figure A1.3. Same as Figure A1.1 but for event 9.

(a)

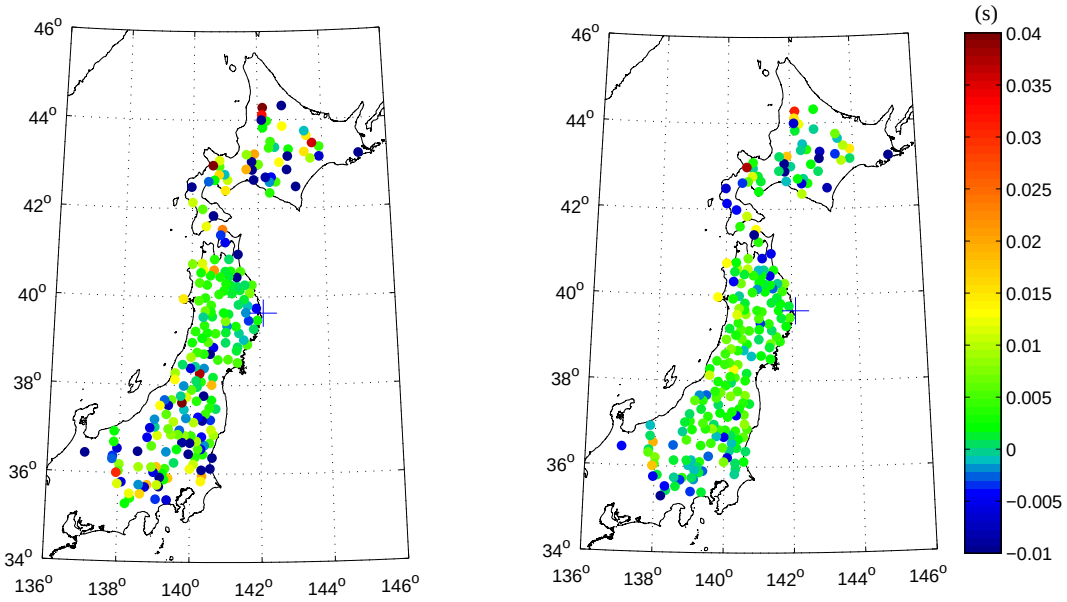

(b)

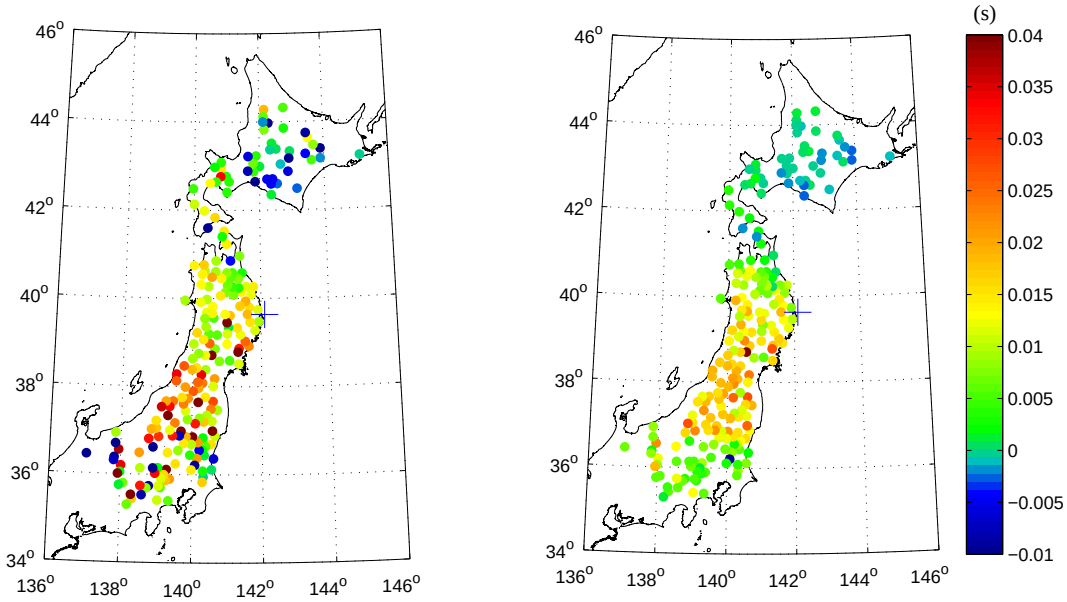

Figure A1.4. Same as Figure A1.1 but for event 10.

(a)

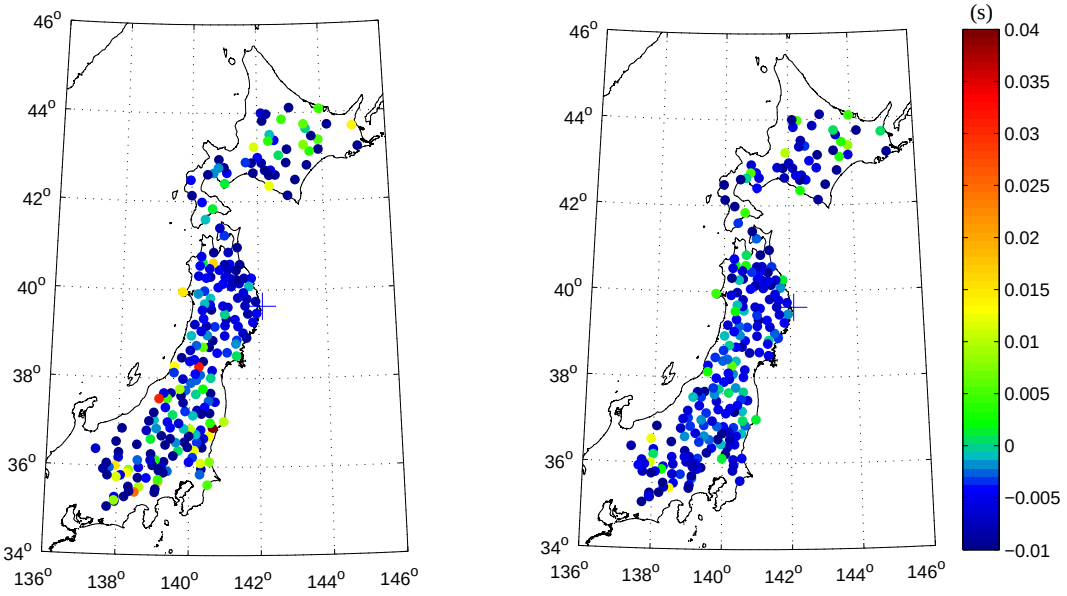

(b)

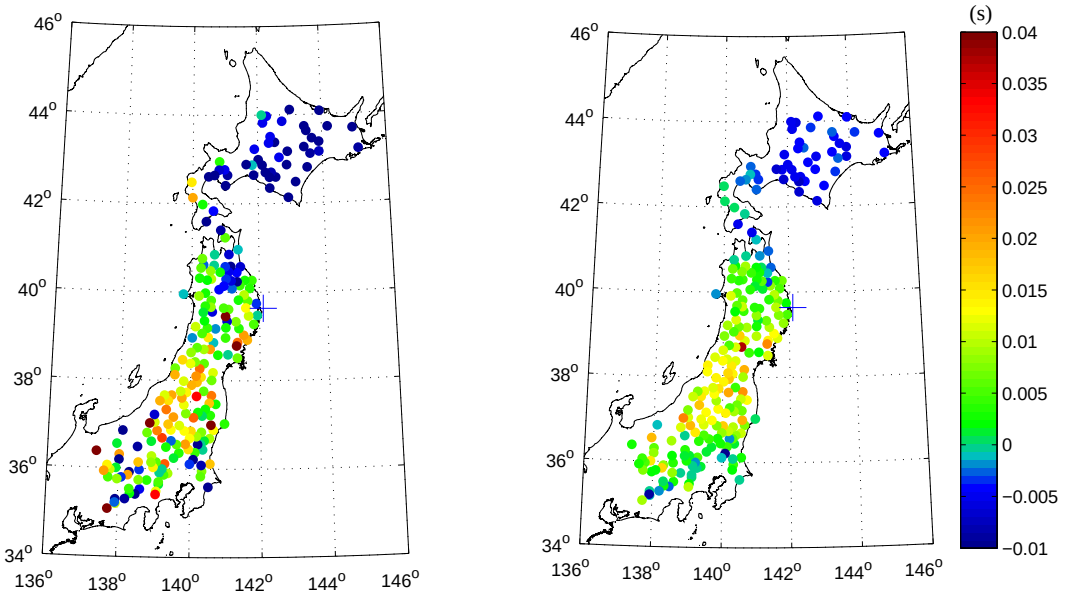

Figure A1.5. Same as Figure A1.1 but for event 11.

(a)

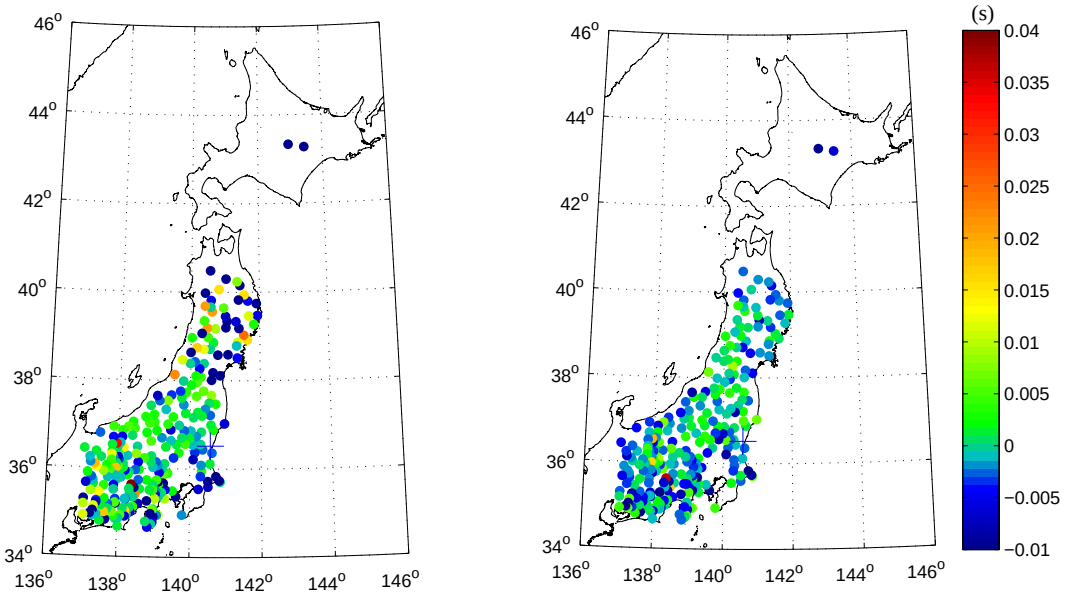

(b)

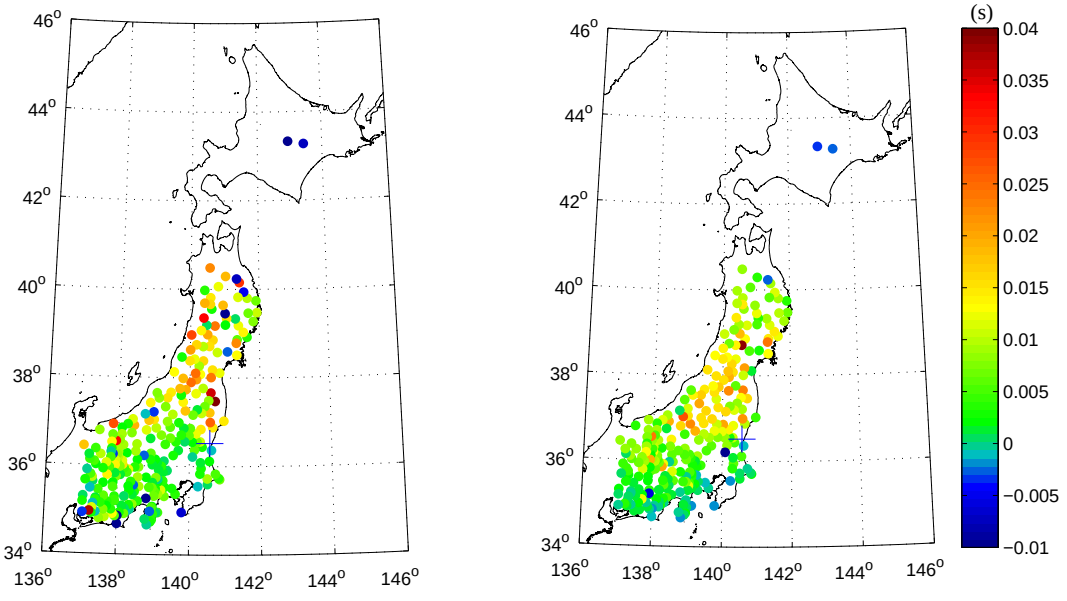

Figure A1.6. Same as Figure A1.1 but for event 12.

(a)

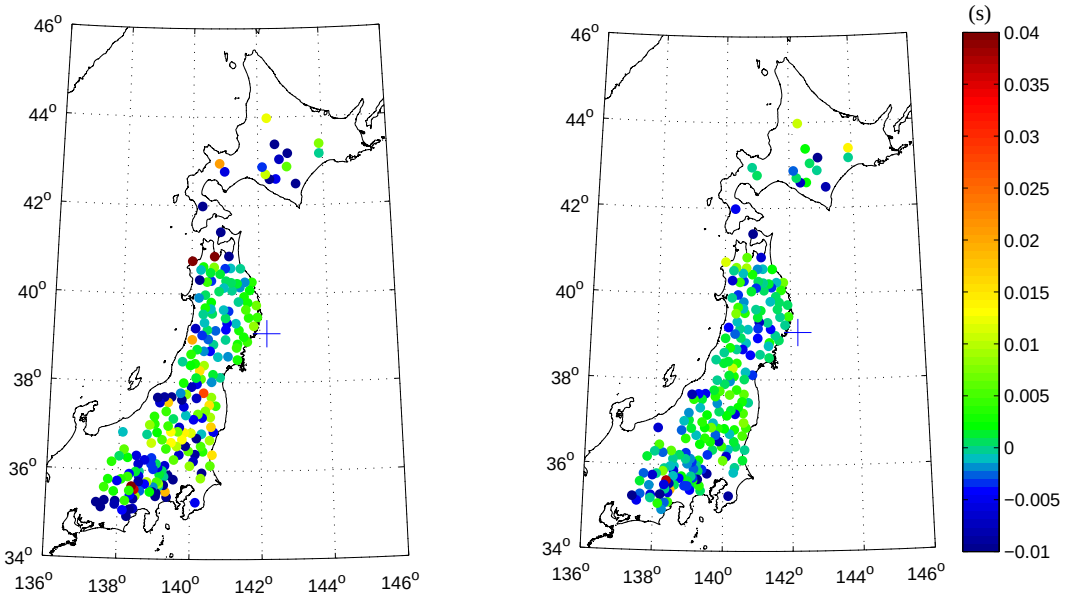

(b)

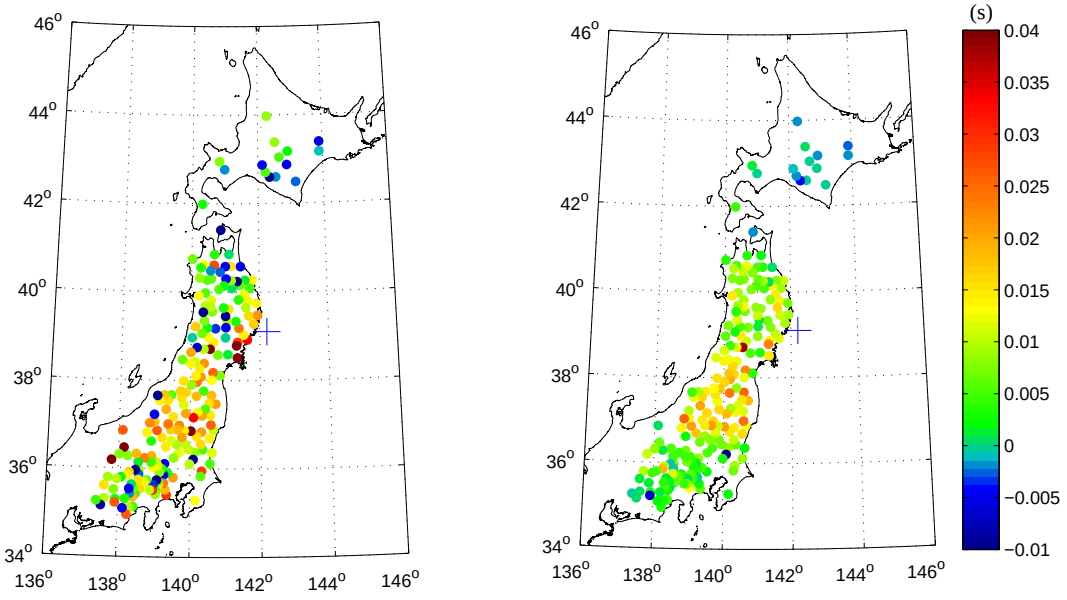

Figure A1.7. Same as Figure A1.1 but for event 13.

(a)

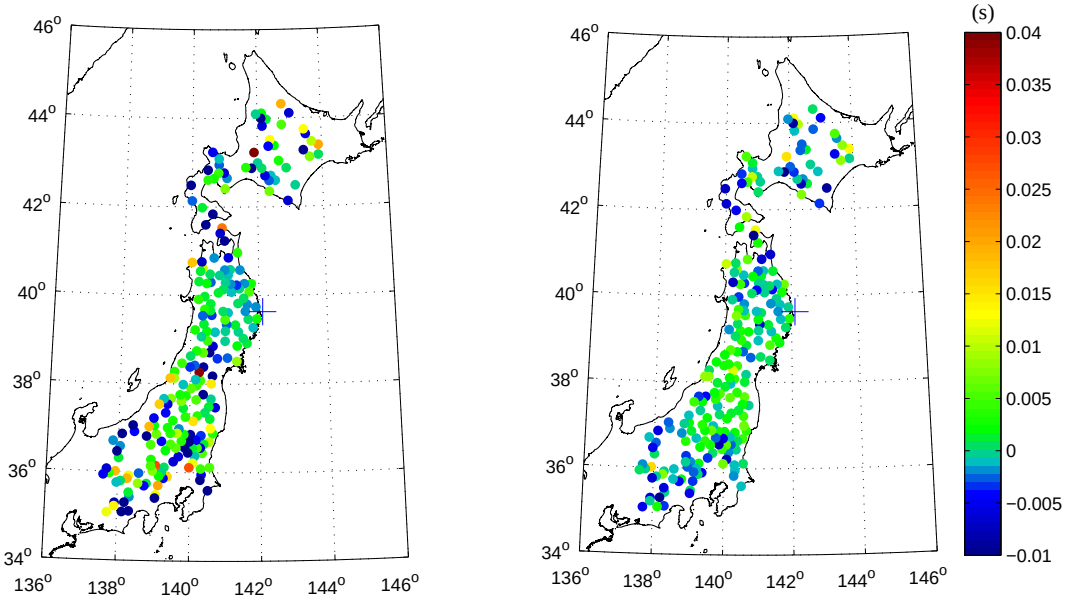

(b)

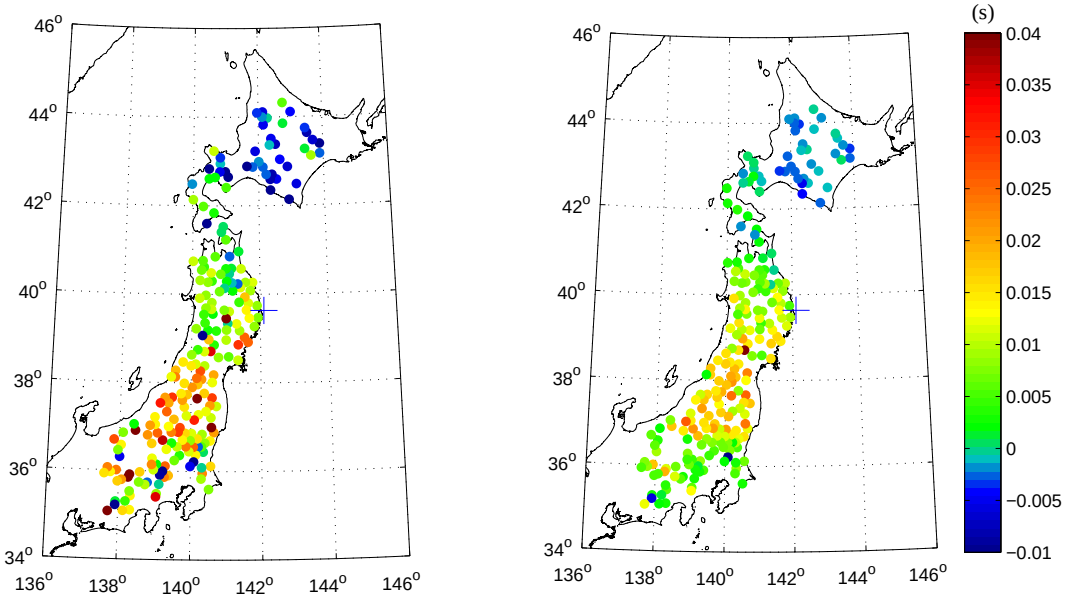

Figure A1.8. Same as Figure A1.1 but for event 14.

(a)

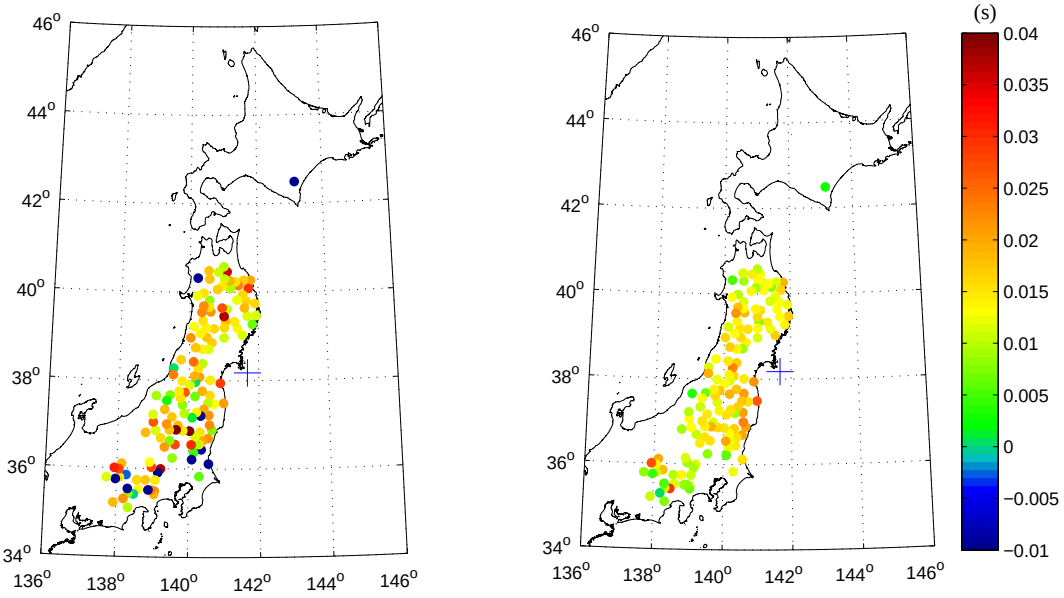

(b)

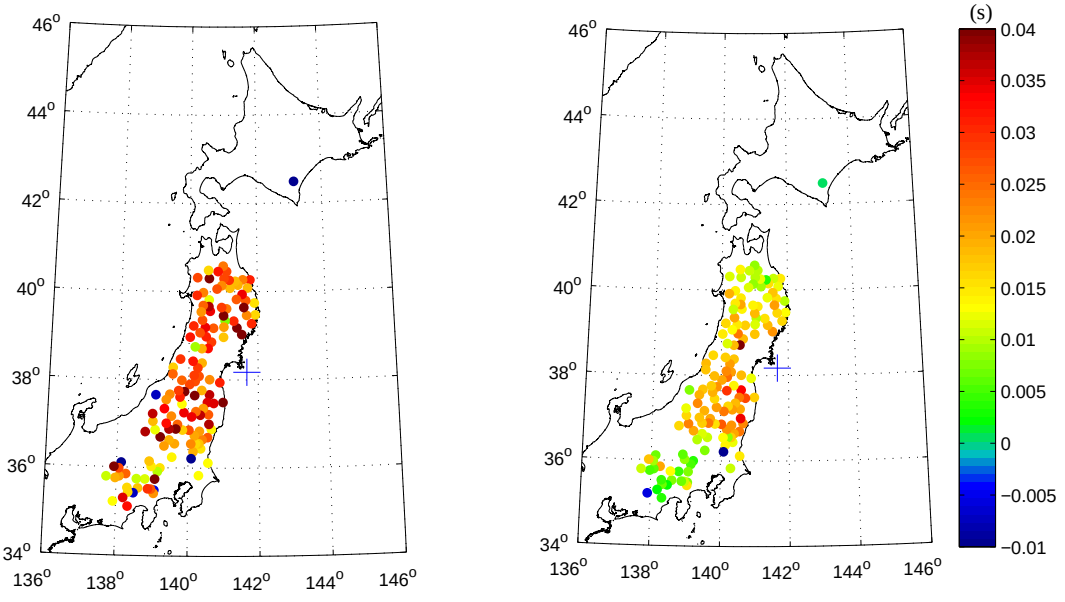

Figure A1.9. Same as Figure A1.1 but for event 15.

(a)

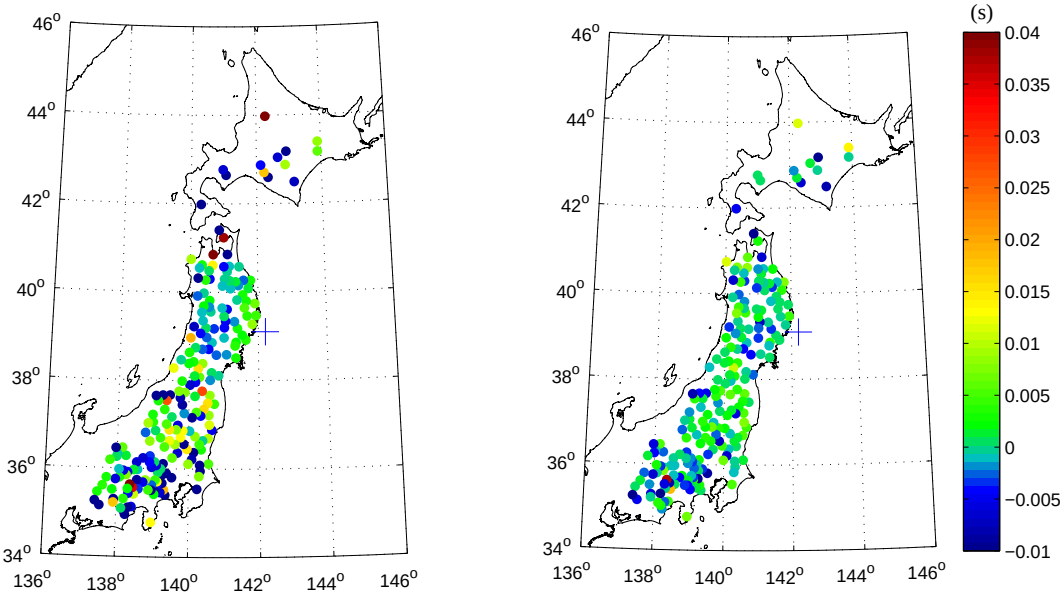

(b)

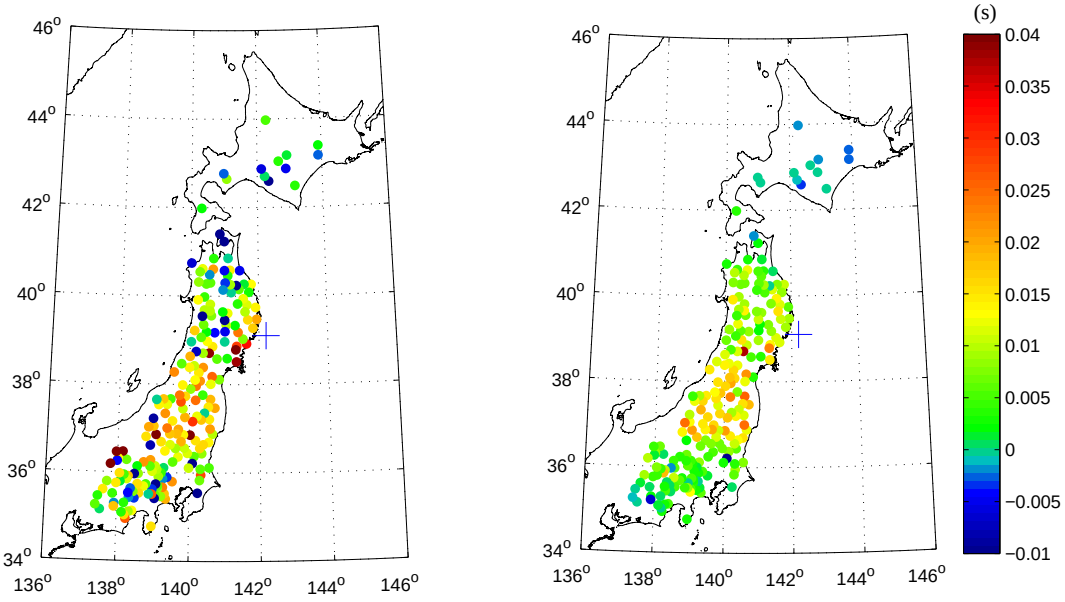

Figure A1.10. Same as Figure A1.1 but for event 16.

(a)

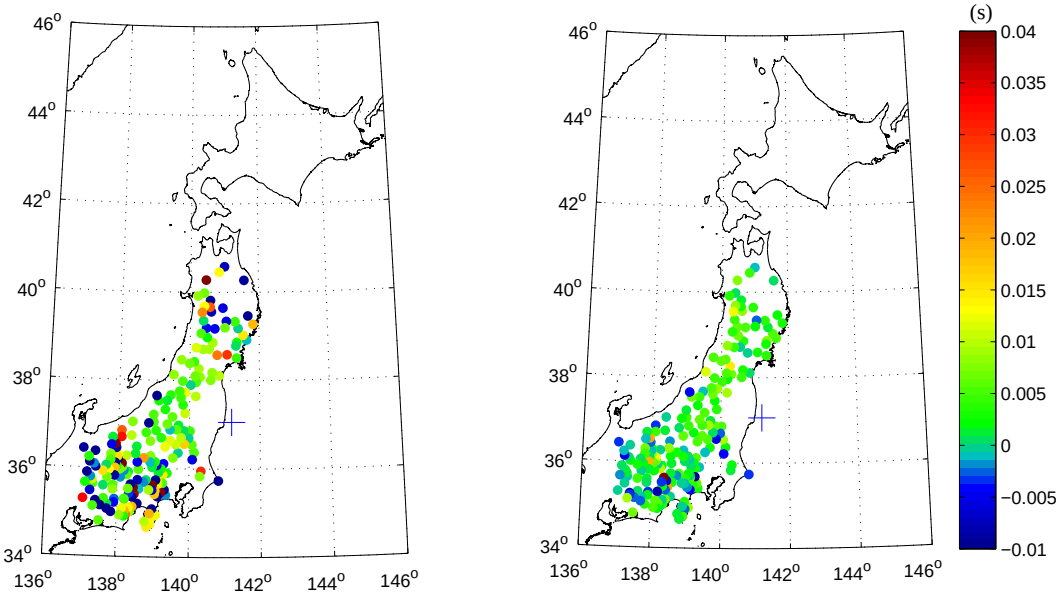

(b)

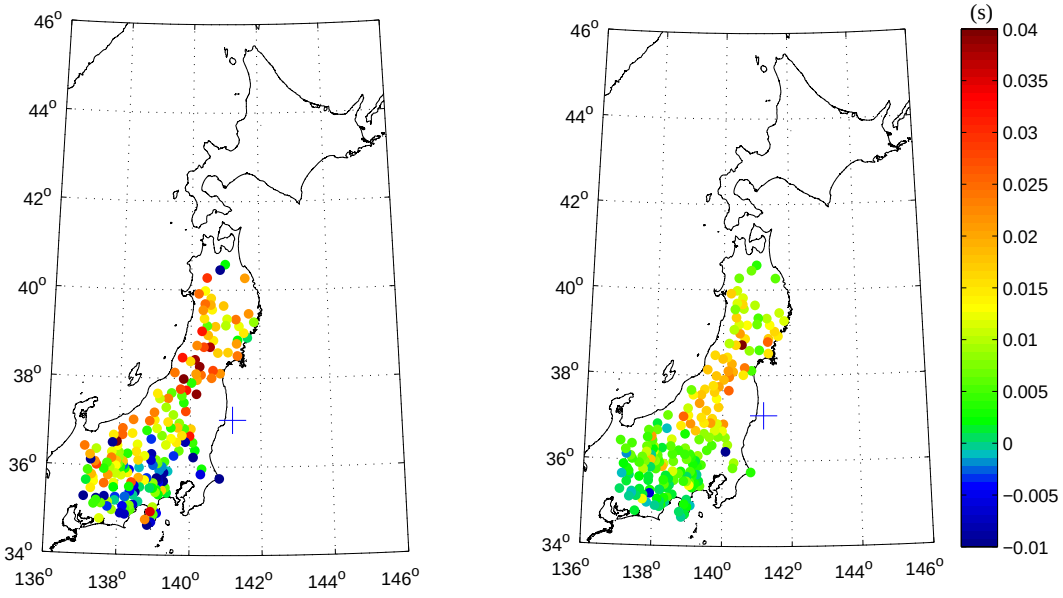

Figure A1.11. Same as Figure A1.1 but for event 17.

(a)

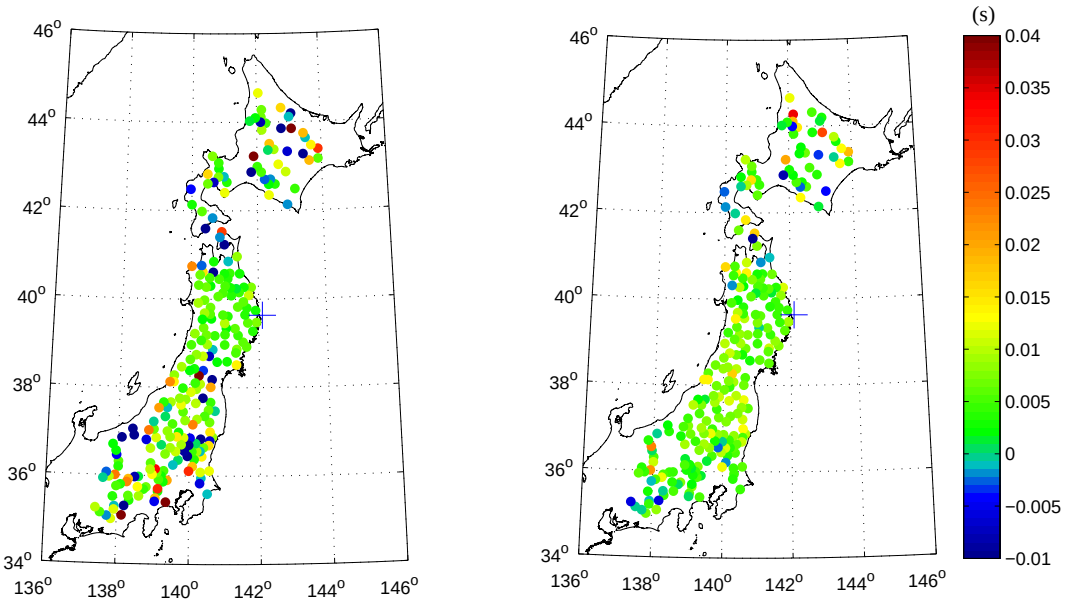

(b)

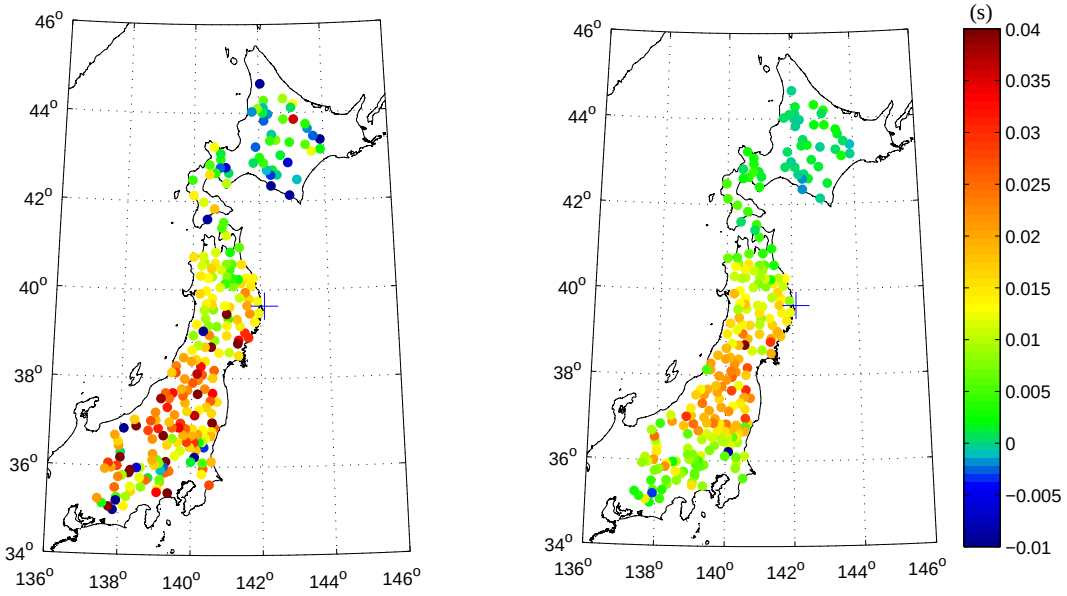

Figure A1.12. Same as Figure A1.1 but for event 18.

(a)

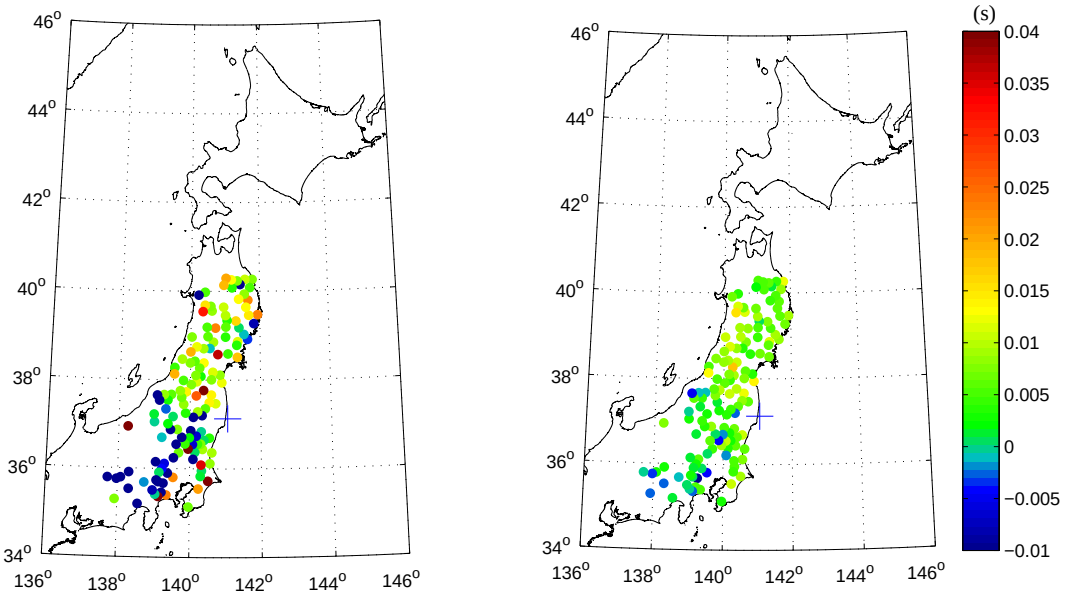

(b)

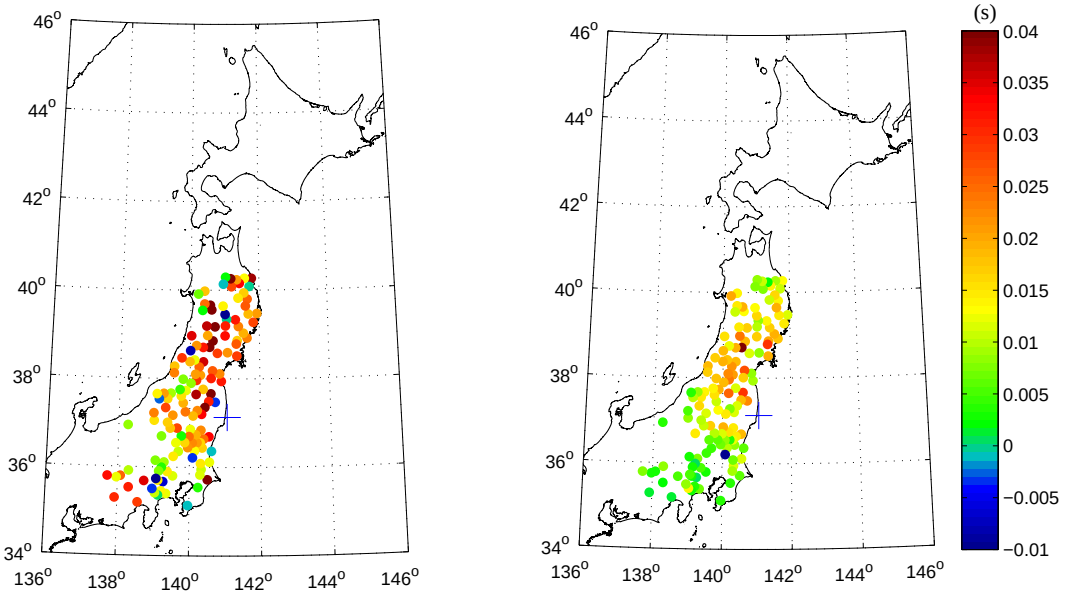

Figure A1.13. Same as Figure A1.1 but for event 19.

(a)

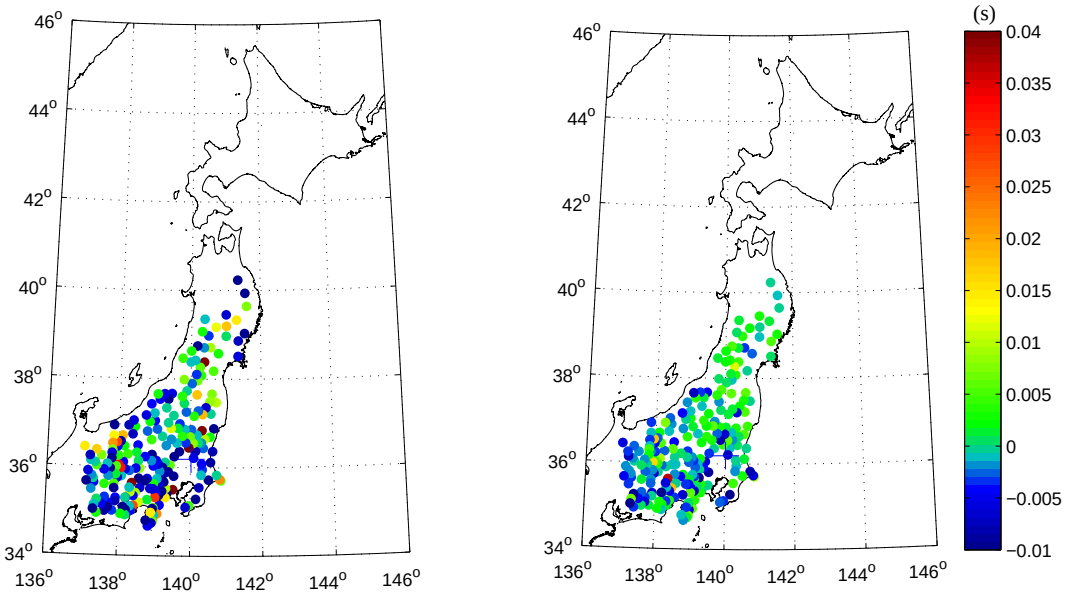

(b)

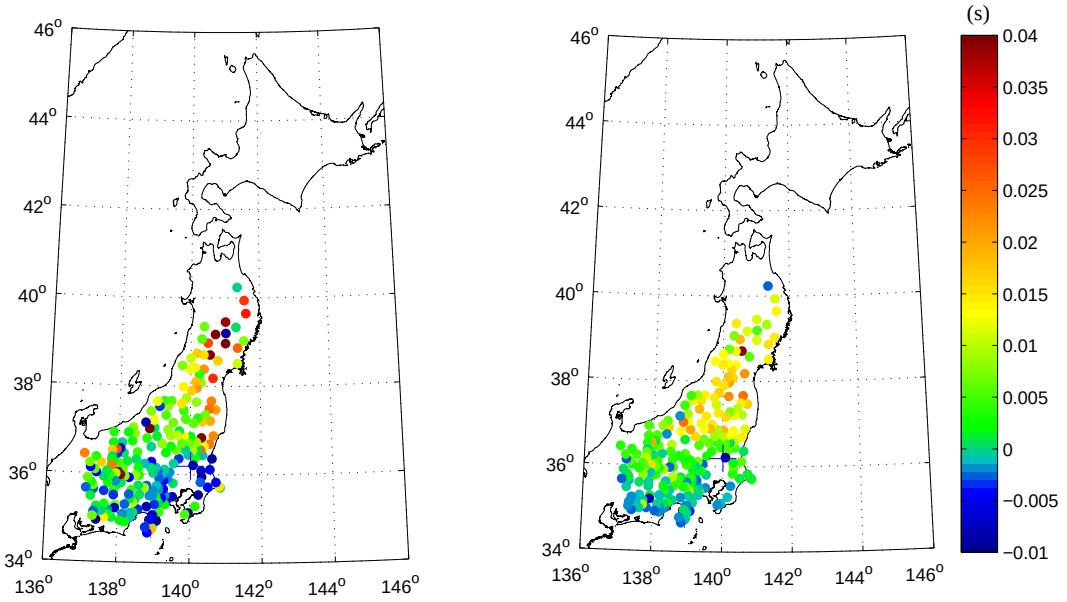

Figure A1.14. Same as Figure A1.1 but for event 20.

(a)

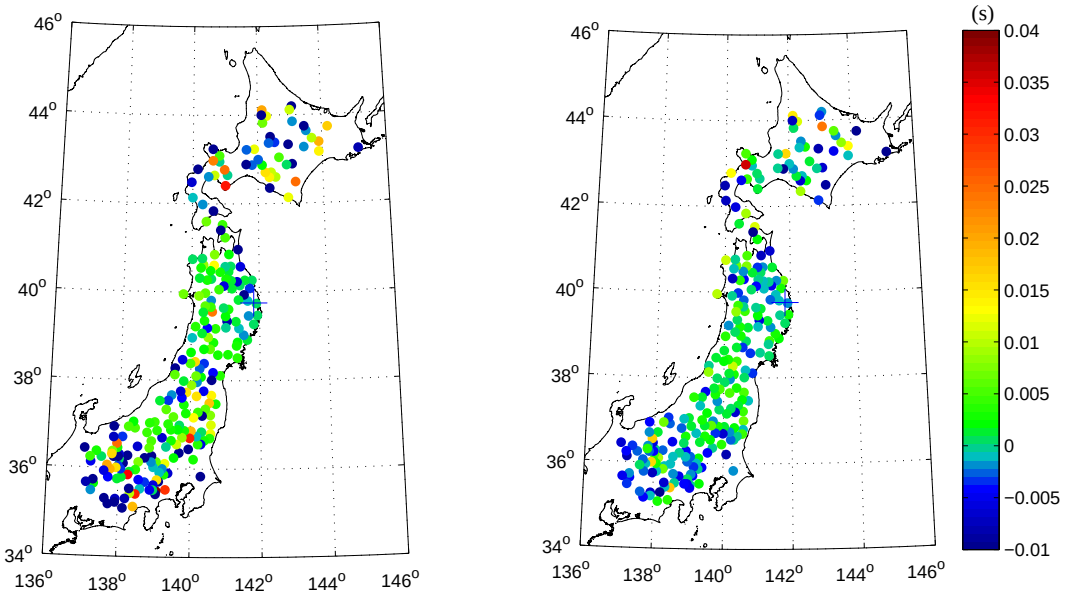

(b)

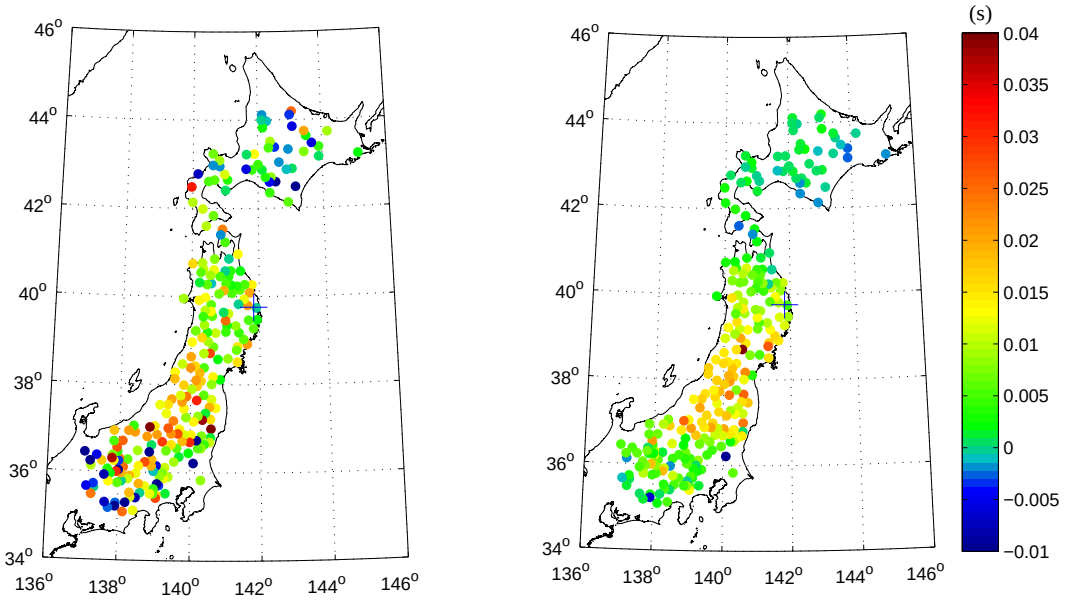

Figure A1.15. Same as Figure A1.1 but for event 21.

(a)

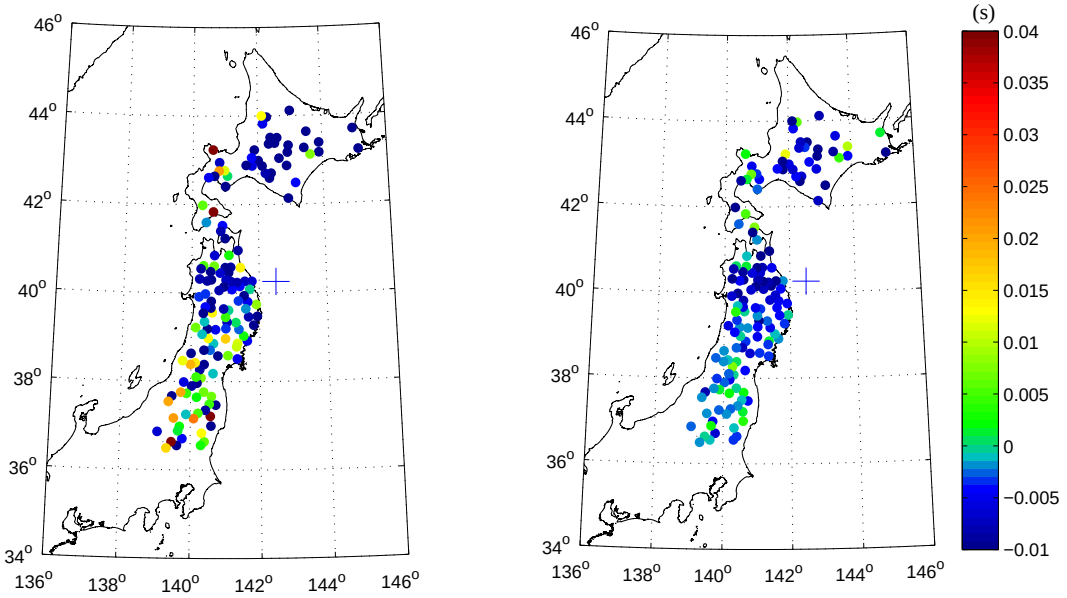

(b)

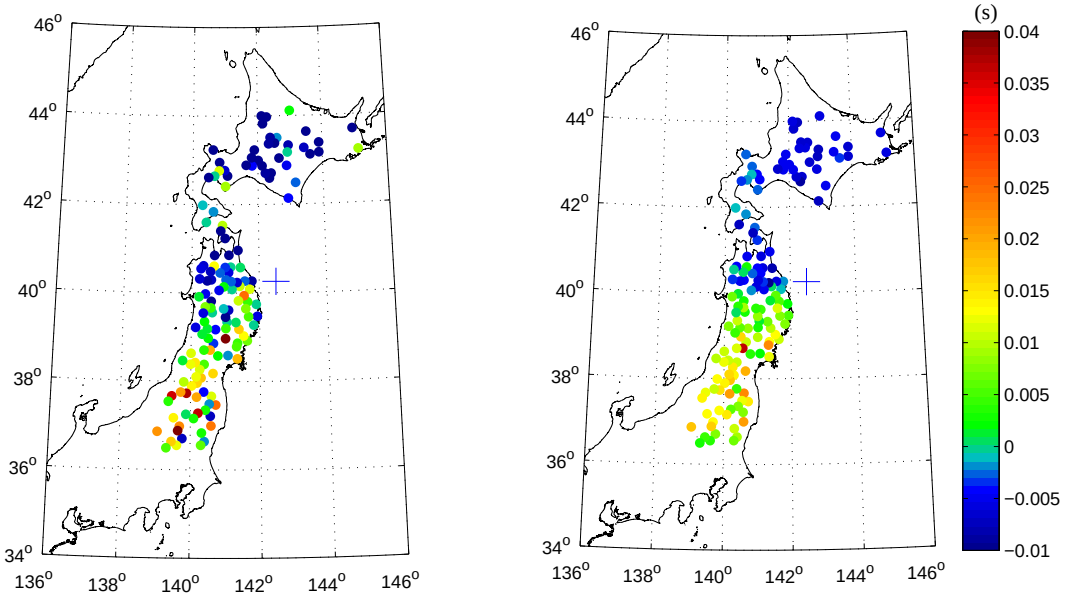

Figure A1.16. Same as Figure A1.1 but for event 22.

(a)

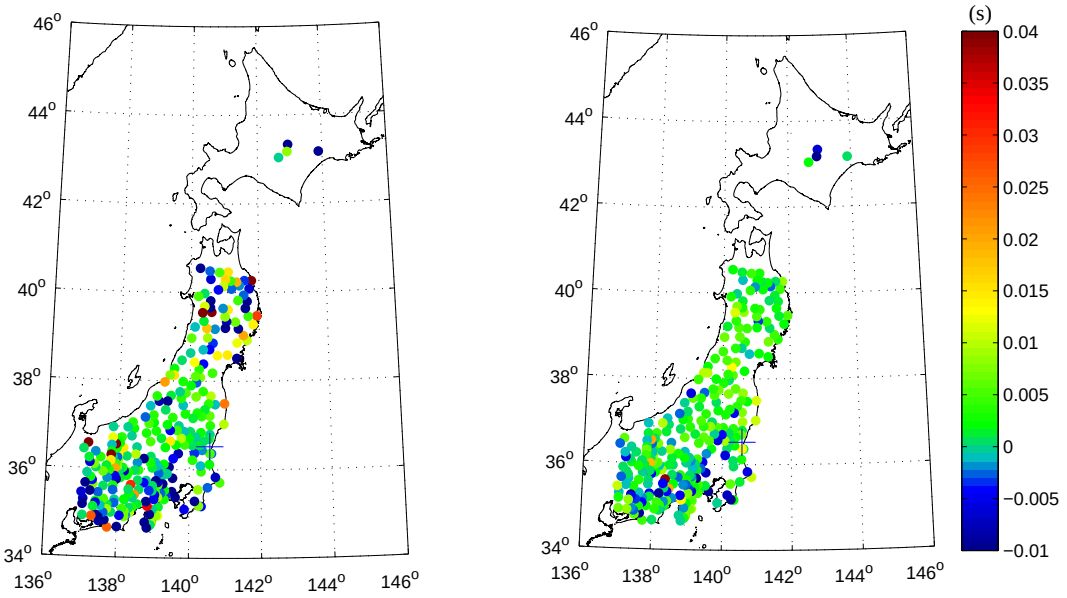

(b)

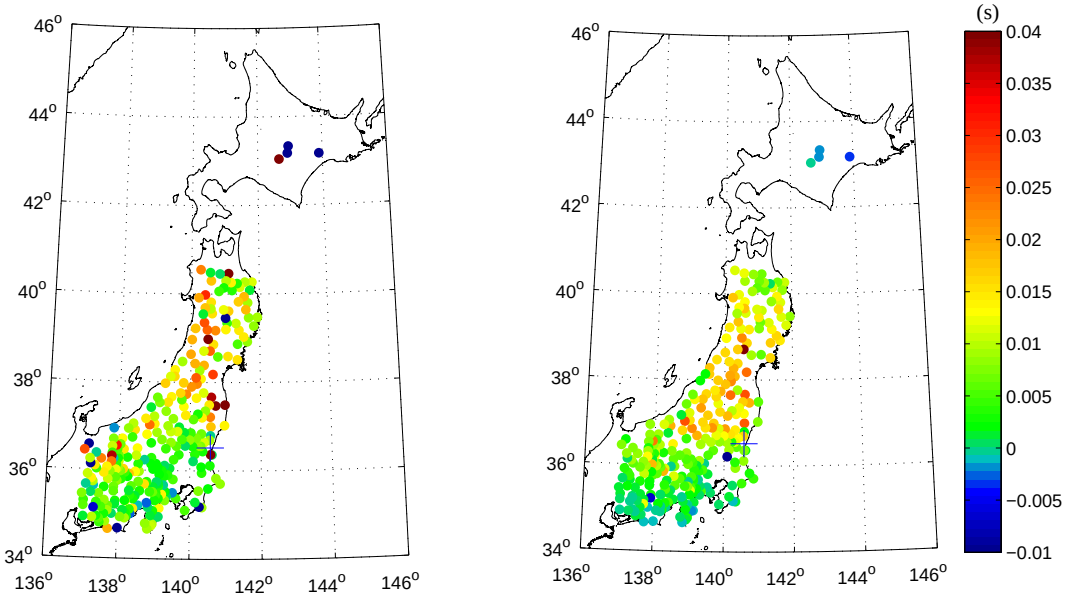

Figure A1.17. Same as Figure A1.1 but for event 23.

(a)

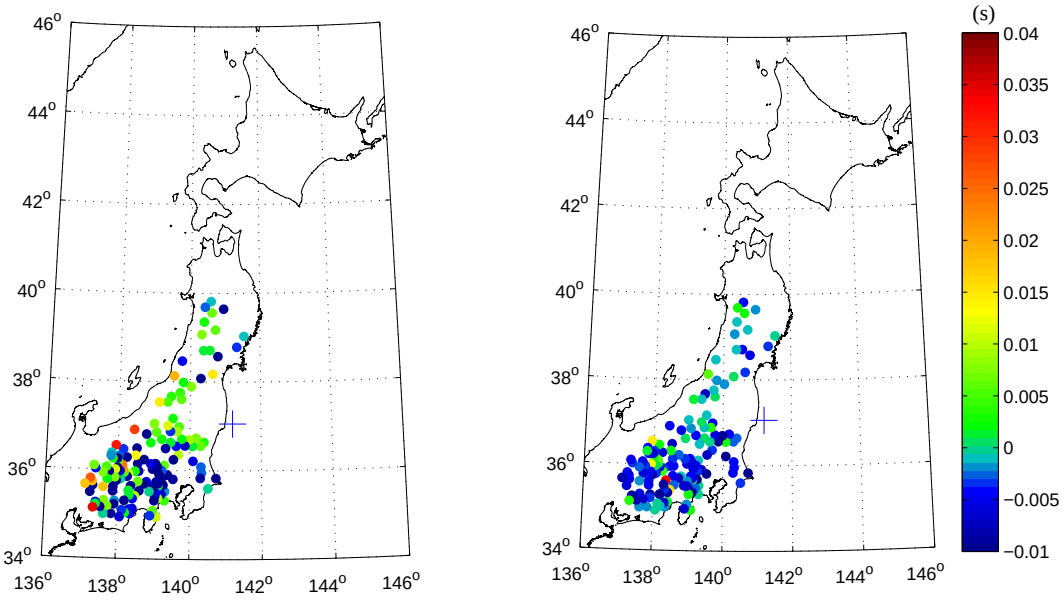

(b)

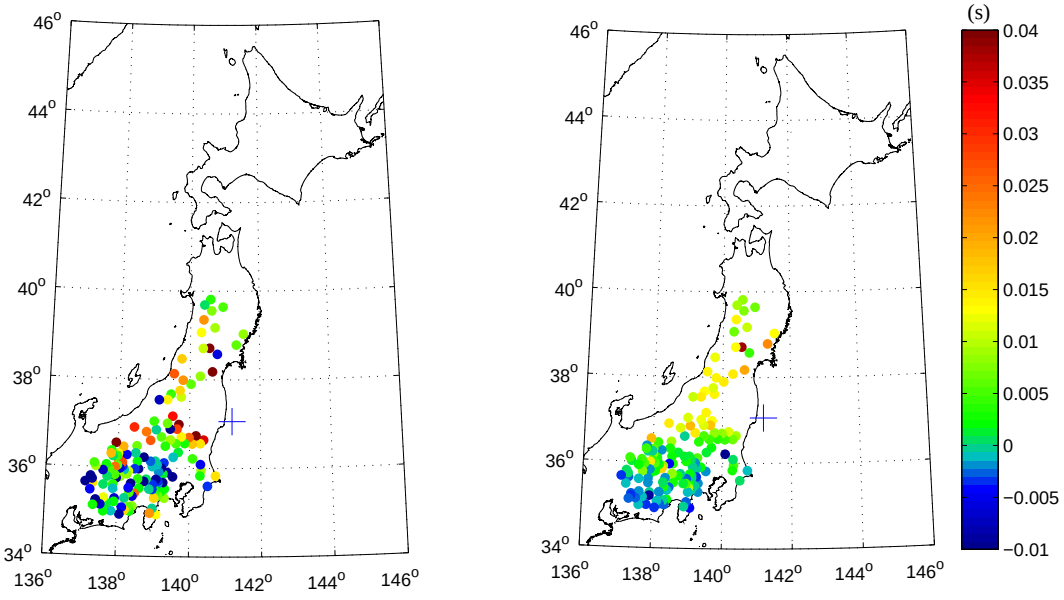

Figure A1.18. Same as Figure A1.1 but for event 24.

(a)

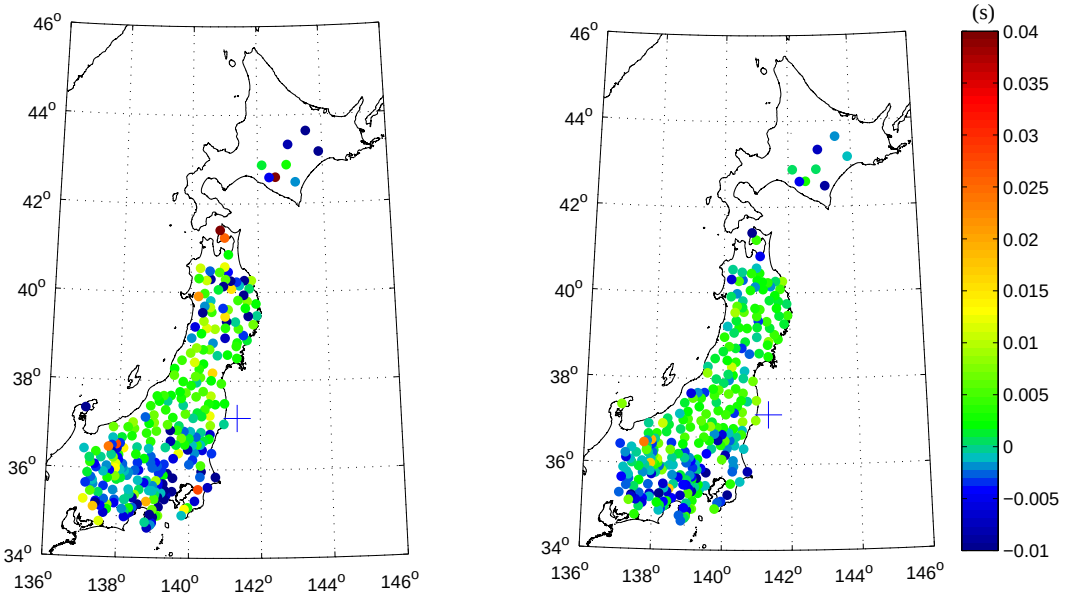

(b)

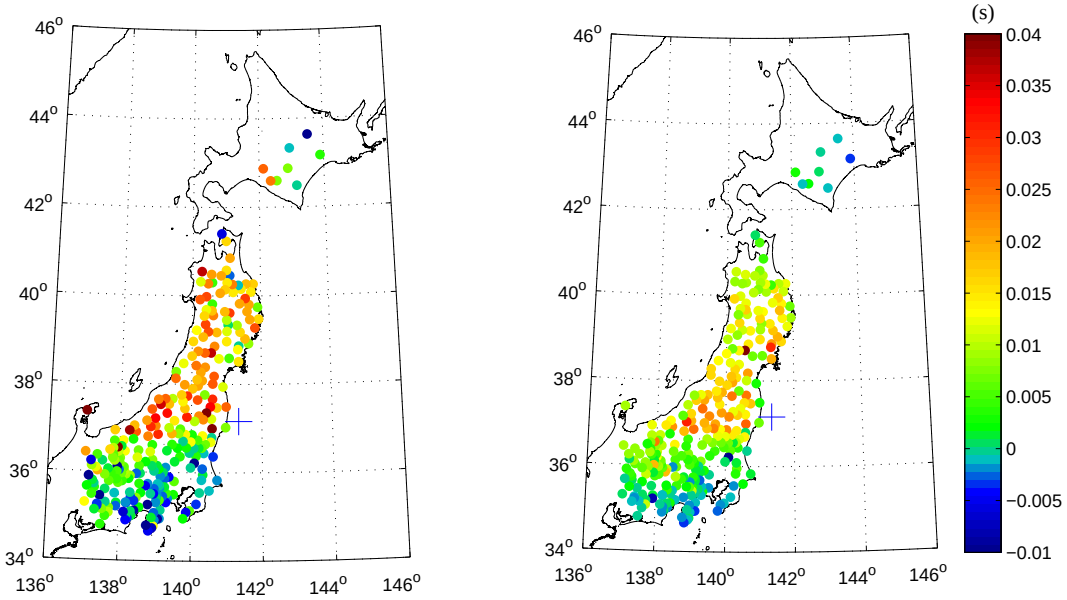

Figure A1.19. Same as Figure A1.1 but for event 25.

Appendix.A2

Figures A2.1-A2.6 show EW-component seismograms of events 1-6 recorded by stations of KiK-net network at the borehole (a) and ground surface (b).

(a)

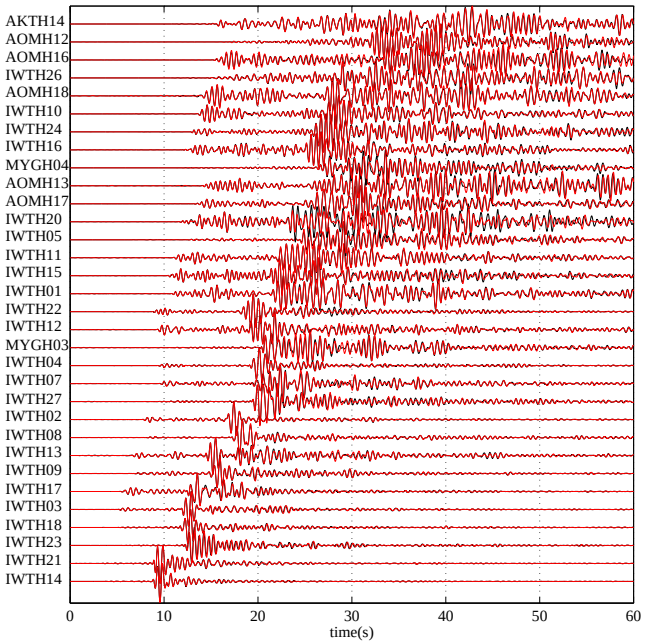

(b)

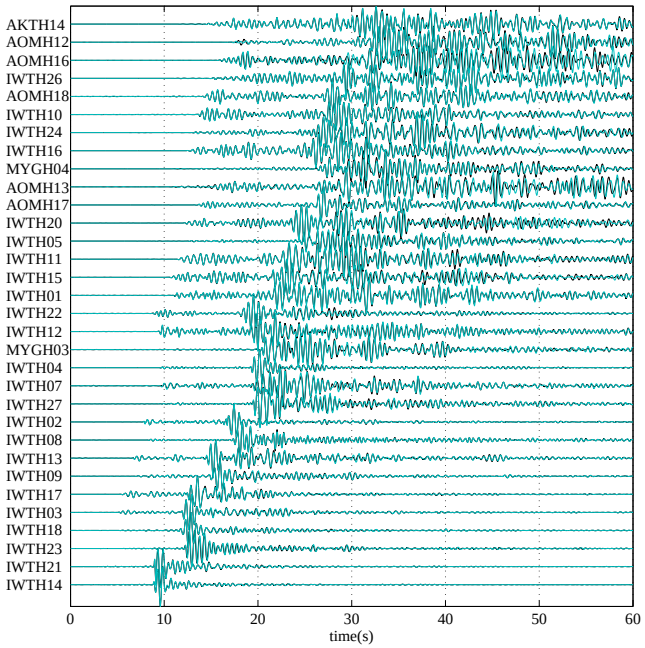

Figure A2.1. Waveforms observed at the borehole (a) and ground surface (b) sensors of KiK-net seismic network. Station code is indicated in the left. Black and red (or blue) lines correspond to the waveform recorded before and after the Tohoku-Oki earthquake, respectively. This figure shows the case of event 1.

(a)

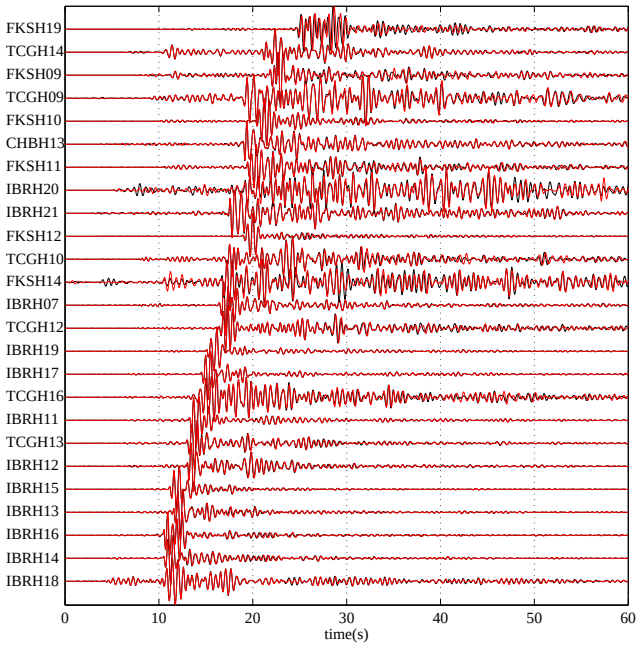

(b)

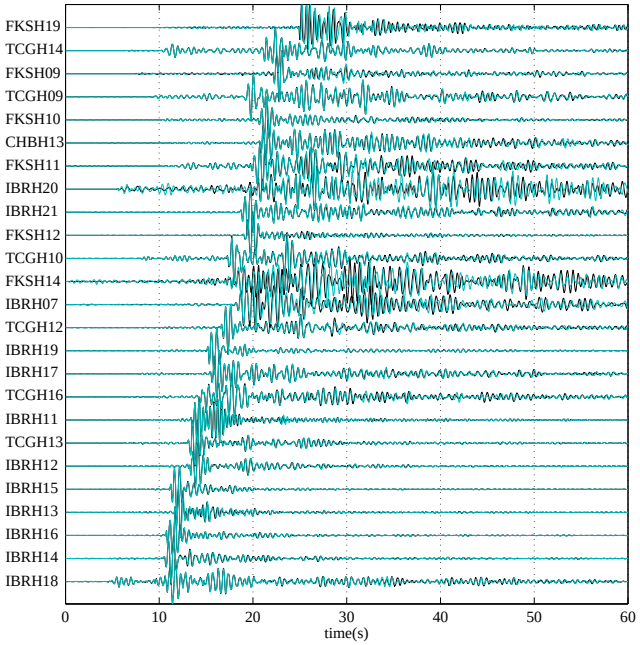

Figure A2.2. Same as Figure A2.1 but for event 2.

(a)

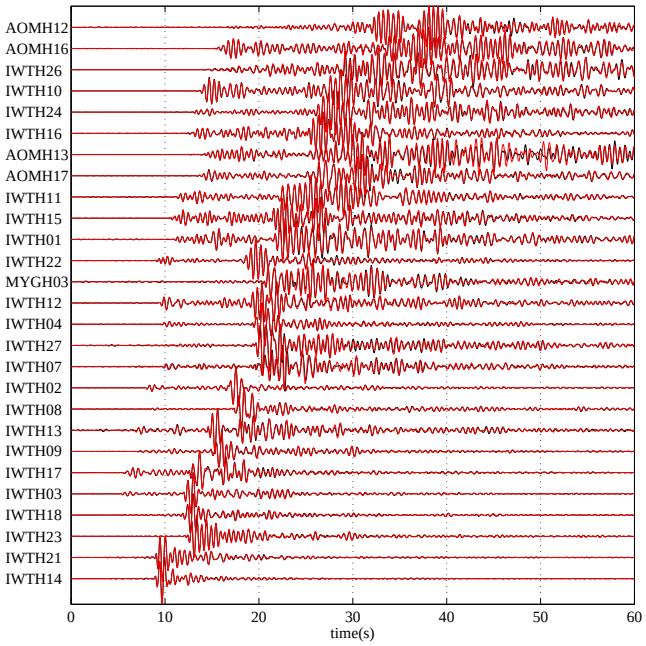

(b)

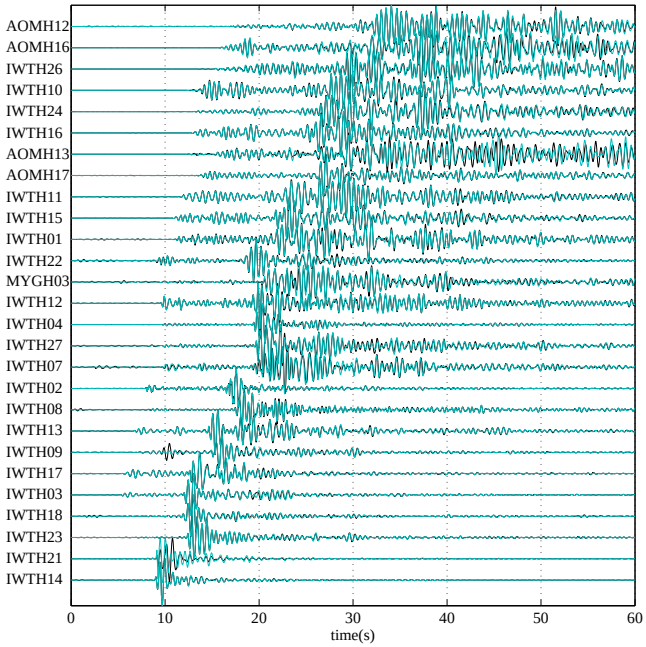

Figure A2.3. Same as Figure A2.1 but for event 3.

(a)

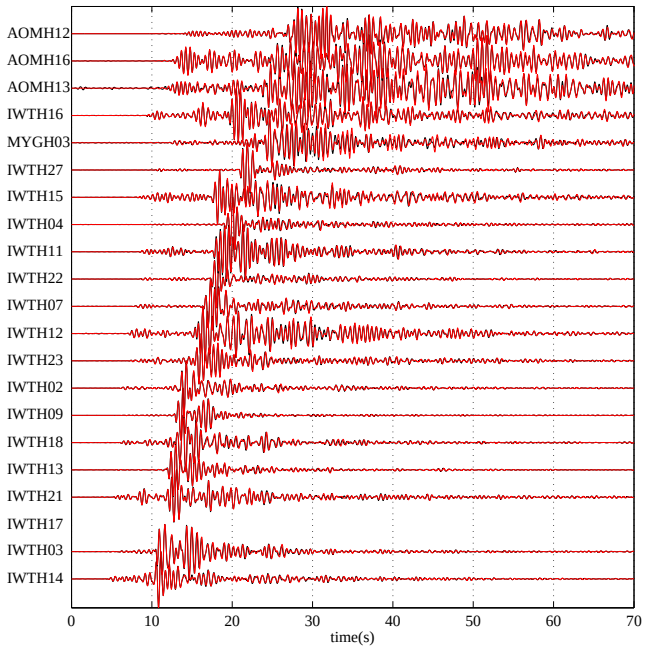

(b)

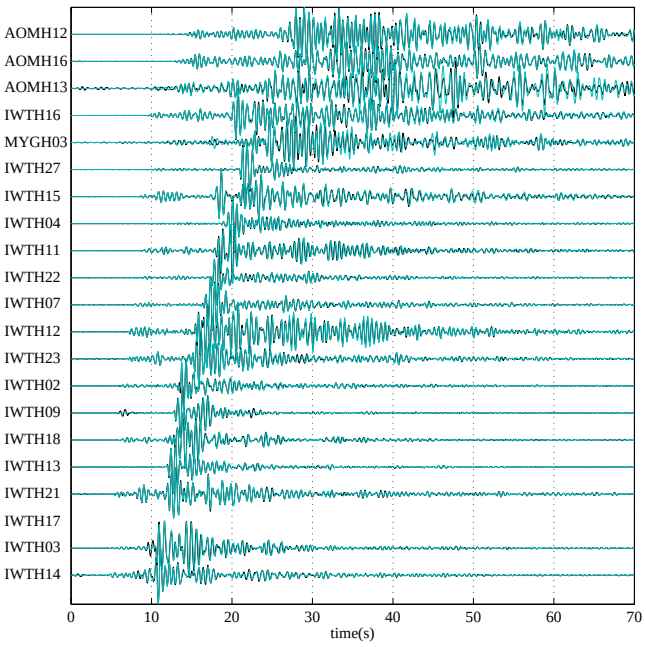

Figure A2.4. Same as Figure A2.1 but for event 4.

(a)

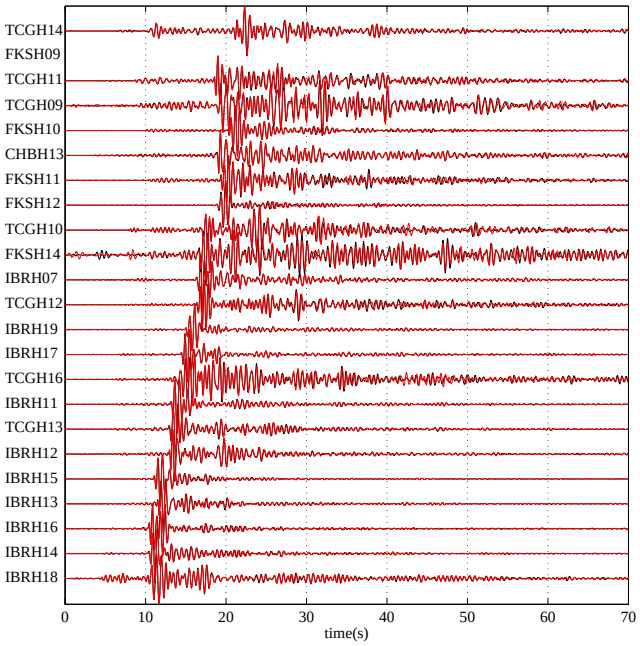

(b)

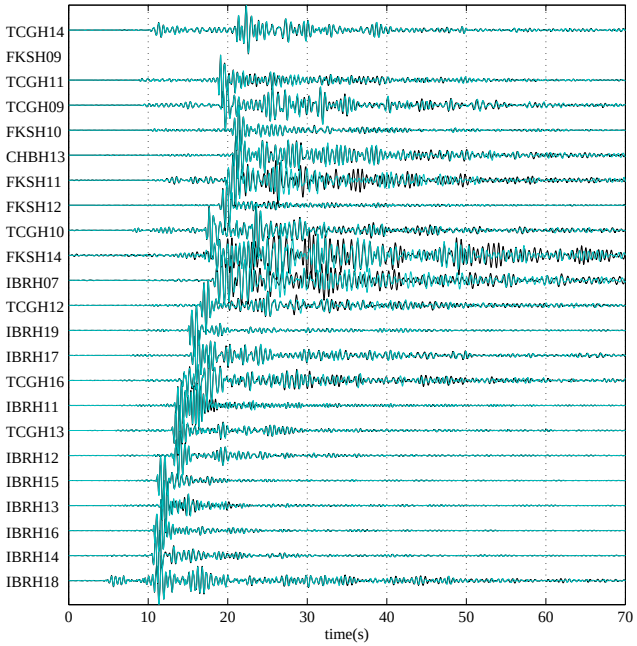

Figure A2.5. Same as Figure A2.1 but for event 5.

(a)

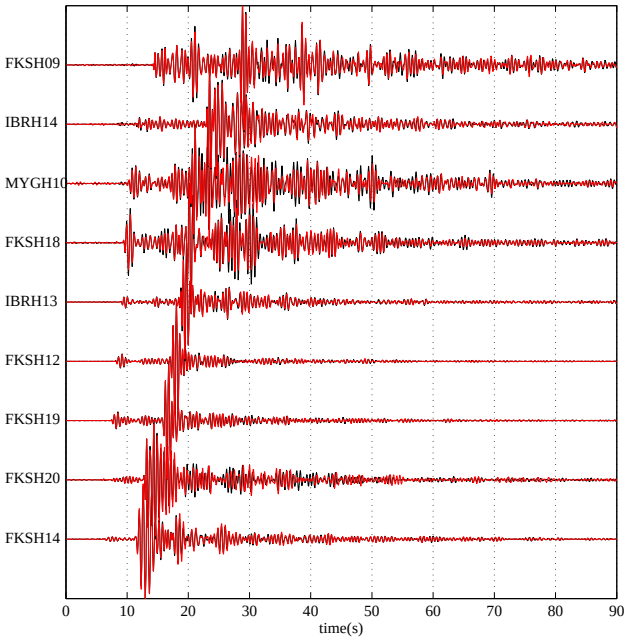

(b)

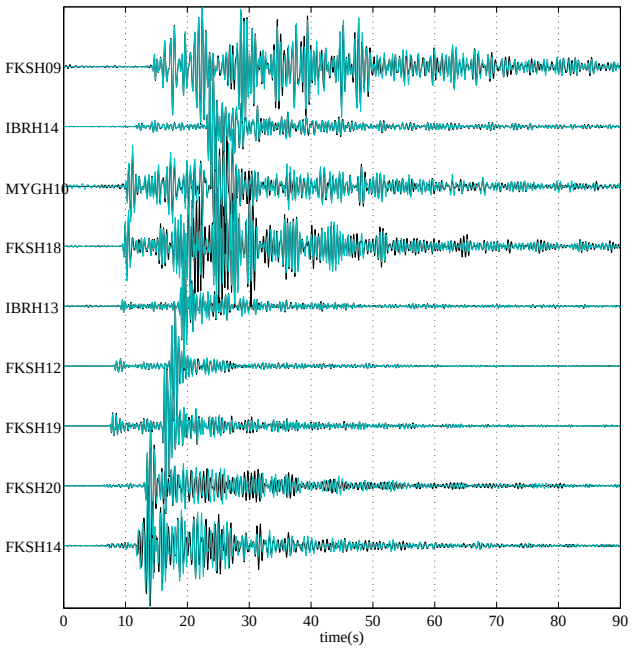

Figure A2.6. Same as Figure A2.1 but for event 6.

Appendix.A3

Figures A3.1-A3.7 show the results of the Jackknife that is applied to 25 pairs of repeating earthquakes (see text in detail). Each figure shows histograms of the estimated hypocenter parameters with the mean value and standard deviation.

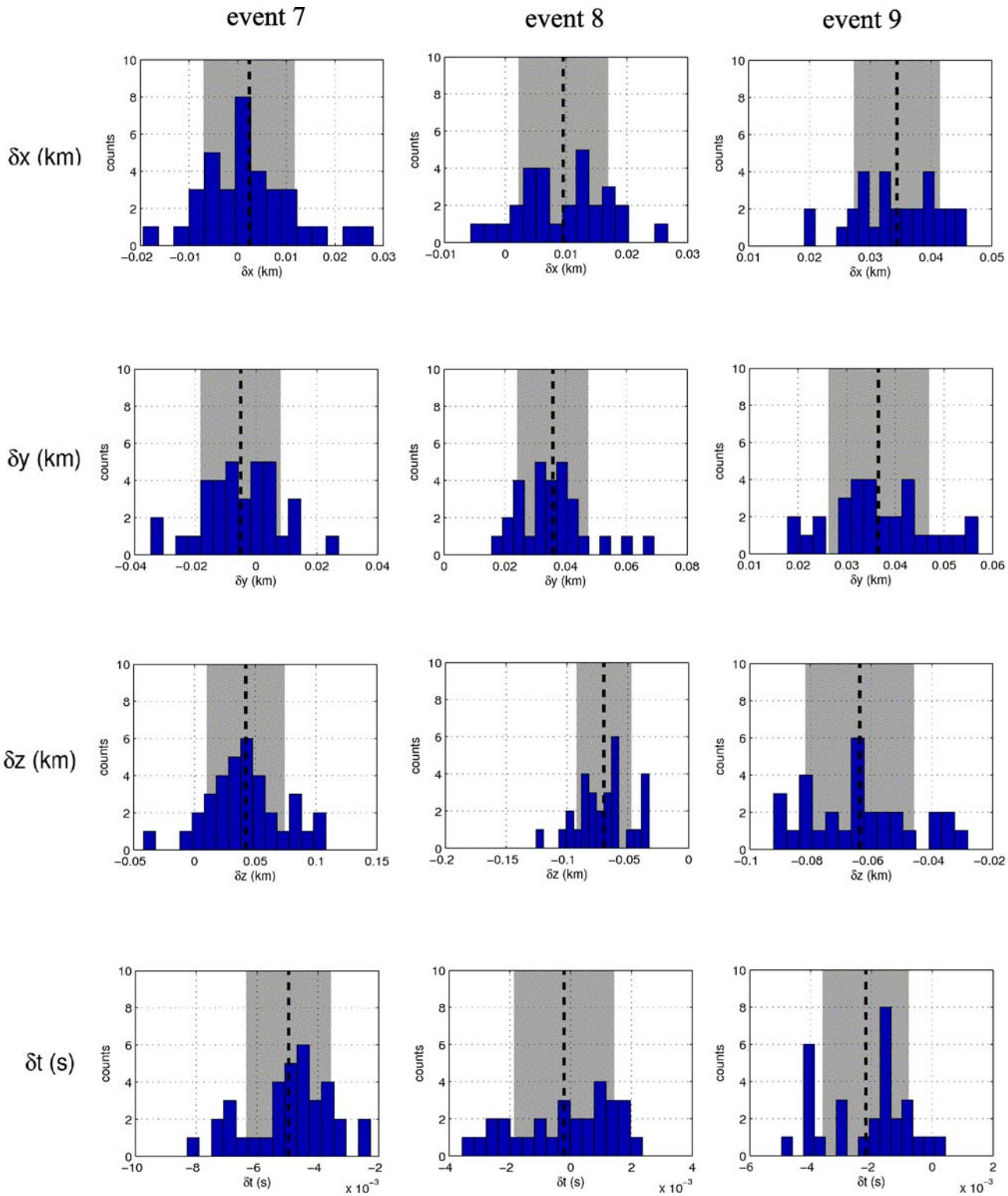

Figure A3.1. Histograms of hypocenter parameters estimated from the Jackknife test. Panels in each row correspond to the four hypocenter parameters δx_j, δy_j, δz_j, and δt_j, respectively. Dashed lines indicate the mean values and shaded zone one standard deviation. The figure shows the results of events 7, 8, and 9.

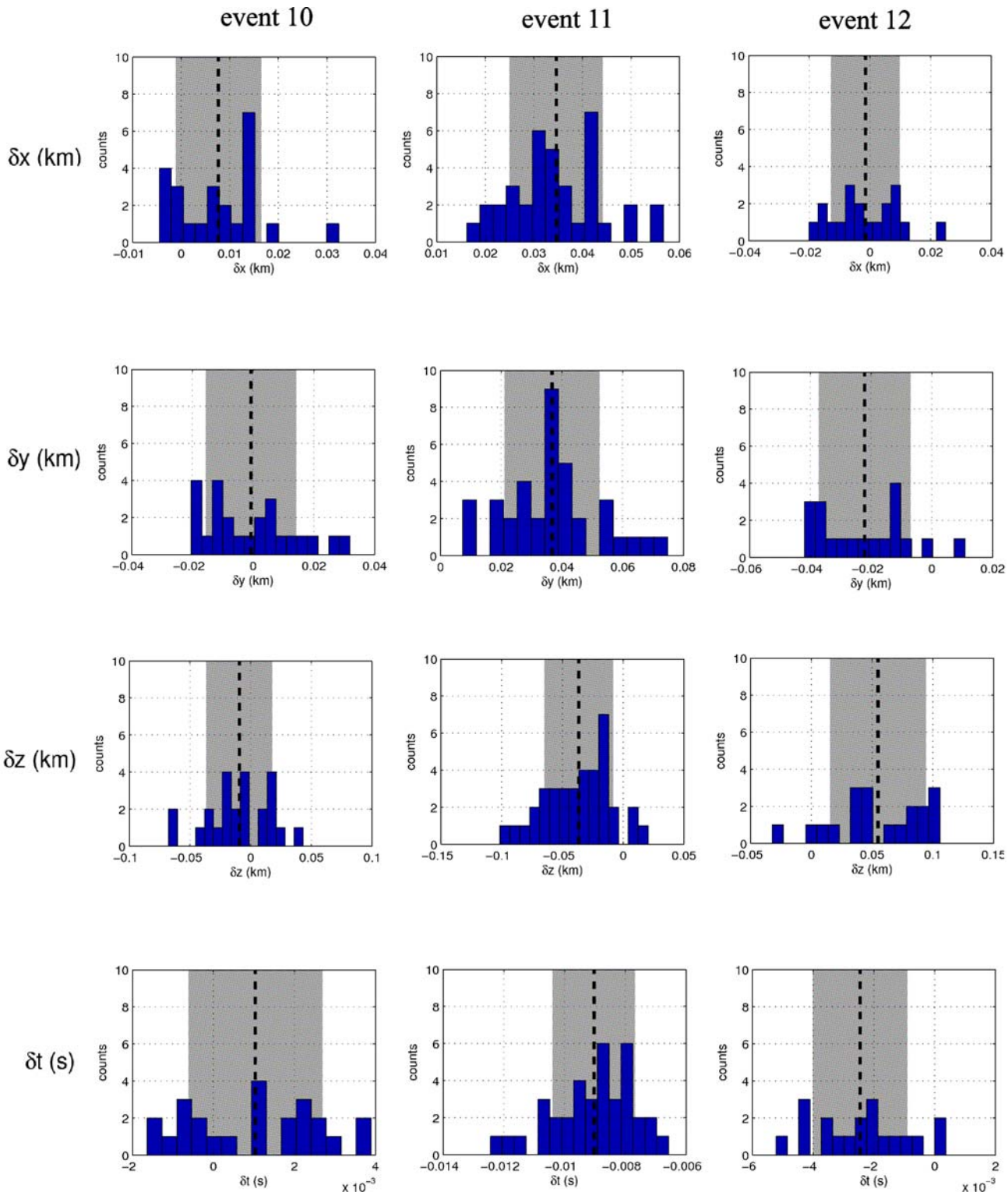

Figure A3.2.Same as Figure A3.1 but for events 10, 11 and 12.

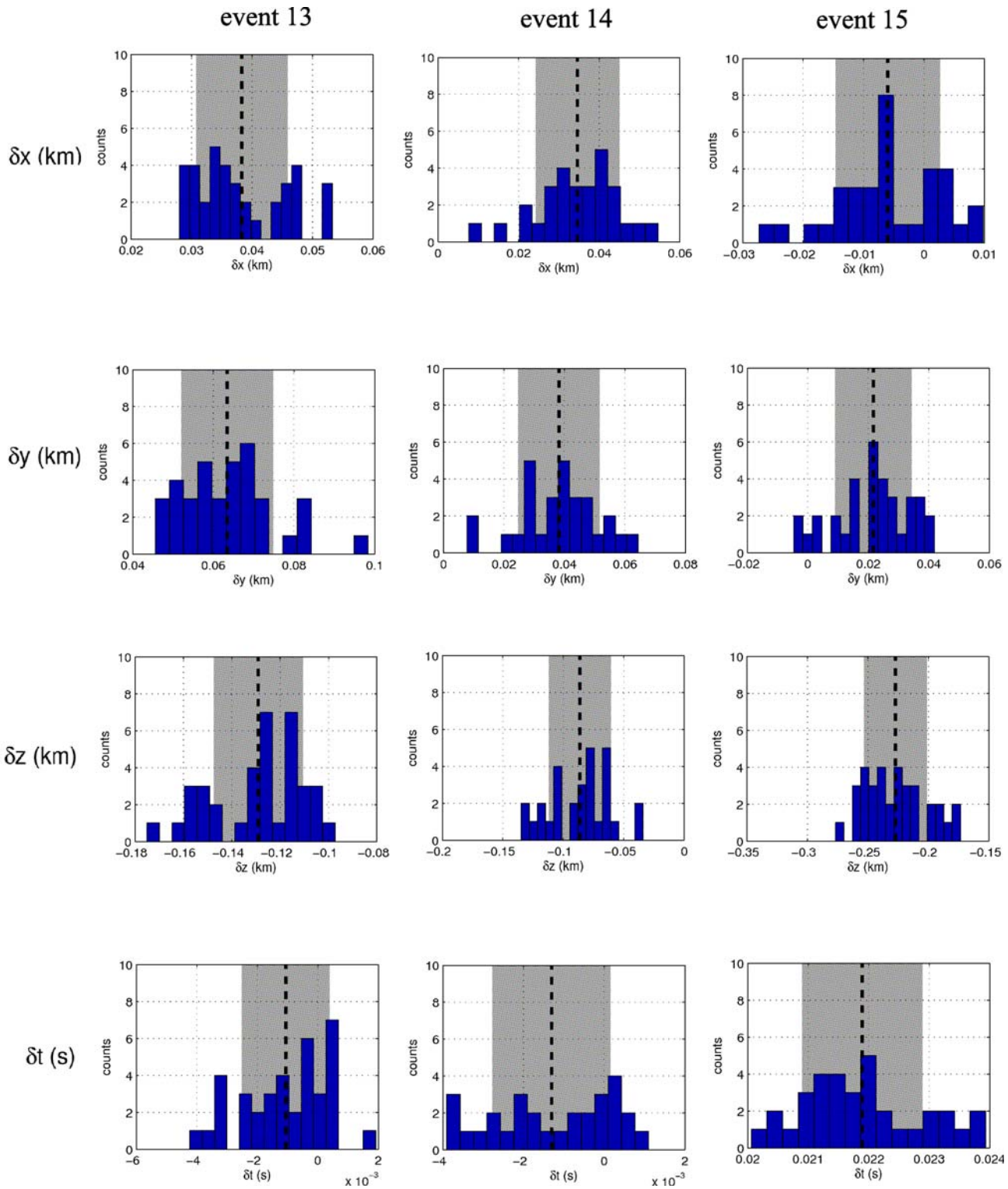

Figure A3.3.Same as Figure A3.1 but for events 13, 14 and 15.

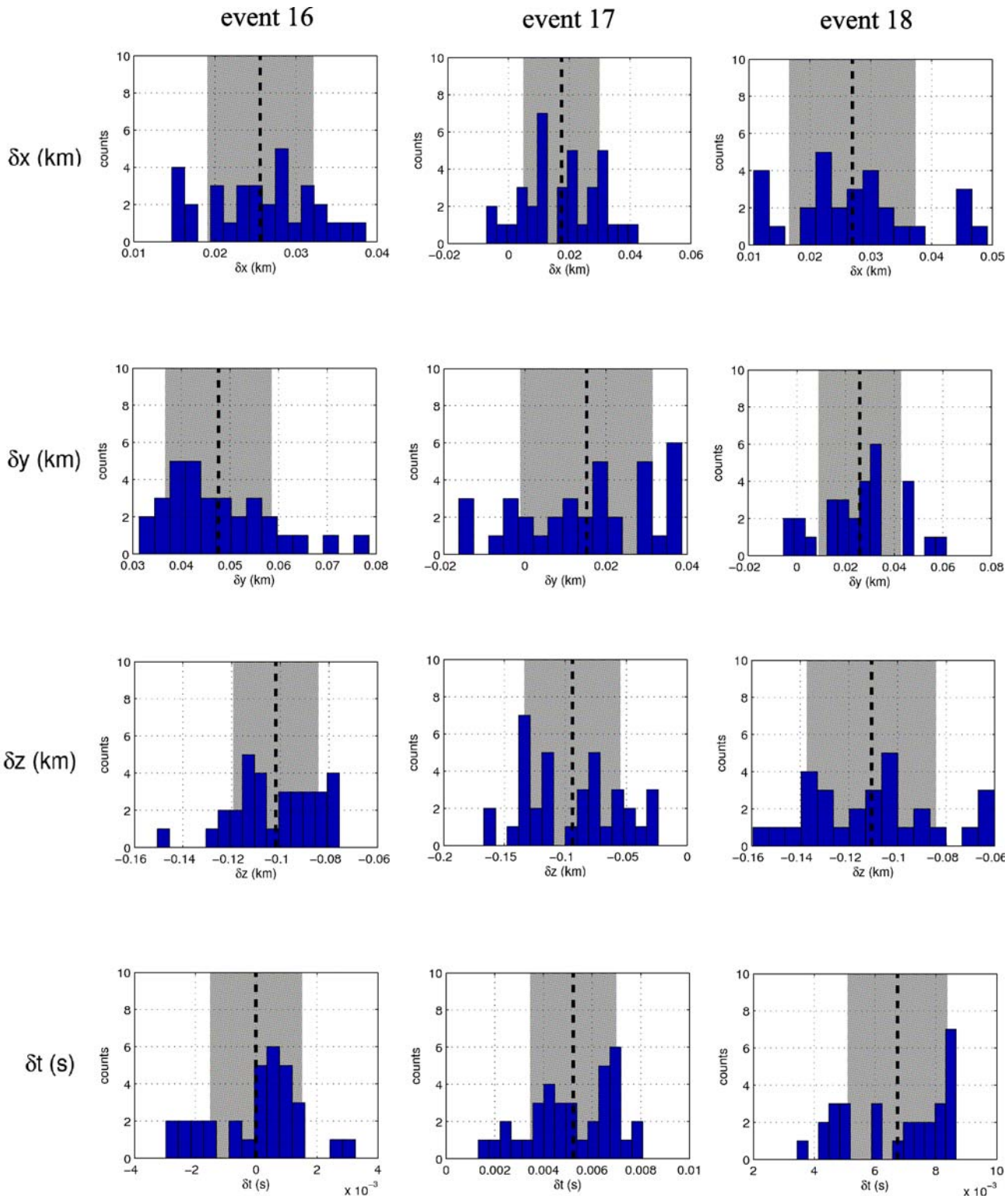

Figure A3.4.Same as Figure A3.1 but for events 16, 17 and 18.

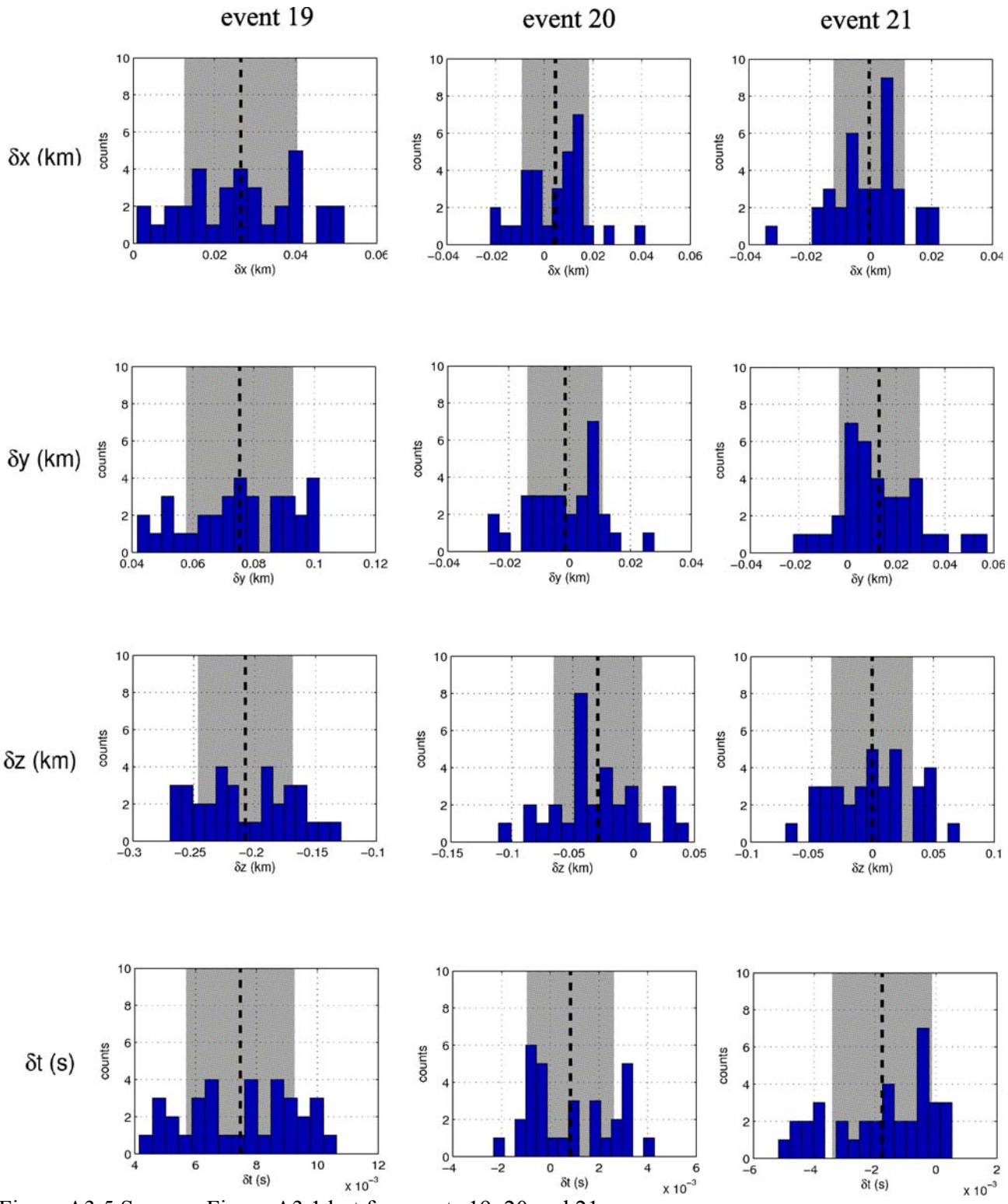

Figure A3.5.Same as Figure A3.1 but for events 19, 20 and 21.

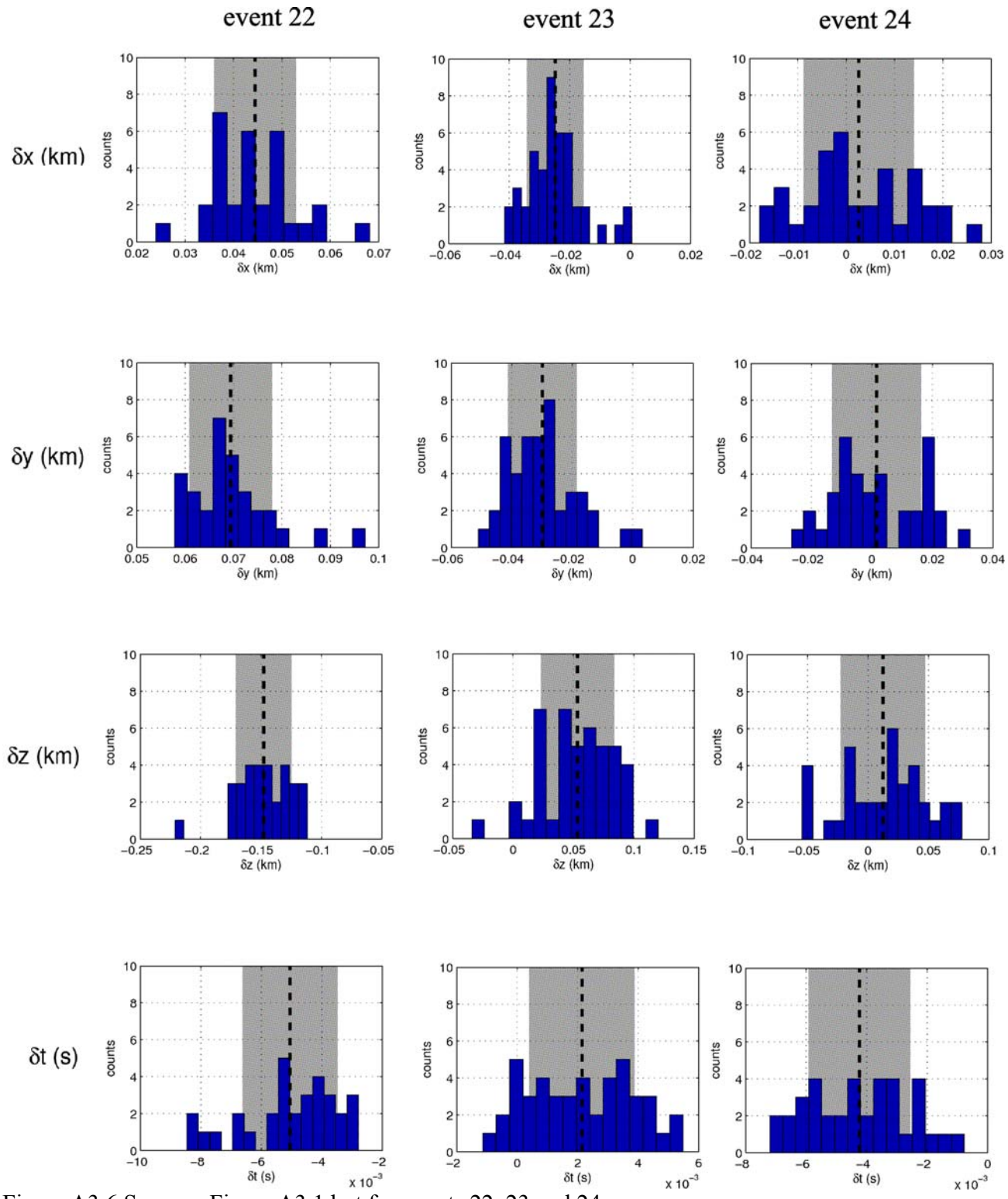

Figure A3.6.Same as Figure A3.1 but for events 22, 23 and 24.

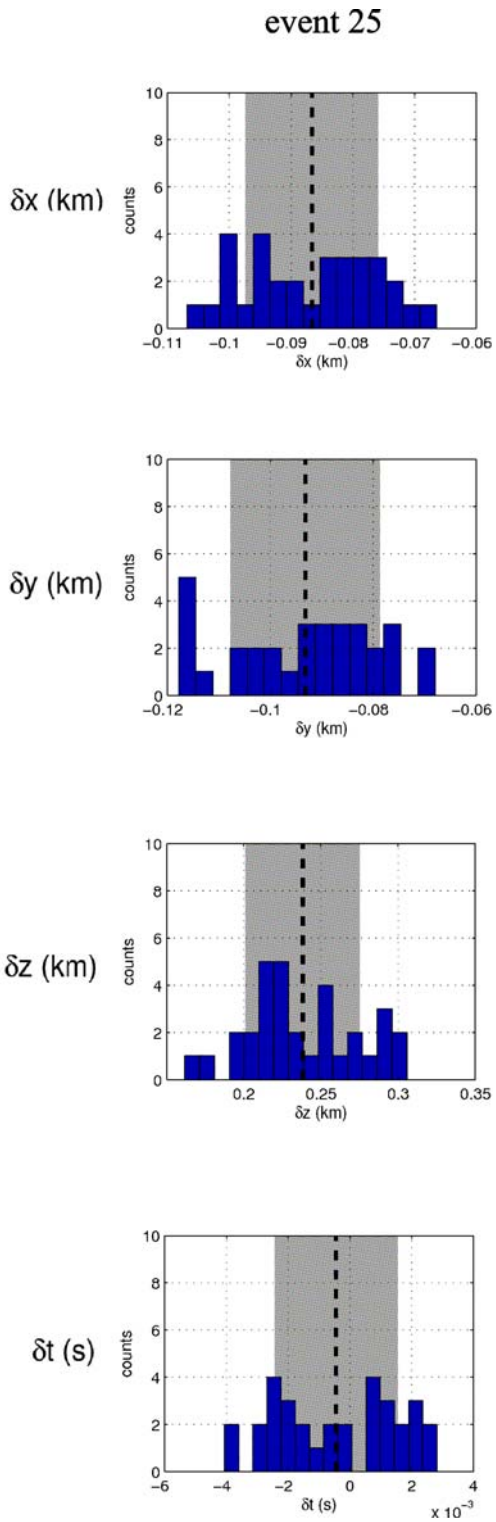

Figure A3.7.Same as Figure A3.1 but for event 25.